Technical Report
TR-20-06
December 2020

Creep testing of copper intended for nuclear waste disposal – overview of studies from 1985 to 2018

Henrik C M Andersson-Östling

SVENSK KÄRNBRÄNSLEHANTERING AB

SWEDISH NUCLEAR FUEL
AND WASTE MANAGEMENT CO

Box 3091, SE-169 03 Solna
Phone +46 8 459 84 00
skb.se

SVENSK KÄRNBRÄNSLEHANTERING

ISSN 1404-0344
SKB TR-20-06
ID 1869474
December 2020

Creep testing of copper intended for nuclear waste disposal – overview of studies from 1985 to 2018

Henrik C M Andersson-Östling
Swerim AB

Keywords: Creep, Tensile, Copper, Phosphorus doped, Testing.

Abstract

Creep in copper for applications in canisters for spent nuclear fuel disposal is surveyed. In the time period studied, 1995–2018, copper has been studied by creep testing, tensile testing, fracture mechanics testing and by metallographical studies. List of reports and publications produced by Swerim AB (formerly Swerea KIMAB, Kimab AB and SIMR) have been collated. All physical tests are also collated, and the results are compared. The effect of phosphorus doping of copper on the mechanical properties is given particular importance in the comparisons.

A limited amount of testing has been performed on nodular cast iron that is used for the inner, load-bearing structure of the canister. Since studies on cast iron at these temperatures are scarce in the published literature, these results have been included in this report.

The significant conclusions made from the research publications presented in this report are given under the heading “Conclusions”. The most significant are repeated below:

- Oxygen-free copper generally shows brittle behaviour during creep at temperatures from 75 to 450 °C, and very low creep ductility has especially been observed between 180 and 250 °C. The creep ductility including loading strain often stays well below 20 %.
- Phosphorus-doped copper shows high creep ductility at temperatures between 75 and 450 °C, higher than that of oxygen-free copper. This is valid for at least 20 years, since the longest-running tests are of this duration. Once the influence of phosphorus on ductility is established for long times, predictions about creep ductility can be made.
- Creep properties are negatively affected only for the very largest grain sizes tested (2000 μm).
- A content of 6 or 12 ppm sulphur has no effect on the creep properties for the two test series that have been examined.
- The loading rate has an effect on the creep strain. The total experienced strain, loading plus creep strain, tends to remain the same through all of the tested loading times.
- Creep testing of electron beam welds and friction stir welds show that the latter have generally better creep characteristics that are often undistinguishable from those of the base metal. Electron beam welds concentrate all deformation to a very narrow band, and the overall properties are thus worse than friction stir welds (FSW).
- Indentations in the tests performed do not have a large effect on the creep properties of the specimen as a whole. No large cracks have been found in conjunction with the impressions, but smaller cracks have been found. The extent of these cracks and their long-term effect have not yet been studied.

Sammanfattning

Kryp i koppar avsett för slutförvaring av utbränt kärnbränsle har studerats. Publikationer rörande kryp, dragprovning, varmdragprovning, brottmekanisk provning och metallografiska studier från perioden 1985–2018 har sammanfattats. En lista över de publikationer som tagits fram av Swerim AB (tidigare Swerea KIMAB, Kimab AB och Institutet för Metallforskning) har sammanställts. Samtliga tester som genomförts i dessa studier är tabellerade och resultaten har jämförts med varandra. I synnerhet har effekten av små mängder fosfor i koppar och dess inverkan på de mekaniska egenskaperna studerats.

En begränsad mängd prov har även utförts på det gjutjärn som formar den inre lastbärande strukturen. Eftersom krypstudier på gjutjärn i de aktuella temperaturerna saknas i publicerade källor har även de medtagits här.

Alla slutsatser som dragits från forskningen som presenteras i denna rapport ges under rubriken ”Conclusions”. De viktigaste repeteras här nedan:

- Syrefri koppar (“OF”) visar i regel ett sprött krypbeteende i temperaturomfånget 75 till 450 °C, och särskilt låg krypduktilitet har observerats mellan 180 och 250 °C. Krypduktiliteten inklusive den initiala pålastningstöjningen understiger ofta 20 %.
- Fosfordopad koppar (”OFP”) visar högre krypduktilitet i temperaturomfånget 75 till 450 °C, högre än duktiliteten hos syrefri koppar. Detta har visats för tidsperioder upp till 20 år, då det är så långt som det längsta krypprovet har gått. När fosforns påverkan på duktiliteten har fastställts för långa tidsperioder kan förutsägelser om krypduktiliteten göras.
- Endast för de största kornstorlekarna som har provats, 2 000 µm, ses en negativ påverkan på krypegenskaperna.
- En svavelhalt på 6 eller 12 ppm har ingen påverkan på krypegenskaper för de två testserier som gjorts.
- Pålastningshastigheten har en påverkan på kryptöjningen. Men den totala töjningen, det vill säga pålastningstöjning plus kryptjöning, tenderar att vara densamma för alla testade lasttider.
- Krypprovning av elektronstråle- och friktionssvetsar visar att den senare har bättre krypegenskaper, ofta oskiljbara från grundmetallen. Elektronstrålesvetsar koncentrerar all deformation till ett mycket snävt band och överlag är egenskaperna därför sämre än hos friktionssvetsar.
- Intryck har i testerna som gjorts inte haft någon stor påverkan på provstavarnas krypegenskaper. Inga stora sprickor har hittats nära intrycken, dock har små sprickor hittats. Sprickornas utbredning och påverkan under långa tidsperioder har inte studerats ännu.

Contents

1 Introduction

Copper is a most interesting metal. It is one of the earliest metals known to man, and one of the most used. An early known use of copper is as material for weapons. Copper weapons were found to be more durable than edged stone weapons and could be resharpened when dulled by use. Body armour could also be made from copper, and for both of these applications, the ductility of pure copper was the key property. Later, among other applications, copper was used to make nails for shipbuilding, cooking pots and personal jewellery. In addition to ductility, the toughness, high thermal conductivity and ability of copper to be polished to a high sheen are important for these applications. Currently, the most important use for copper is in electrical appliances where a high electrical conductivity is the most important material property.

Another early use for copper was as a protective sheeting material for ship hulls. Initially, copper was used was to stop the growth of seaweed and other bio-organisms by exploiting the slight biotoxicity of copper. However, it was noted that the copper also resisted corrosion to a great extent. Thus, a hull sheeted with high-quality copper could remain intact for several decades. Copper is a relatively inert metal in most environments and particularly in water. The corrosion process is accelerated only in fast-flowing water. The good properties of copper in water make it an ideal material for the manufacturing of corrosion-protective containers.

Since the beginning of modern science, copper has been used as a model material for experiments. In particular, creep of metals was studied using copper as a model material, and much of the early knowledge regarding dislocation movements and grain boundary sliding was obtained in the studies of copper specimens (Gifkins 1994). These early studies of copper creep behaviour were incorporated in the deformation map published by Frost and Ashby (1983).

It has been found that creep in copper arises from the movements of dislocations in the copper matrix and the build-up of a substructure of intertangled dislocation lines. The dislocation lines appear when a stress is applied to the material and two moving dislocation lines of opposite sign meet are annihilated upon encountering each other in a process called creep recovery. The balance between dislocation generation and creep recovery determines the creep response of the material.

The operation of nuclear power plants produces radioactive waste that must be treated and disposed without harming the environment. Spent nuclear fuel is more radioactive than natural uranium for more than 100 000 years. The safe method for the disposal of such spent nuclear fuel found by SKB and the planned method in Sweden is based on the so-called KBS-3 concept, where the spent nuclear fuel is placed in canisters (Figure 1-1), which are deposited in the bedrock at a depth of approximately 500 m (Figure 1-2).

The canisters have an inner load carrying insert made from nodular cast iron with quadratic channels where the nuclear fuel elements are placed. The cast iron inserts are then placed inside thick-walled (50 mm) copper shells that are sealed by welding. Copper is chosen for this purpose because it is resistant to corrosion under reducing conditions in the bedrock and because of its high ductility. The spent nuclear fuel elements are placed in the holes drilled in the bedrock and are embedded by a bentonite clay buffer. The surrounding ground water will seep into the buffer over a period of many years, the bentonite will swell and increase the hydrostatic pressure. Due to this pressure, the copper shell of the canister will plastically deform by creep. If the material does not deform due to creep, it will crack during this process, and therefore, the creep properties of copper are of fundamental importance for KBS-3. The deformation will continue until the gap between the copper shell and the cast iron insert is closed. The purpose of the present report is to survey the studies of creep in copper that are related to spent nuclear fuel disposal.

Figure 1-1. *Spent nuclear fuel disposal canisters of Swedish design (SKB).*

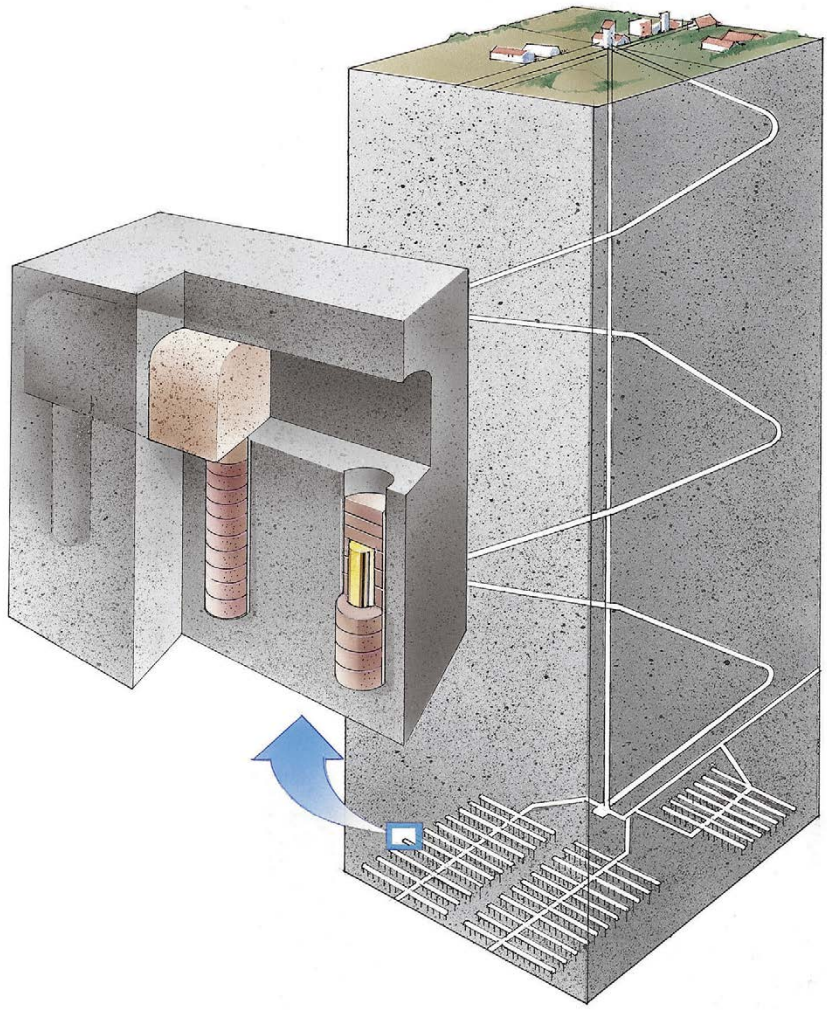

Figure 1-2. *Swedish design of canister repository (SKB).*

2 Research at Swerim

2.1 How it started

Research on canisters for spent nuclear fuel started in Sweden in the mid-1970s. It was soon decided that a canister with an outer copper shell is the preferred option for spent nuclear fuel storage. This is because safe corrosion properties could be anticipated due to the thermodynamic stability of copper in the repository. Initially, the creep properties of copper were considered. It was not until a public enquiry about the disposal concept in 1983 that the creep properties of copper were first discussed in this context.

During the 1970s, it was discovered that failures in structures and plants exposed to creep mainly occur in weldments. During this period, a vast number of creep cracks and failures were observed in fossil fuel-fired power plants. This phenomenon is due to three effects. First, the creep properties vary across the welds because the weld metal, the heat-affected zone, and the parent metal almost invariably have different creep properties, giving rise to stress concentrations. Second, the creep ductility and strength are often lower for the welds than for the parent material. Third, the creep properties were rarely taken into account in design at that time.

In the beginning of the 1980s, the Swedish Institute for Metals Research (SIMR, then Swerea KIMAB and now Swerim) and British CEGB were the internationally leading organisations in the study of creep in weldments. Tests were performed on uniaxial specimens as well as tubes under internal pressure. The experiments were successfully combined with finite element model (FEM) modelling (Ivarsson and Sandström 1980). It was therefore proposed that SKB will study the weldments in the copper canisters. Pure copper had been used extensively as a model material for creep studies with regard to different aspects of materials as well as their design. Although most of these investigations were conducted at temperatures of 300 °C and higher and thus were well outside the typical design temperatures for copper, no one anticipated the serious problem with the extremely low creep ductility that was discovered later.

2.2 Quality assurance requirements and internal reports referred to in this document

All of the work performed at Swerim and its predecessors has been reported in either internal Swerim (SIMR, Swerea KIMAB) reports or in international scientific publications. Some reports have been published as SKB reports and for some studies, several different report types have been used. Many of these, especially older documents, do however not comply with SKB´s current quality assurance requirements for public reports due to, for instance, public availability of the document and formalities in the review process and are therefore not allowed to be used as references in SKB TR series of reports. Although these documents are not formally acceptable as references they still contain valuable information and are relevant for an overview report such as the present report since they contain valuable data which validity has not been questioned. The actual test data from the studies have been included in this survey report both as the tabulated individual data points and as graphs, but, to indicate that they do not meet current requirements, references to these documents are given in *italics* and these documents are not included in the reference list. Instead Appendix 1 provides a comprehensive list of all these reports with a short description of the content. Some documents have not only been published as internal Swerim (SIMR, Swerea KIMAB etc.) reports but also in, for instance, conference proceedings. If so, this reference is included in the Report list. Since other internal documents might use the internal reference and not the reference to, for instance, the conference proceeding there is still a need to include these documents in the Report list.

2.3 Timeline of research

A timeline for the work on creep in copper at Swerim in cooperation with KTH is presented in Table 2-1. Studies with an experimental component have been included in the table. Pure modelling studies have been included in the cases where they are directly related to experiments. Work on creep in copper at Swerim started in 1984 with a literature study (*Yngrén 1985*)[1]. This was followed in 1988 by a pilot creep study on a Cu-OF standard high purity copper material (Ivarsson and Österberg 1988, Ivarsson et al. 1989, Henderson et al. 1992). In 1992, a creep programme was started on phosphorus-doped copper Cu-OFP (*Lindblom et al. 1992*, *Henderson 1994*). Further studies on the same material were reported in 1995 and included studies of creep crack propagation, tensile tests and the effect of specimen size on the creep results. The first extrapolation efforts were also reported in that year (*Lindblom et al. 1995*, *Henderson and Seitisleam 1995*, *Henderson and Lindblom 1995*, *Seitisleam et al. 1995*). In 1996, further work on creep in Cu-OFP was reported (*Seitisleam and Henderson 1996*, Henderson and Werme 1996). In 1998, a thorough analysis of creep ductility results on Cu-OF was published (Henderson and Sandström 1998). In 1999, the first slow rate tensile tests were performed at KTH for cold-worked Cu-OFP (Yao and Sandström 2000).

At the same time, the final copper alloying composition was selected, and a new programme was initiated involving creep-tested extruded bars with different phosphorus and sulphur levels as well as different grain sizes (Andersson et al. 1999, 2001). A new method for the extrapolation of creep strain data was developed (Sandström 1999). Starting in 2004, the creep test studies focused on welds. Both electron beam welding (EBW) and friction stir welding (FSW) were studied (Andersson et al. 2004, 2005). New creep crack propagation tests were also performed at this time (*Andersson 2005*). The work progressed and new results were published in 2007 (Andersson et al. 2007).

In 2008, studies on the effect of hydrogen in copper were initiated. A study on the depth of penetration during electrochemical charging was published in 2012 (Martinsson and Sandström 2012). Two studies on the in situ charging of copper during creep were published in 2014 and 2017, respectively (*Leijon and Ahlström 2014*, Leijon et al. 2018).

In the repository, the rate of load application depends on the water ingress and saturation of the bentonite clay. While, geologically speaking, this process can be either slow or fast, on the laboratory timescales, this process is always slow. Studies on the loading rate effect begun in 2009, and their results were published in 2011 and 2014 (Andersson-Östling and Sandström 2011, Mannesson and Andersson-Östling 2016). Slow strain rate tests have also been performed at KTH (Sandström and Hallgren 2012, Sui and Sandström 2016) and Swerim (Björck et al. 2019), which in a sense also deal with the load application rate.

During the manufacturing of a copper canister, it is important that cold working of the copper is not introduced inadvertently. Several studies (Martinsson and Andersson 2009, Mannesson et al. 2013, Mannesson and Andersson-Östling 2014b, Wu and Sandström 2015) explored the properties of copper with both macroscopic levels and microscopic levels of cold work. Further work was also performed on the multiaxial stress states and the subcell structure within the copper grains (Wu et al. 2009, 2014). Finally, a study was performed on copper materials from different copper tubes that exhibited different sound attenuation during ultrasonic non-destructive testing (Mannesson and Andersson-Östling 2014a). The difference in sound attenuation is most likely an effect of the different grain sizes in the material.

More studies on creep crack growth experiments were performed in 2011 (Wu et al. 2011), and a critical review of crack and rupture surfaces was undertaken. This was published in 2017 (Björkblad and Faleskog 2018).

[1] References given in italics do not meet SKB´s quality assurance requirements for public reports, see further Section 2.2. These references are presented in the Report list in Appendix 1.

In 2018, results from Finnish studies that showed oxide inclusions in FSW lines emanating from the root of the weld and up along the advancing side became available. In this research effort, creep studies were performed to evaluate the effect of these inclusion lines on the overall properties of the weld (*Wu 2011a*, *b*, *c*, Björck et al. 2019). Starting with theoretical studies performed in 2013, efforts have been made to elucidate the role of phosphorus in copper creep and its positive effect on the creep ductility. The results of these investigations were published in Sandström and Wu (2013), Wu et al. (2014, 2015a), Wu and Sandström (2015), Sandström (2016a, 2017), Andersson-Östling et al. (2018) and Josefsson and Andersson-Östling (2019).

Details are provided in the publication list in Appendix 1. A small study was also carried out on non-phosphorus-doped oxygen-free copper in 2017. Cu-OF had not been studied since 1999, and the methods of creep testing have been significantly refined since then. These refinements consist of better temperature logging, better load control and the absence of resets in load applications that were necessary in previous studies. Using modern testing methods, the new study (Danielsson and Andersson-Östling 2018) verified that the earlier results were valid.

Generally, the results obtained in different years are broadly comparable, but owing to the different production methods of the examined copper materials, a direct comparison of individual results cannot be performed. For instance, prior to 1999, the tested copper samples were commercial-grade copper bought on the open market. In 1999, a study was performed on 16 mm extruded bars. Starting in 2001, 50 mm thick hot-rolled materials were used in the studies. Starting approximately 2004, only 50 mm extruded tube and forged lid materials were used, which are similar to the material of the proposed canister with regard to both the chemical composition and the production method. From this point on, even individual tests may be compared if the material conditions are considered (i.e., as-received, annealed or cold-worked). These material conditions are noted in the reports along with the test results.

In Sandström and Jin (2008) and Sandström (2012) a creep model for primary and secondary creep has been developed and applied to finite element calculations on a copper canister shell using creep data from previous investigations.

Table 2-1. A timeline of work on creep in copper for spent nuclear fuel disposal at Swerim and KTH.

1984 Literature survey
1988 Creep study of Cu-OF at 75 to 145 °C
1992 Creep study of Cu-OF at 180 to 250 °C
1992 Creep study of Cu-OFP at 200 to 350 °C
1995 Creep study of Cu-OFP at high temperatures
1995 Initial creep crack growth studies
1995 Specimen size studies
1996 Creep test series 600, 700 and 800
1999 Extruded copper studies at 175 °C. P, S and grain size effect
1999 Extrapolation of creep strain data
1999 Hot working investigations
1999 Slow strain rate tensile tests of cold work material
2001 FSW tool material development literature survey
2004 Initial weld studies, EBW and FSW
2005 Second creep crack growth investigation
2005 Creep loading procedure studies
2007 Creep investigations on extruded material welds
2007 Modelling of creep ductility on the basis of creep cavity nucleation and growth
2007 Modelling the effect of phosphorus on copper creep
2007 Fundamental constitutive equations for creep during power-law breakdown
2007 Slow strain rate tensile tests of annealed copper
2007 FEM modelling of creep in copper canisters taking secondary creep into account
2008 Effect of hydrogen in Cu
2008 Fundamental model for slow strain rate flow curves
2008 FEM modelling of creep in copper canisters taking primary creep into account
2009 The effect of cold deformation on creep in copper
2009 Extremely slow creep loading of copper
2009 Studies on the role of multiaxial stress state during creep
2011 Third creep crack growth studies
2011 Studies on processing line inclusions and the effect on the creep properties of the weld
2012 Hydrogen charging of copper and the resulting depth profile
2012 Slow strain rate tests on copper (KTH)
2013 The effect on phosphorus on the creep ductility of copper
2013 The effect of local deformation imprints on the creep properties of copper
2014 In situ hydrogen charging of copper
2014 Second study on the slow loading of copper creep tests
2014 Creep properties of copper with different NDT sound attenuation responses
2014 Further studies of the effect of local deformation imprints on the creep properties of copper
2014 Subcell structure studies using transmission electron microscopy
2015 Studies of grain boundary sliding during creep testing
2015 Creep properties of copper with different levels of phosphorus
2015 Second study on creep in copper with cold work and intentional notches
2016 A dislocation model for the cell structure in the cold deformed Cu-OFP was formulated
2016 Further studies on the effect of phosphorus on creep. Overview of the previous experiments
2016 Second SSRT study on copper (KTH)
2017 A critical evaluation of fracture surfaces on both uniaxial and creep crack growth specimens
2017 New experiments on Cu-OF to verify the early findings using state of the art creep test rigs
2017 A study on modelling of creep curves based on the dislocation model for Cu-OFP developed in 2016
2018 Third study on slow strain rate tests
2018 Embedded oxide particles and the effect on the creep properties of the weld
2019 Ageing and recrystallisation dynamics of Cu-OFP at low temperatures

3 Creep testing techniques

3.1 Materials sampling

All materials used for creep testing must be extracted from the larger delivered pieces. Standard uniaxial creep tests are usually performed with plain cylindrical tests specimens. The smaller specimen used has a gauge length of 50 mm and a gauge diameter of 5 mm, and the larger specimen has a gauge length of 75 mm and a gauge diameter of 10 mm (Figure 3-1).

To manufacture the specimens, the blanks cut from the copper pieces must be larger than the final dimensions of the specimens, which were $9 \times 9 \times 90$ mm and $17 \times 17 \times 180$ mm, respectively.

The placement of the specimens is important. If the material has a texture due to rolling or extrusion, the specimens are usually taken along the working direction. If the material contains a weld, specimens can be taken from either the weld metal, the base metal, the heat-affected zone (HAZ), or a cross-weld position. An example of the extraction of specimens from a weld is shown in Figure 3-2.

Specimens from either the weld constituents or the base metal provide information regarding the properties of homogenous materials. Cross-weld specimens tend to accentuate the weakest region of the weld. These specimens cannot be used for the ductility estimation since the gauge length is undetermined if only a part of the specimen is strained during testing.

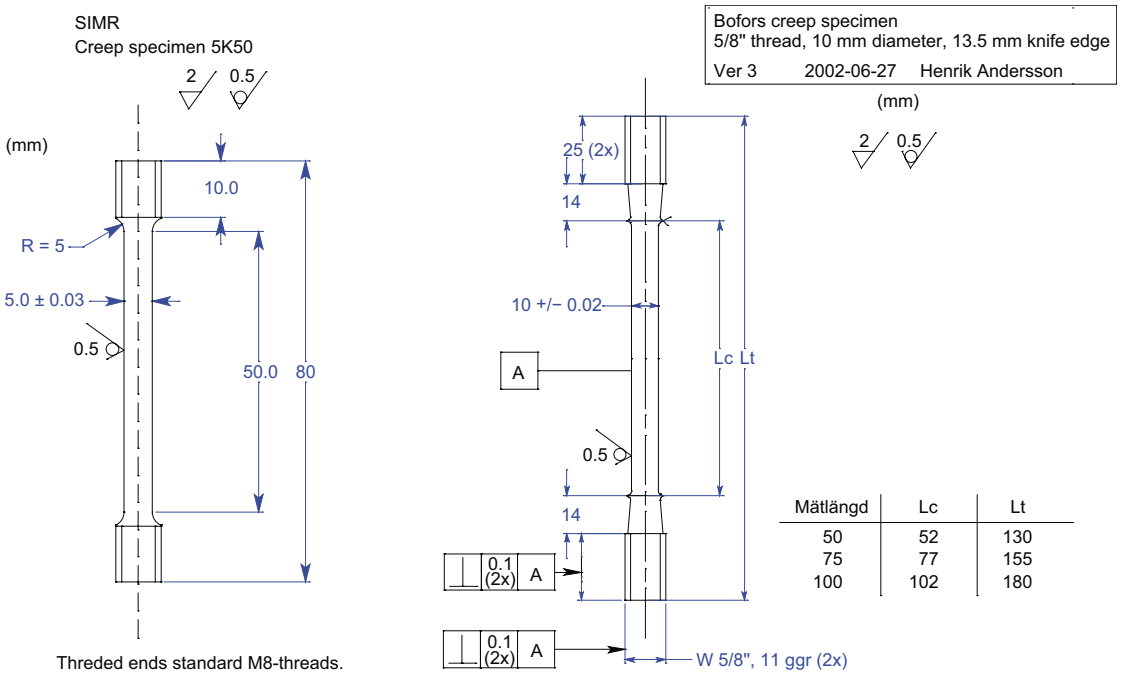

Figure 3-1. *a) Creep specimen type 5K50. The same specimen design is used in a similar specimen called 5K25, where the gauge length is 25 mm. Scale 1:2. b) Creep specimen type Bofors. The same design is used with the gauge lengths of 50–100 mm by altering the distance between the knife edges.*

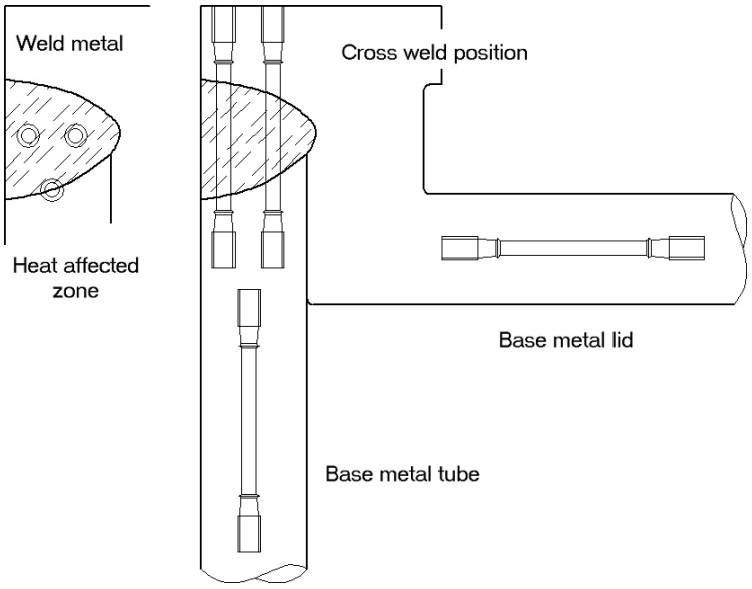

Figure 3-2. *An example of the extraction of specimens from a friction stir weld. Specimens from the base metal lid and tube as well as the cross-weld, weld metal and heat-affected zone specimens are marked in the image. Taken from the 2007 study of friction stir welds at 75 °C (Andersson et al. 2007).*

3.2 Test procedures in a dead weight lever test rig

All of the creep tests performed up to 2008 were conducted on standard dead weight, lever creep test rigs. All of these test rigs operated in a similar manner despite the variations in the design of the individual test rig. A schematic drawing of the operating principle of such a rig is given in Figure 3-3. Until 2012, Swerim had over 70 of these test rigs with different configurations that were all equipped with high-temperature furnaces (Figure 3-4).

The set-up of a creep test is as follows. The load train is calibrated by placing a calibrated load cell in the test rig instead of the specimen. The lever arms have a ratio of 1:16, 1:20 or 1:25, but by using the actual lever arm and load with actual weights until the correct reading is reached on the load cell, a correct load value is obtained for each test. The weights are then removed. The specimen is placed inside the furnace and preloaded with the empty lever arm, yielding a load of approximately 100 N. Thermocouples are tied to the gauge length, and the specimen is heated to the test temperature. The thermocouples, known as type S (Pt/PtRd wires), are made from certified metals, and new metal is used for the thermal junction for each new test. After a soaking time of at least 2 h, during which the temperature gradient is adjusted and minimised, the previously calibrated weights are loaded onto the lever arm, and the test is started. The maximum tolerances allowed are ± 1 °C for temperature stability and ± 2 °C for the axial gradient. For all of the tests carried out up to 2006, the load was applied within 2 minutes.

If the creep strain in the specimen is sufficiently large, the lever arm must be reset to ensure that it has an approximately horizontal position. During the reset, the specimen is temporarily unloaded by the insertion of a manual lever arm between the fulcrum and the weights. The weights are lifted, and the nut on the top of the load train is adjusted until the angle of the lever arm is once again +5°. The weights are lowered, and the load is slowly reapplied to the specimen. The specimen temperature remains constant during this operation.

Strain and temperature are recorded automatically using extensometers mounted on the knife edges immediately outside the gauge length on the specimens (Figure 3-3). In the case of the small specimen (Figure 3-1), the knife edges are mounted on the adapters in which the specimens are mounted. The extensometer rods are fed to the capacitive transducers that measure the strain in the specimen. Usually, two transducers are used for each test. The signals from the transducers are recorded along with the specimen temperature and the ambient temperature by a computerised logging system. The logging interval can be individually adjusted. The standard interval is 1 hour. As a backup, the measurements are noted on paper protocols once every workday.

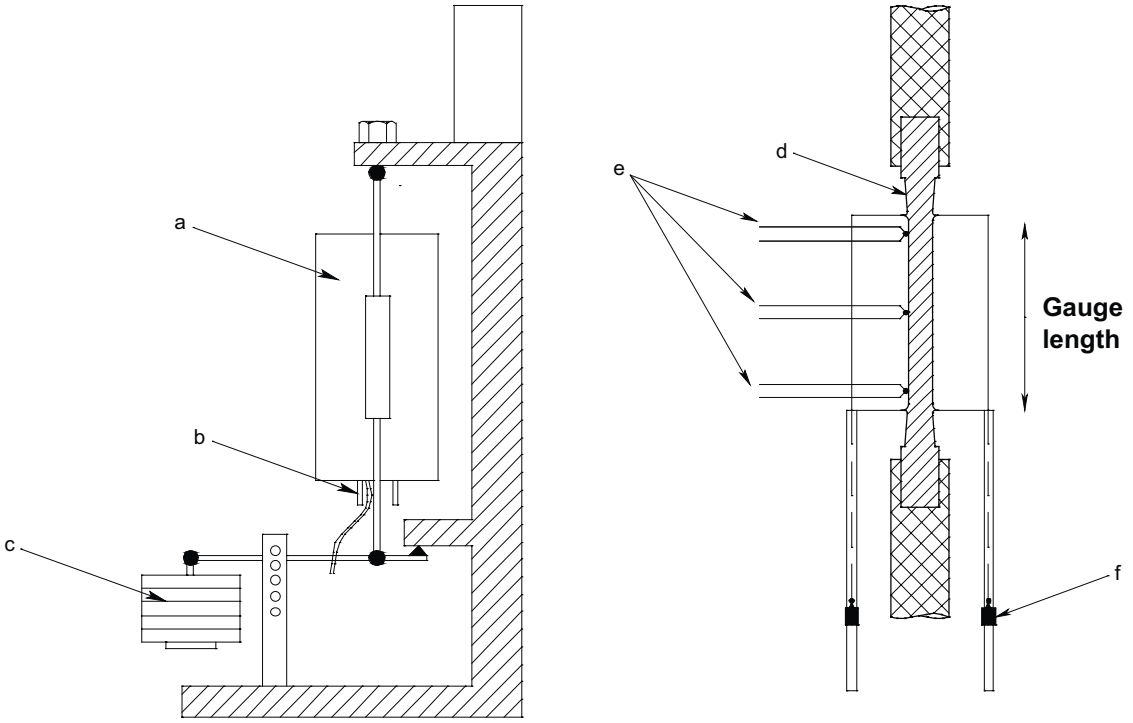

Figure 3-3. *Principle of creep testing. Schematic drawings of a creep test rig (left) and a creep specimen (right); a: furnace with specimen, b: extensometer transducer, c: weights and lever arm, d: specimen, e: thermocouples, f: transducer. The gauge length is marked in the right image.*

The main attractive feature of capacitive transducers is their inherent ability to avoid the signal drift from the correct measurement value. The signal only depends on the dielectric properties of the medium between the electrodes in the laboratory air.

The creep laboratory is climate controlled and is maintained at a constant temperature and humidity, so that the signals from the transducers do not vary except due to the strain measurement. The signals are linear with a theoretical accuracy of 10 nm; however, 100 nm is the practical limit of the measurement accuracy. If a mechanical malfunction occurs, it usually only affects one of the two transducers, which can be removed and repaired while the test is monitored by the other transducer.

One drawback of the dead weight lever creep testing is that it is not compensated for the lever arm movement. The horizontal distance between the fulcrum and the load application point depends on the angle of the arm. This error can be neglected with confidence for small angle shifts, and the used testing machines allow max ± 5° arm travel. Thus, the standard procedure is to start the test with the arm at the top limit and to reset the arm as the angle reaches the bottom limit. In practice, this means a maximum travel of 5 mm at the specimen end of the lever. Depending on the gauge length, the test must be reset every 5 or 10 % engineering strain.

Figure 3-4. *Creep testing laboratory showing the creep rigs. Inset: a close-up of the lever arm.*

3.3 Test procedures in an active load control test rig

In 2007, the newly developed test machines for which the load is applied using a step motor connected to a gearbox started to be used. This equipment allows 35 mm of travel of the load arm without the need for unloading of the specimen (Figure 3-5). The load can also be applied very slowly. Starting in 2012, the majority of the test rigs at Swerim were converted to the new configuration, and all copper tests performed subsequently were conducted using the active test rigs.

The procedure of using the active control test rigs is similar to the dead weight lever test rigs, with the application of the load as the only difference. A test is started by calibrating the load using an external calibrated load cell. The specimen is then placed in the furnace using the same procedures as with dead weight lever test rigs and is heated. Then, the test is started by increasing the load using the step motor. The load is applied using a continuous stroke. The loading time for the standard copper specimens is 15–20 minutes, and the loading strain is automatically logged. During the creep part of the test, the load is held within ± 5 N. The test is usually interrupted immediately prior to fracture for practical reasons with the machine feedback.

The test rig allows the precise control of the loading procedure, and extremely long loading times of up to 6 months can be easily implemented.

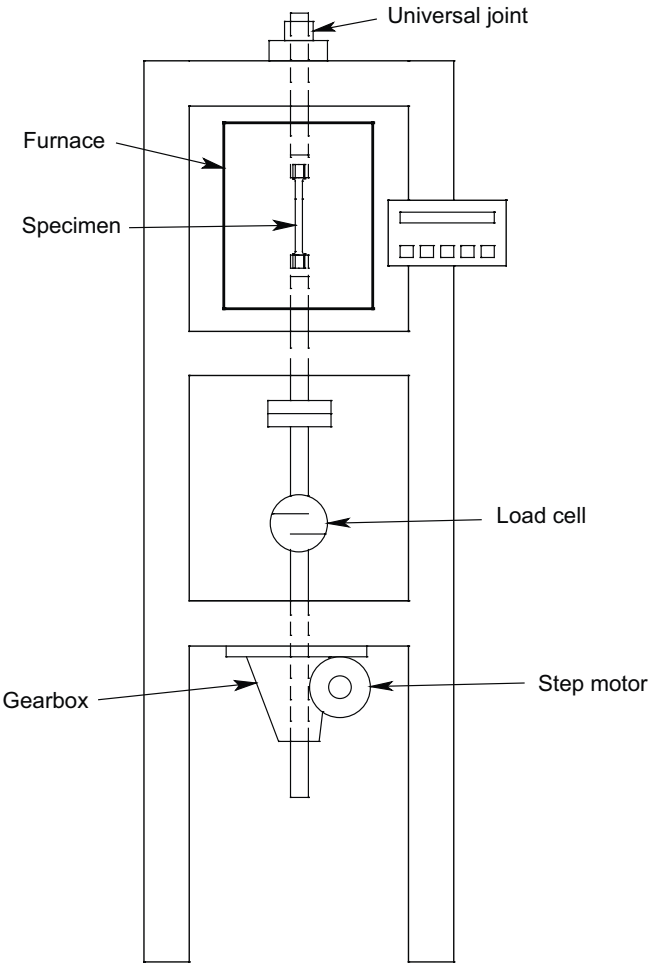

Figure 3-5. *Schematic drawing of the active load control test rig.*

3.4 Testing – plastic strain on loading

A creep experiment is started by placing the specimen in the furnace and heating it to the test temperature. The load is then applied as smoothly as possible until the desired stress has been reached on the specimen. During the loading process, the specimen is strained by the load. This strain is not the true creep strain since the test timescale is several minutes rather than hundreds of hours. Early experiments did not distinguish between this plastic strain and the subsequent creep strain. Most testing at the creep laboratories up to this point had been performed on ferritic steels where the initial strain is low, typically below 2 %. In the case of copper, and especially for annealed copper, the initial plastic strain can be as high as 15 %, and thus is a substantial part of the total strain. Later experiments recorded the initial strain, but it was not included in the reported creep strain. This means that early and late creep results are not fully comparable, and the later results reported starting in 1999 are conservative with respect to ductility.

In the repository, the canister is exposed to the hydrostatic pressure due to the ground water. At a depth of 500 m, the hydrostatic pressure is 5 MPa. In addition, a swelling pressure from the bentonite is also exerted on the canister. When fully saturated, this pressure is 5–13 MPa. Thus, the total pressure on the canister can reach 10–18 MPa. Depending on the hydraulic conductivity of the rock and the associated rate of the water inflow, up to one hundred years are required for the full saturation of the bentonite.

During the loading phase the stresses in the canisters will be quite low, so the secondary creep rate is negligible. However, the strain on loading and the primary creep can still be significant.

3.5 Testing – resets

All tests carried out prior to 2007 were performed using dead weight lever tests rigs. In these tests, the standard practice was to keep the arm ± 5° from the horizontal direction. This allows a maximum amount of strain before the lever arm must be raised. If the lever arm is not raised, the weight hanging on the arm lands on the floor. The strain can be either 5 % or 10 % depending on the test rig. Since the total strain in many copper creep tests is 40 % or higher, the lever arm must be reset several times. Some tests have been reset as many as five times. Annealed or close to annealed copper exhibits a creep tests curve that consists of almost exclusively primary and tertiary creep with almost no steady state secondary creep between the primary and tertiary creep regions. During a reset, if the material is in a primary or early tertiary stage, new primary creep is initiated. This is manifested as a series of bumps on the creep curves. A likely cause of this phenomenon is that during the reset the specimen is temporarily unloaded, and the dislocation substructure is relaxed. When the load is then reapplied, a new dislocation substructure is created, yielding a new primary stress redistribution stage. If the specimen is reset well into the tertiary stage, an accelerated tertiary stage is developed, and the specimen rupture is accelerated. Since many of the tests have been reset several times, it is imperative to determine the effect of the unloading/reloading on the creep properties. However, exactly how the reset affects the creep properties has not yet been established: the deformation introduced in a reset may harden the material and enhance creep life or may cause material damage and shorten creep life. In both cases, the difficulty of the modelling of the creep behaviour is increased by this effect.

For instance, it is not clear to which curve a model should be applied. The two options are the incomplete unbumped curve or the envelope of the bumped curve. In the study on extremely slow creep loading (Mannesson and Andersson-Östling 2016), the newly developed test rigs do not need to be reset. Thus, creep tests can be allowed to continue uninterrupted to rupture even if the creep strain approaches 100 %. Modelling of the results and extrapolations of the results should be made easier by this approach. As a general recommendation, the number of resets should always be kept to a minimum.

3.6 Testing – geometrical considerations

Creep testing of copper has been performed using two different types of specimens. The early experiments concentrated on the 5 mm diameter specimen shown in Figure 3-1. The gauge length has varied, but a gauge length of 50 mm was usually used. Later experiments had predominately used the standard

Bofors 10 mm diameter specimens with a gauge length of 50–80 mm. The difference between these two specimen designs lies in the manufacturing of the specimens. When a slender 5 mm specimen is turned on the lathe, work hardening can result from the vibration of the specimen when the cutting tool is applied to the surface. The 10 mm specimens are much bulkier and are more resistant to vibration. Thus, the 5 mm specimens are slightly cold-worked and exhibit a longer creep life than the 10 mm specimens even if they are made from the same block of material. This was demonstrated by a series of experiments performed in 1995. While not published externally at the time, the results can be found in Chapter 6.2 below and the results of the actual creep tests are presented in Table A4-3.

When the 5 mm specimens were annealed for 5 minutes at 600 °C followed by a water quench, the creep results became similar to those obtained for the 10 mm specimens. The 10 mm specimens were tested as-machined. Thus, it is recommended for all future testing to use 10 mm specimens when possible and to anneal all 5 mm specimens prior to testing.

3.7 Temperature

In the creep testing performed at the institute, test temperatures in the copper creep tests have varied from a minimum of 75 °C to a maximum of 600 °C. Under repository conditions, the temperature may be as high as 125 °C in the cast insert and is approximately 100 °C in the copper shells during the initial years and then slowly decrease to room temperature over many hundreds of years. It is therefore interesting to perform creep tests of copper at the temperatures relevant to the repository. Copper is known to creep at room temperature and above, but for practical reasons test times must be kept to a reasonable length, and the creep test must be accelerated. There are two possible approaches for performing accelerated testing: either the temperature is increased, or a higher applied load is used. Both approaches have been used in the investigations surveyed in this work. Earlier testing concentrated on increasing temperature to 175–250 °C. This produced creep lives that were suitable for the project timeframe. When the temperature is increased above the intended service temperature, there is always a risk of the test results exhibiting a creep damage accumulation behaviour that is different from that at the service temperatures. In part for this reason, later work shifted towards the use of the temperatures close to 75 °C, which is a reasonable average of the temperature of the copper over the first years in the repository.

The resulting creep strain curves and the creep ductility at rupture were similar for the test series at higher and lower temperatures. This does not apply to the Norton exponent, which is the slope in the plot of the strain rate versus stress. As the temperature decreases, the Norton exponent increases, which is referred to as the power-law breakdown. This behaviour has been fully explained and quantitatively modelled assuming climb control (Sandström 2018). This also makes extrapolation to longer creep times more difficult. A slope of 3–5 that is typical in the power-law creep makes it easier to extrapolate the data to longer times than a slope of 50 or 70. A small mistake or scatter in the results gives a very large change in the extrapolated rupture time results. Power-law breakdown is the dominating creep mechanism in the repository.

3.8 Material condition

The treatment of specimens before testing has been different for the older and the newer investigations. In the beginning it was not fully realized that plastic deformation history of the material could have a large impact on the results of the creep testing. From approximately 2008 all specimens have been annealed before testing to give the material a maximum softness. Before this time, hot rolled and extruded materials could be tested as received and with no special consideration for the hardness of the material being tested. For all testing the treatment of the materials was noted in the report, and this has been quoted in this overview report as well. But the difference in heat treatment could affect the results making a direct comparison difficult.

4 Creep of oxygen-free high-conductivity copper

A literature survey was carried out prior to the selection of material for creep testing. The published literature data from 1945 to 1982 were surveyed, and creep data were extracted. It was concluded that most data were from short term creep tests that had not reached the secondary creep stage, but graphical illustrations of this fact were not published. The temperatures of the studies ranged from 0 to 300 °C. The materials were usually annealed prior to testing. Nevertheless, modelling of the limited data was performed, and constitutive relations were identified. The average value of the Norton exponent n in the power law equation (Equation (4-1)) was found to be 2.5, and the activation energy for creep Q was 1.0×10^5 J/mol.

$$\dot{\varepsilon} = A_0 \exp(-\frac{Q}{RT})\sigma^n \qquad (4\text{-}1)$$

None of these results are consistent with the results of subsequent tests.

The first creep tests were performed on oxygen-free high-conductivity copper (Cu-OF) (Ivarsson and Österberg 1988, Ivarsson et al. 1989). The chemical composition was not reported but was most likely in accordance with the EN 1976 Cu-OF1 specifications. Base metal, weld metal, cross-weld and simulated HAZ) specimens were tested for electron beam welds. The best match for the real HAZ was found for a heat treatment at 800 °C for one hour, followed by air cooling. A total of 30 creep tests were conducted, and 29 of these ended with rupture. The standard 5K50-specimen with a gauge length and diameter of 50 mm and 5 mm, respectively, was used (Figure 3-1). The results of these tests can be found in Table A4-1 and Figure 4-1, and the Norton plot for the same results is presented in Figure 4-2.

It can be observed that the Norton exponents are in the 10–27 range, indicating a power-law break-down behaviour. The measured elongation values of the creep tests depended strongly on the applied stress, with higher ductility obtained for higher stresses (Figure 4-3). The simulated HAZ showed the lowest ductility values. Low elongation values of approximately 5 % were obtained at stresses below 100 MPa. The authors comment that a large variation in the creep response was observed for the different parts of the weld and the base metal.

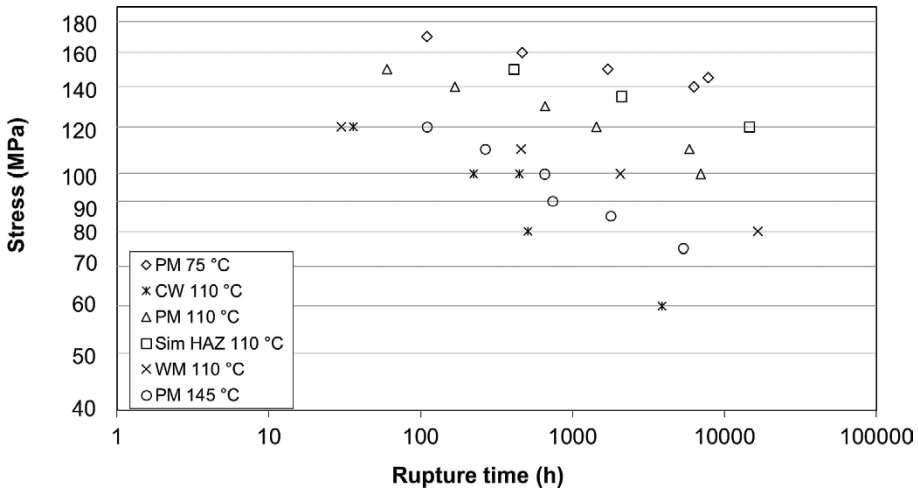

Figure 4-1. *Influence of applied stress on the creep rupture time for Cu-OF at 75 to 145 °C (Ivarsson and Österberg 1988). PM parent metal, CW cross weld, Sim HAZ simulated HAZ, WM weld metal.*

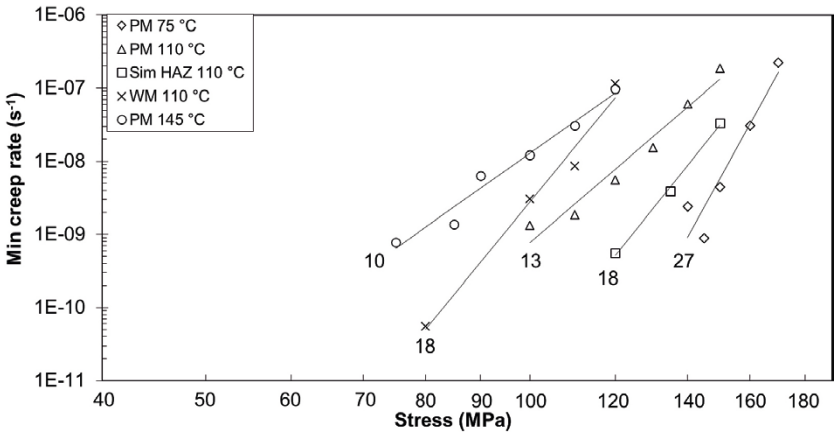

Figure 4-2. *Norton plot for Cu-OF at 75 to 145 °C (Ivarsson and Österberg 1988). The Norton exponents are marked in the graph.*

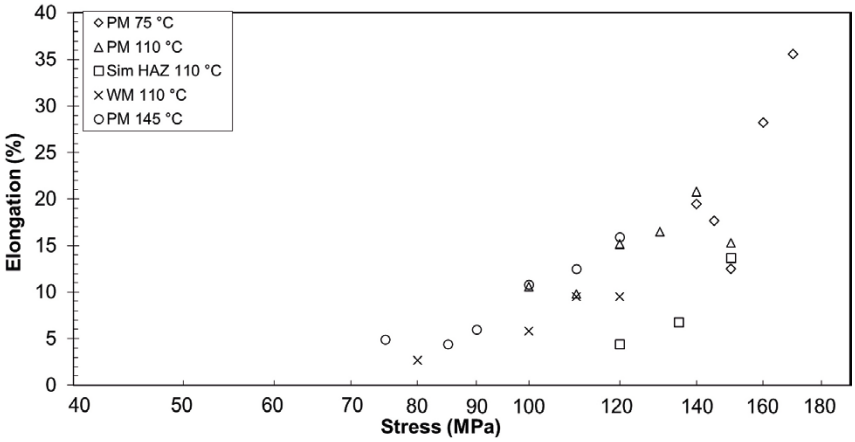

Figure 4-3. *Rupture elongation versus creep stress for Cu-OF at 75 to 145 °C (Ivarsson and Österberg 1988).*

In 1992–94, the results from the next series of creep tests on Cu-OF were published (Ivarsson and Österberg 1988). Oxygen-free copper was studied in the forged (000-series), extruded (200-series), and electron beam welded (100-series) states.

The results from the creep testing are given in Table A4-2 and Figure 4-4, and the Norton plot can be found in Figure 4-5. The extruded material had a significantly longer creep life than the forged material. The Norton exponents were between 4 and 7, which is in the power-law regime. The rupture elongation results are presented in Figure 4-6, and it is evident that the forged material shows almost no creep ductility. This has dramatic consequences because this makes Cu-OF unacceptable as a material for spent nuclear fuel canisters. The extruded material has a modest creep ductility of approximately 10 %.

In the discussion of the results, it is mentioned that the grain size affects the creep ductility of copper. The results from the published literature indicate that maximum ductility is obtained with a grain size of 50–100 μm, and the authors did not find any results that contradict these findings.

The effect of sulphur is also discussed, and it is stated that sulphur has a detrimental effect on the creep ductility. Auger microscopy showed that sulphur migrates to the grain boundaries and is found on the inside faces of cavities, possibly contributing to the formation of cavities.

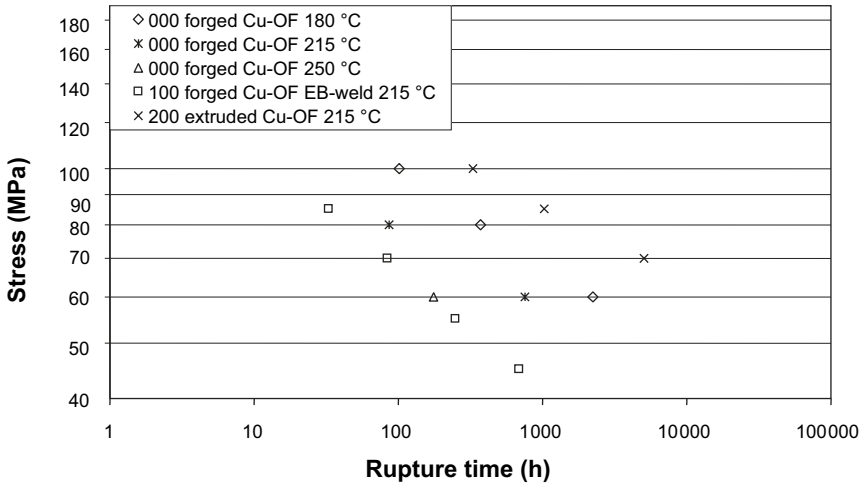

Figure 4-4. *Influence of applied stress on the creep rupture time for Cu-OF at 180 to 250 °C (Ivarsson and Österberg 1988).*

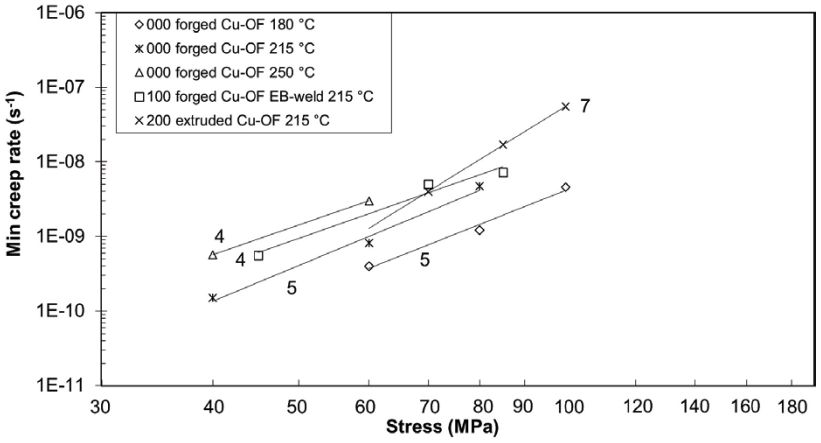

Figure 4-5. *Norton plot for Cu-OF at temperatures from 180 to 250 °C (Ivarsson and Österberg 1988). The Norton exponents calculated are marked in the graph.*

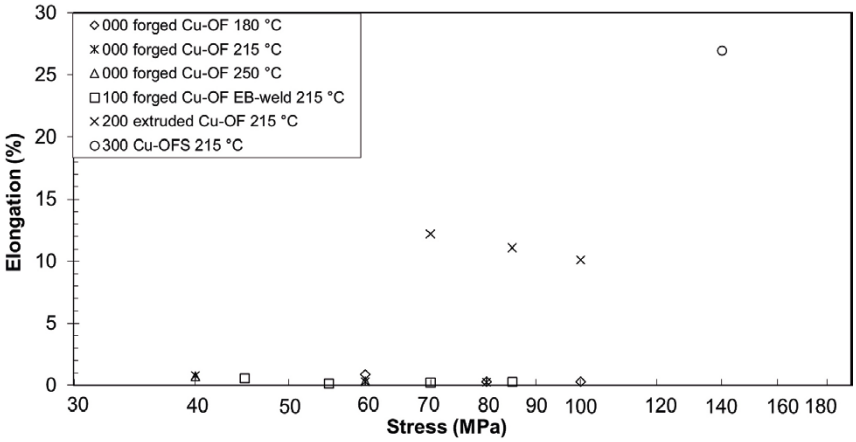

Figure 4-6. *Influence of creep stress on rupture elongation for Cu-OF at temperatures from 180 to 250 °C (Ivarsson and Österberg 1988).*

Raj and Langdon published the creep rate data for Cu-OF in 1989. The lowest test temperature was 350 °C. Thus, these results do not overlap with the results presented above. In Chapter 9.1, a model for the creep rate is applied to the different sets of data.

The 600-series electron beam welded (EB-welded) specimens were cut from a Cu-OF block and examined (*Seitisleam et al. 1995*, *Seitisleam and Henderson 1996*)[2]. All of the 600-series specimens were obtained from the weld metal and were taken either longitudinally along the weld or transverse through the weld depth. The results of the testing can be found in Table A4-4 and in Figure 4-7 and Figure 4-8, respectively. No significant difference could be measured for the longitudinal and transverse specimens, but compared to the previously tested materials, both the creep life and the ductility were considerably lower. In the same graphs, the results obtained in the testing of the catalytically deposited copper are presented (series 800). Neither the longitudinal nor the transverse direction signifies a special grain orientation as in the weld specimens, but rather, the specimens are taken in two different directions in the received slab. The results were quite poor, and no further testing was performed on the catalytically deposited copper.

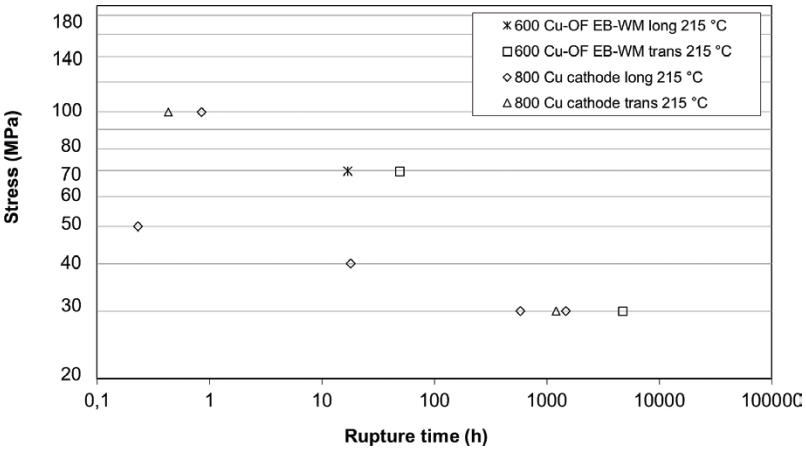

Figure 4-7. *Influence of applied stress on the creep rupture time for EB-welds and cathode deposits for Cu-OF (Seitisleam et al. 1995, Seitisleam and Henderson 1996).*

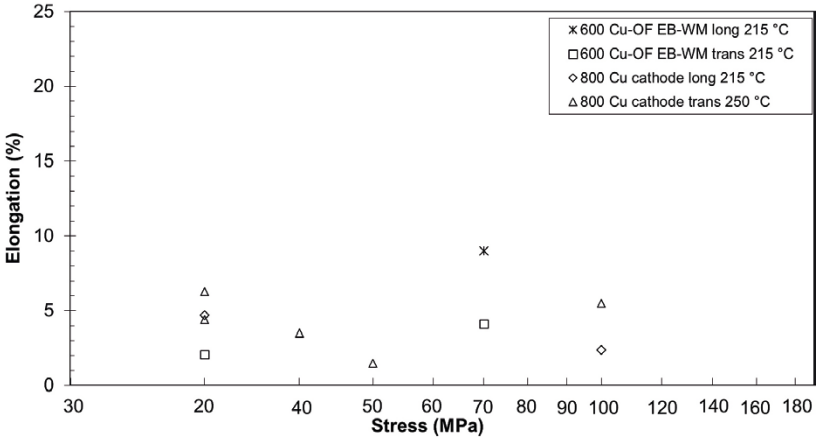

Figure 4-8. *Rupture elongation for EB-welds and cathode deposits for Cu-OF (Seitisleam et al. 1995, Seitisleam and Henderson 1996).*

[2] References given in *italics* do not meet SKB´s quality assurance requirements for public reports, see further Section 2.2. These references are presented in the Report list in Appendix 1.

As mentioned in Chapter 3.3, new active control creep test rigs were placed in operation in 2005–2007. These test rigs did not need to be reset by unloading the specimen, and furthermore, the load application rate could be kept at a very low value and was continuous with no stress increments. Several more Cu-OF specimens were tested in 2017 to evaluate whether the test procedure affected the obtained results. The results are given in Table A4-15 and Table 4-1. The Cu-OF testing results showed that the obtained values were similar to the previously measured values for both the rupture time and the ductility. A single Cu-OFP test was conducted at 215 °C using the same stress as that for the Cu-OF test, and this specimen exhibited much higher creep ductility and longer time to rupture. It was concluded from these tests that the test procedure was not a factor in the low ductility of Cu-OF measured in the initial creep studies.

Table 4-1. Creep testing of Cu-OF and Cu-OFP for the evaluation of the test procedure. From Danielsson and Andersson-Östling (2018). *Running.

Specimen	Temp. °C	Stress MPa	Rupture time h	Elongation H
Cu-OF01	215	85	175	0.81
Cu-OF03	175	85	1 495	1.26
Cu-OFP02	215	85	30 400*	

5 Creep of phosphorus-doped copper, Cu-OFP

5.1 High-temperature testing

Extensive creep testing on Cu-OFP was performed for two batches, named 400 and 500 (*Lindblom et al. 1995*)[3] The chemical compositions of the copper tested together with other batches are found in Table A2-1. The product forms used in these tests are summarised in Table A2-2. The material tested was extruded Cu-OFP, and the test temperatures varied from 200 to 450 °C. It was shown that the low creep ductility found for Cu-OF was not observed for in Cu-OFP. Figure 5-1 and Figure 5-2 show the results of the tests in graphical form, and the results are also tabulated in Table A4-3.

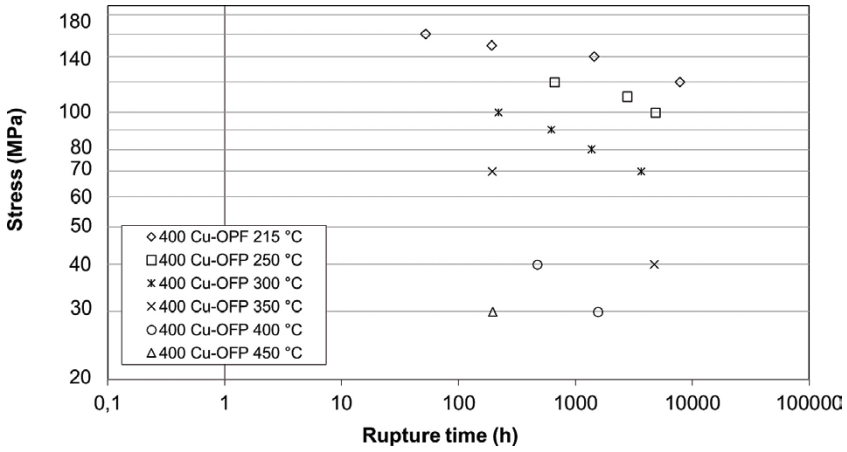

Figure 5-1. *Influence of applied stress on the creep rupture time for Cu-OFP (400 series) (Lindblom et al. 1995).*

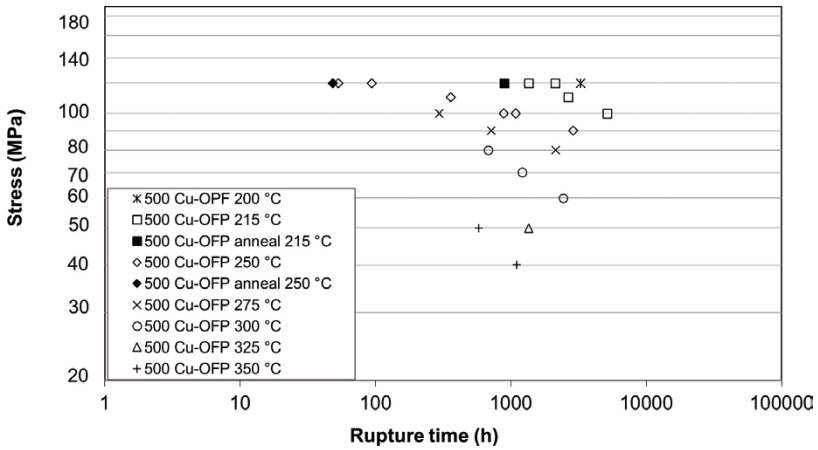

Figure 5-2. *Influence of applied stress on the creep rupture time for Cu-OFP (500 series) (Lindblom et al. 1995).*

[3] References given in *italics* do not meet SKB´s quality assurance requirements for public reports, see further Section 2.2. These references are presented in the Report list in Appendix 1.

The creep strength of Cu-OFP is much higher than that of Cu-OF (see Figure 4-4). The variation in strength between the 400 and 500 series is pronounced in spite of their similar compositions. It is noteworthy, that a strong dependence on temperature was observed for both series 400 and series 500. The Norton exponent falls between 5 and 17 for both series (Figure 5-3 and Figure 5-4).

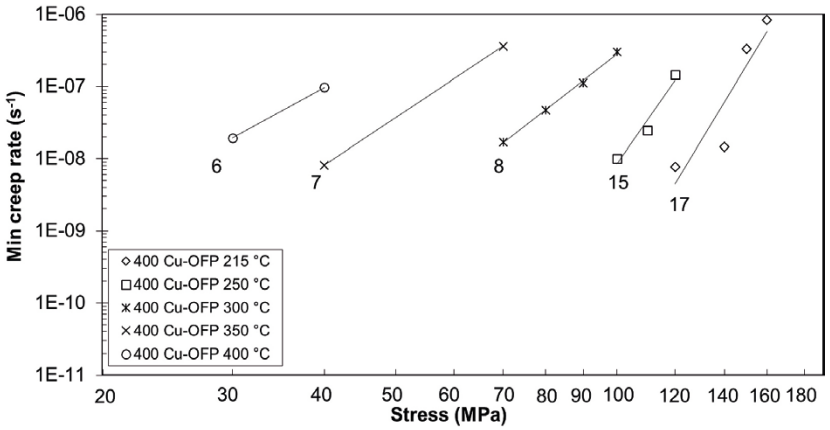

Figure 5-3. *Norton plot for the 400 creep test series (Cu-OFP) (Lindblom et al. 1995). The Norton exponents are marked in the graph.*

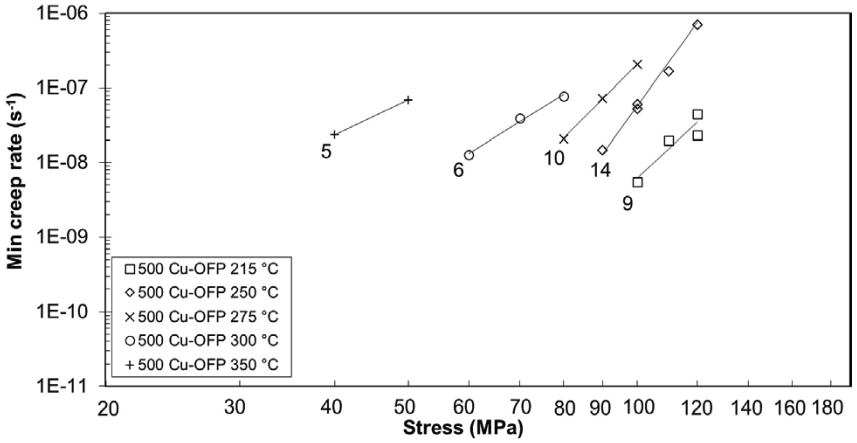

Figure 5-4. *Norton plot for the 500 creep test series (Cu-OFP) (Lindblom et al. 1995). The Norton exponents are marked in the graph.*

Low Norton exponents were obtained at higher temperatures, indicating that at temperatures over 300 °C, the creep mechanism is predominately power-law creep, while at lower temperatures, the creep shows increasingly stronger power-law breakdown behaviour. Creep ductility was found to be dependent on the applied stress for series 500 and to some extent for series 400, with higher ductility for higher stresses (Figure 5-5 and Figure 5-6). In all cases, the creep elongation was above 10 %. Below 300 °C, the creep elongation exceeded 30 %, which is highly satisfactory. For the 500 series, two specimens were annealed for 5 minutes at 600 °C and most likely were air cooled as well (*Seitisleam et al. 1995*). The annealed specimens displayed similar creep lives as the unannealed specimens, but show a marked increase in ductility (Figure 5-6). When examined metallographically, a slight increase in the grain size was found, but this is not considered to be sufficient to explain the higher ductility.

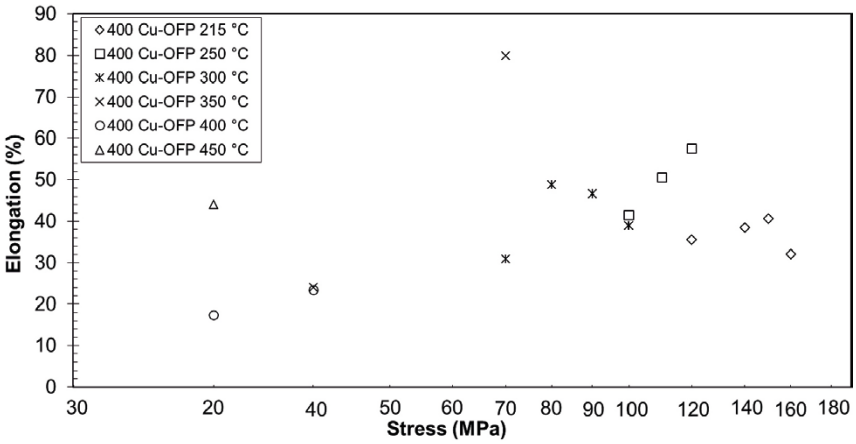

Figure 5-5. *Rupture elongation versus creep stress for the 400 creep test series (Cu-OFP) (Lindblom et al. 1995).*

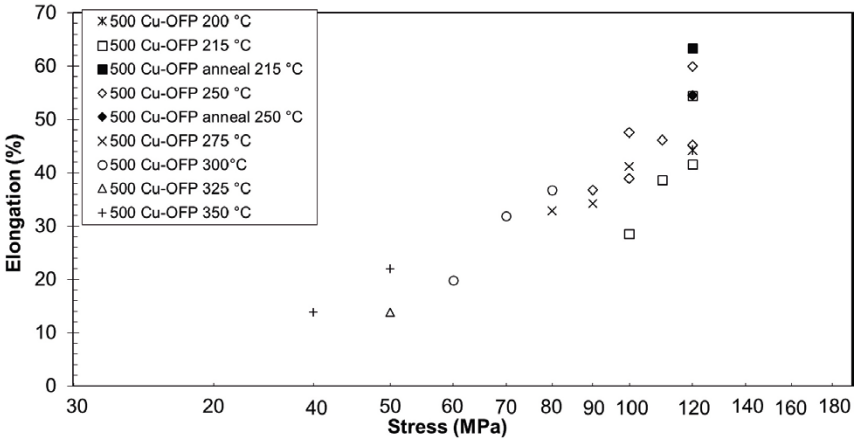

Figure 5-6. *Rupture elongation versus creep stress for the 500 creep test series (Cu-OFP) (Lindblom et al. 1995).*

Five specimens were tested at 600 °C (Figure 5-7). Two of these specimens ruptured, and the others were stopped before failure. The ductility measured for the ruptured specimens was between 10 and 15 % (Figure 5-8). The purpose of these tests (which were carried out at a very low stress) was to examine whether the creep deformation was diffusion controlled (Nabarro-Herring creep), as suggested by the Frost-Ashby deformation maps. However, the obtained creep exponents were 2–3, which rules out Nabarro-Herring creep, which is associated with a creep exponent of unity.

It was concluded from the work that the addition of 50 ppm phosphorus increased creep ductility from 0 to 10 % for Cu-OF to 30–50 % for Cu-OFP below 300 °C at longer testing times. The addition also significantly increased the creep life.

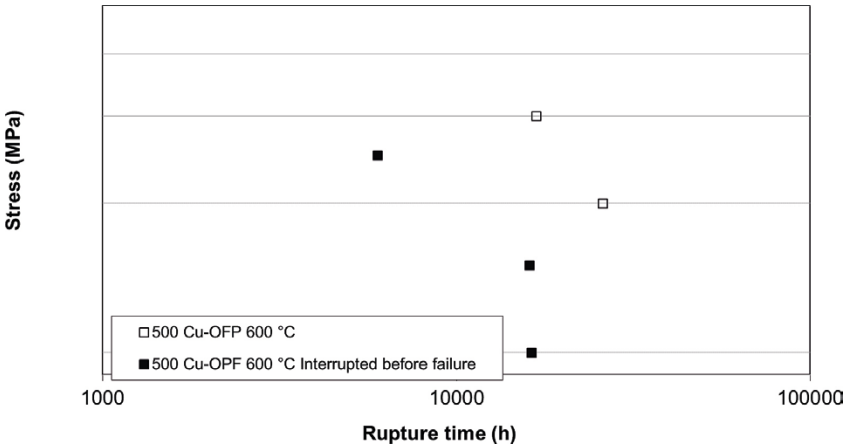

Figure 5-7. *Influence of applied stress on the creep rupture time for Cu-OFP tested at 600 °C (Lindblom et al. 1995).*

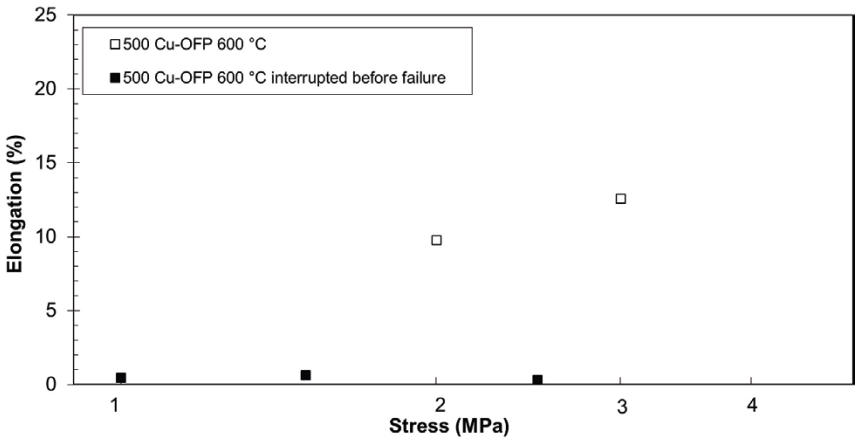

Figure 5-8. *Rupture elongation for the 500 creep test series tested at 600 °C (Lindblom et al. 1995).*

The 700 series is divided into two types of specimens referred to as the 700 and 720 series, where both series of specimens were electron beam welds made from OFP copper (*Seitisleam et al. 1995*, *Seitisleam and Henderson 1996*). In the 700 series, longitudinal and cross-weld specimens were tested. The cross-weld specimens were taken from different heights in the weld, as described in Table A4-4, but since no significant variation was measured, they are presented as one cross-weld series in Figure 5-9. The 720 series consisted of the specimens cut from a weld that was made to simulate a lid weld made from Cu-OFP. Longitudinal, transverse and cross-weld specimens were tested, and the obtained results overlap those obtained for the 700-series, with the transverse specimens exhibiting lower creep strength. Creep ductility was modest at lower stresses (Figure 5-10).

The dependence on the specimen size and annealing prior to testing was investigated in (*Henderson and Lindblom 1995*). Specimens with a 10 mm diameter were compared to the specimens with a diameter of 5 mm for both annealed and as-machined specimens. The annealing process was chosen as 5 min at 600 °C followed by a water quench. It was concluded that the annealed 5 mm specimens gave similar results to those obtained for the as-machined 10 mm specimens. The as-machined 5 mm specimens showed lower ductility measurements and longer creep lives. Tensile tests were affected in a similar manner. The lower ductility of the as-machined 5 mm specimens is attributed to cold working during the machining process.

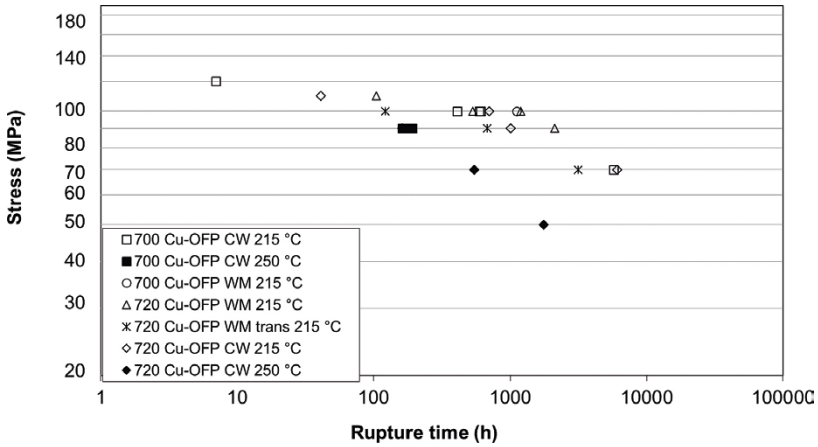

Figure 5-9. *Creep rupture time plotted against applied stress for the 700 and 720 creep test series (Seitisleam et al. 1995, Seitisleam and Henderson 1996).*

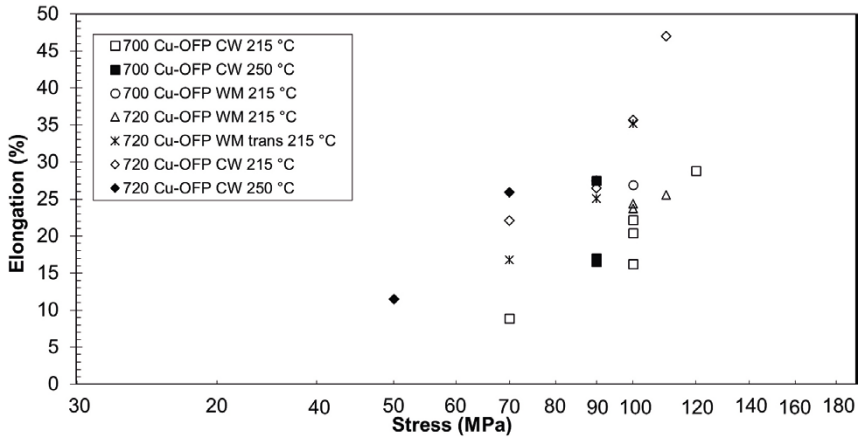

Figure 5-10. *Rupture elongation for the 700 and 720 creep test series (Seitisleam et al. 1995, Seitisleam and Henderson 1996).*

5.2 Influences of grain size and sulphur and phosphorus contents

A creep study was carried out for 20 mm extruded bars with different phosphorus and sulphur contents to evaluate the threshold level of these dopant elements for the effect on creep ductility (Andersson et al. 1999, 2001). The effect of grain size was also investigated. Phosphorus contents of 0 (P free), 30, 60, 65 and 105 ppm were studied. Six grain sizes of 300, 350, 450, 800 and 2 000 µm were investigated. With a single exception, all test series samples had a sulphur content of 6 ppm. The series of samples with 12 ppm S showed the same creep properties as the corresponding samples with 6 ppm S. All testing was performed at 175 °C, and the obtained results can be found in Table A4-5 and are presented in graphical form in Figure 5-11 and Figure 5-12.

As can be observed from the results, the obtained values generally overlap for all material conditions, with only two exceptions, the material without phosphorus and the material with the largest grain size. Both of these are outliers are due to their low creep ductility and short creep lives compared to those of the other materials (Figure 5-13). For the other series, the rupture elongation is approximately 30 % or higher. The creep exponent is approximately 45 (Figure 5-31).

It was concluded from these studies that very large grain sizes (> 800 µm) and phosphorus contents below 29 ppm should be avoided to prevent low ductility.

Subsequently, reassessments of the Cu-OFP results presented in Chapters 5.1 and 5.2 were performed by Sandström and Andersson (2008a, b), where extensive modelling of the results was also included.

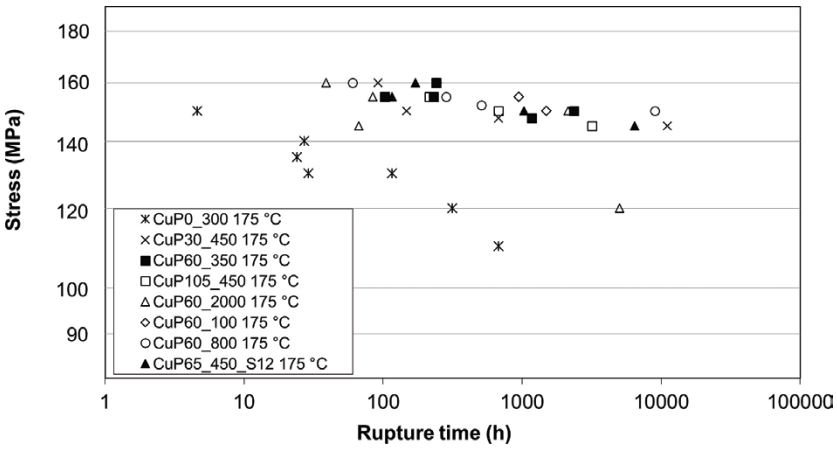

Figure 5-11. *Creep rupture time plotted against applied stress for various sulphur contents, phosphorus contents and grain sizes (Andersson et al. 1999, 2001). The identifier P65_450_S12 means that the sample had 65 ppm P, a grain size of 450 mm and 12 ppm S.*

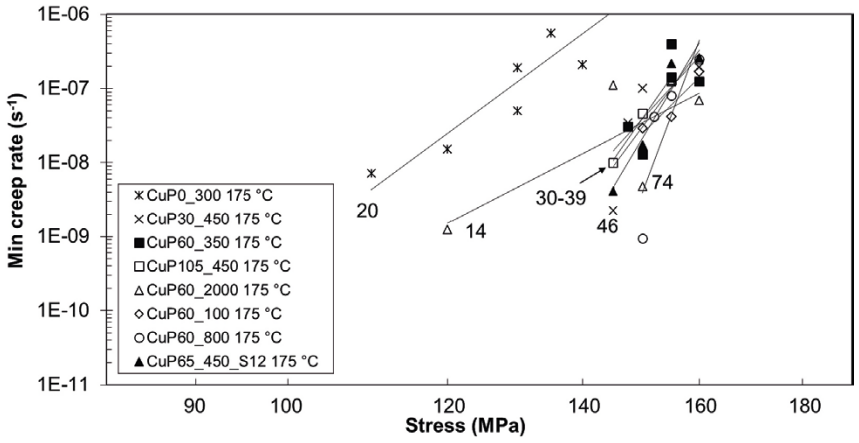

Figure 5-12. *Norton plot for the results in Figure 5-11 for samples with various sulphur contents, phosphorus contents and grain sizes (Andersson et al. 1999, 2001). The Norton exponents are marked in the graph.*

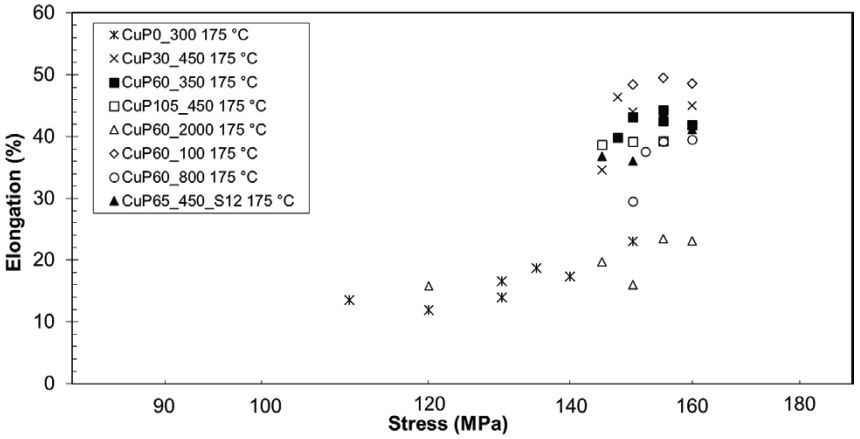

Figure 5-13. *Rupture elongation for the results in Figure 5-11 where the sulphur contents, phosphorus contents and grain sizes of the samples were varied (Andersson et al. 1999, 2001).*

5.3 Influence of phosphorus at 75 and 125 °C

In 2012, a new investigation into the effect of phosphorus on the creep properties of copper was carried out by Wu and Sandström (2015). This study concentrated on creep tests at lower temperatures of 75 and 125 °C. The phosphorus contents were 32–33 wtppm, 65–66 wtppm and 112–115 wtppm. The results of this study are given in Table A4-14. A plot of the obtained time to rupture versus applied stress is given in Figure 5-14. The ductility results are given in Figure 5-15, and the Norton plot is shown in Figure 5-16. The results do not have the optimal quality because the laboratory was moved during the testing of some of the specimens. This means that the testing of some of the specimens was interrupted, and thus, it was not possible to fully evaluate these specimens.

Nevertheless, the overall finding of the study was that variation in the phosphorus content did not significantly affect the creep results. A small decrease in the ductility was measured for the high phosphorus content specimens, and these specimens also displayed a slightly longer creep life. While this may be a material property, the report states that the most likely reason for these results is a test control malfunction leading to a slight stress overload during the testing.

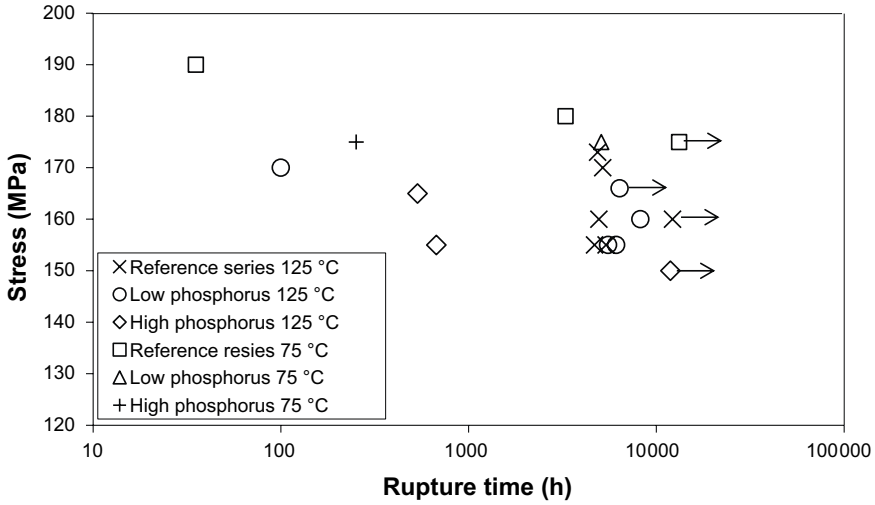

Figure 5-14. *Creep rupture time plotted against applied stress for the Cu-OFP creep tests study of samples with different phosphorus contents (Wu and Sandström 2015).*

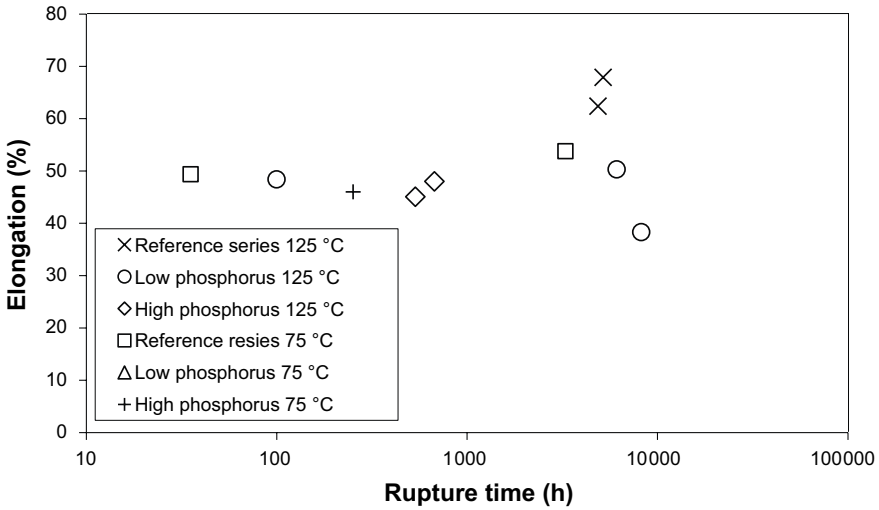

Figure 5-15. *Creep ductility plotted against applied stress for the Cu-OFP creep tests study of samples with different phosphorus contents (Wu and Sandström 2015).*

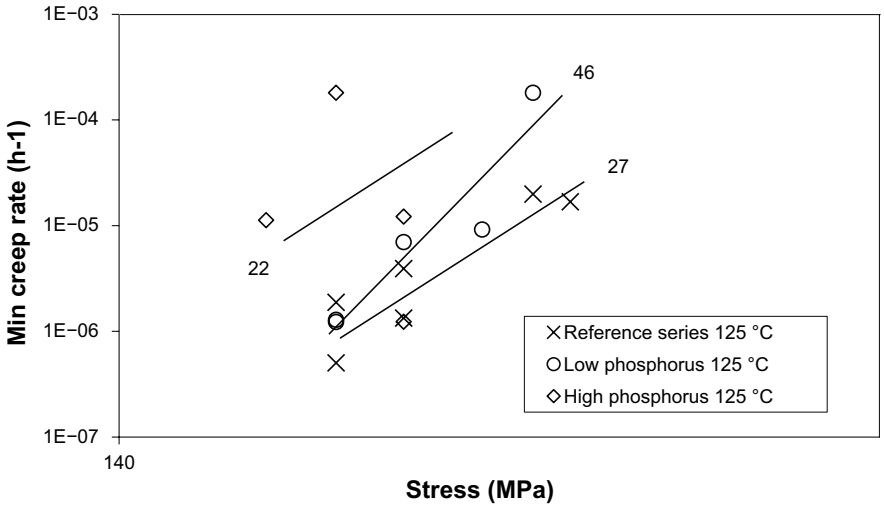

Figure 5-16. *Norton plot for the Cu-OFP creep tests study of samples with different phosphorus contents. Only the results for the specimens tested at 125 °C are included (Wu and Sandström 2015).*

5.4 Grain size effect on creep of Cu-OFP

During manufacturing of the copper tubes for the repository, non-destructive testing (NDT) is used throughout the process to verify that the grain size and other material properties are maintained within the required limits. Ultrasonic inspection is used as the NDT process. A higher sound attenuation in ultrasonic inspection is likely due to a difference in the grain size. Therefore, creep tests were performed on copper samples that exhibited differences in sound attenuation (Mannesson and Andersson-Östling 2014a). The grain size was also studied metallographically and varied from 96 µm to 242 µm. The results from the creep tests are presented in A4-12 and are shown in graphical form in Figure 5-17 to Figure 5-20. It should be noted that while creep ductility appears to be somewhat lower than that found in previous studies, this is not in fact the case. These tests were conducted in the new active test rigs, and since the machine at the time did not allow the specimen to rupture, all of the tests were interrupted within 10 minutes of the final fracture. Thus, the necking process was also interrupted, and the measured values are slightly lower than what they would have been if the specimen had been allowed to rupture.

It was concluded from this project that there is no significant difference in the creep properties for these grain sizes and by extension for the differences in sound attenuation. The small observed difference was attributed to different degrees of cold working in the material prior to testing. No annealing step had been applied prior to testing since this could have affected the grain size and distribution of the sample.

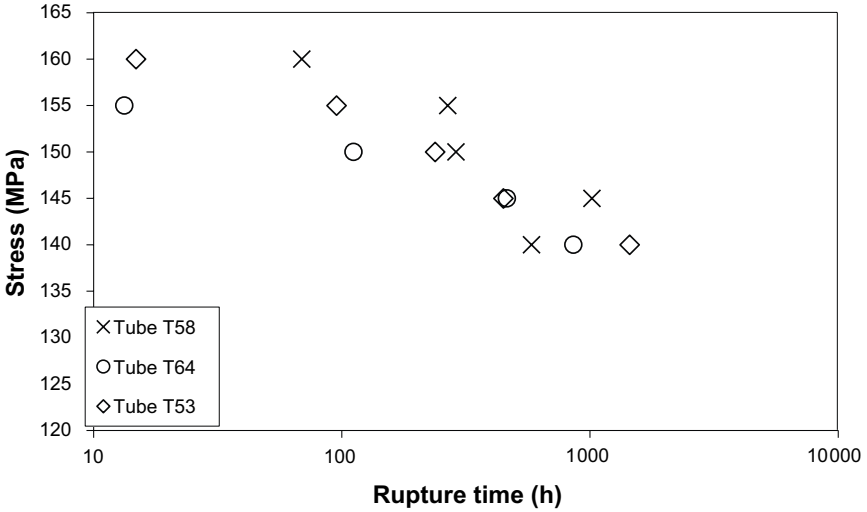

Figure 5-17. *Creep rupture time plotted against applied stress for the different sound attenuation samples studied for Cu-OFP (Mannesson and Andersson-Östling 2014a).*

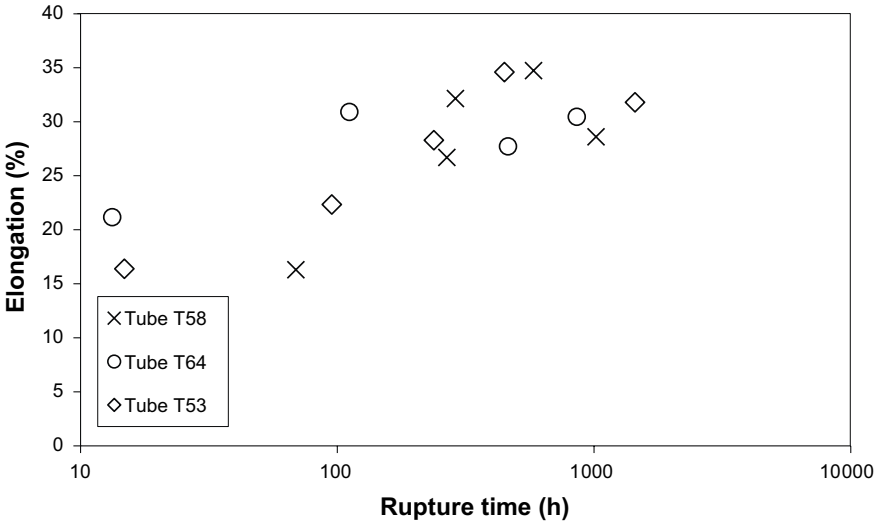

Figure 5-18. *Creep elongation plotted against applied stress for the different sound attenuation samples studied for Cu-OFP (Mannesson and Andersson-Östling 2014a).*

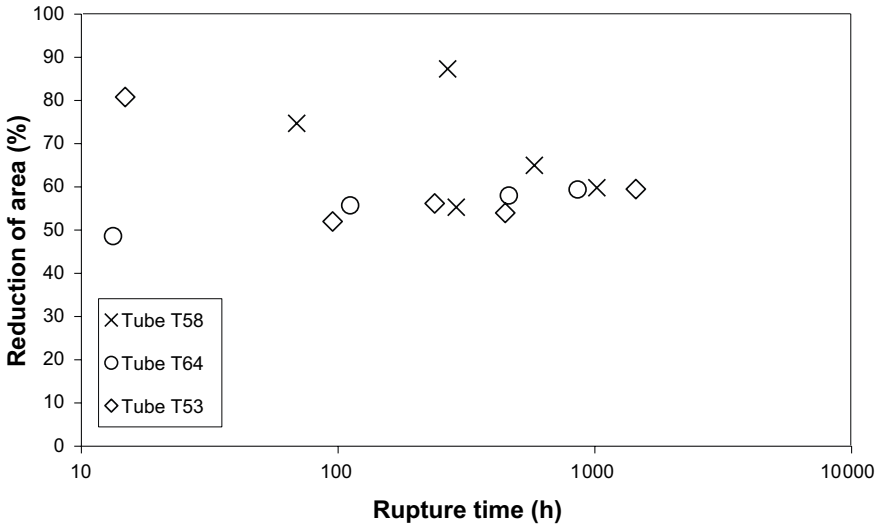

Figure 5-19. *Creep reduction of area plotted against applied stress for the different sound attenuation samples studied for Cu-OFP (Mannesson and Andersson-Östling 2014a).*

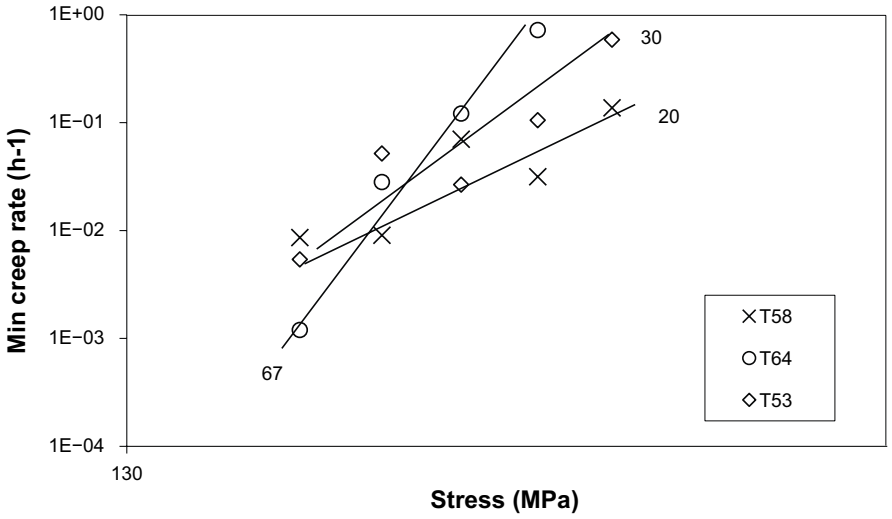

Figure 5-20. *Norton plot for the different sound attenuation samples studied for Cu-OFP (Mannesson and Andersson-Östling 2014a).*

5.5 Loading rate effect on creep

One of the goals in the development of the new active creep test rigs was to obtain a test machine that could load the specimens from unloaded to fully loaded in times longer than 2–5 minutes. The creep testing standard states that the load should be applied as quickly as possible and without mechanical shock. While this is sufficient for most metals, since copper canisters are subjected to an increasing pressure over a significant amount of time, this requirement is not applicable to copper creep tests. The application of the load in the repository depends on the ingress of water and the subsequent saturation of the bentonite clay. This process can take several years or longer depending on the amount of water present in the surrounding bedrock.

An investigation was therefore started in 2006 as a part of the larger study on the friction stir welds in copper (Andersson et al. 2007). In this study, loading times ranging from 2 minutes to 482 hours were studied for the specimens that were otherwise similar with respect to the applied load and temperature. The main result obtained in this study was that while the initial loading strain varied, neither the creep life nor the total elongation of the specimen showed any variation.

In 2010, a more comprehensive study on the effect of the loading rate on the creep of copper was conducted (Andersson-Östling and Sandström 2011). In this study, the loading time was increased significantly with the longest time of 4 320 h or six months. The load was applied in a continuous linear manner without steps or interruptions. The results from these creep tests are given in Table A4-9. Unfortunately, several of the tests had to be interrupted since they slowed to a barely detectable creep and would have progressed for several years longer than the duration of the project. The results are also given in graphical form in Figure 5-21 and Figure 5-22. Figure 5-23 shows the measured strain values both for the loading strain and for the total strain (loading strain + creep strain = total strain or elongation).

The main finding of this study was that the total strain stayed roughly the same for all loading times, while a longer loading time gave a higher loading strain at the expense of the creep strain. This is not surprising since a specimen with a long loading time experiences high stresses for a significant time prior to the full load being achieved. Therefore, the strain experienced by the sample prior to the full load is a mixture of loading and creep strain. The total strain remains constant, meaning that the total strain potential in copper remains unchanged, and only the application of the load and the time period of the load application determine whether the strain is a loading strain or a creep strain.

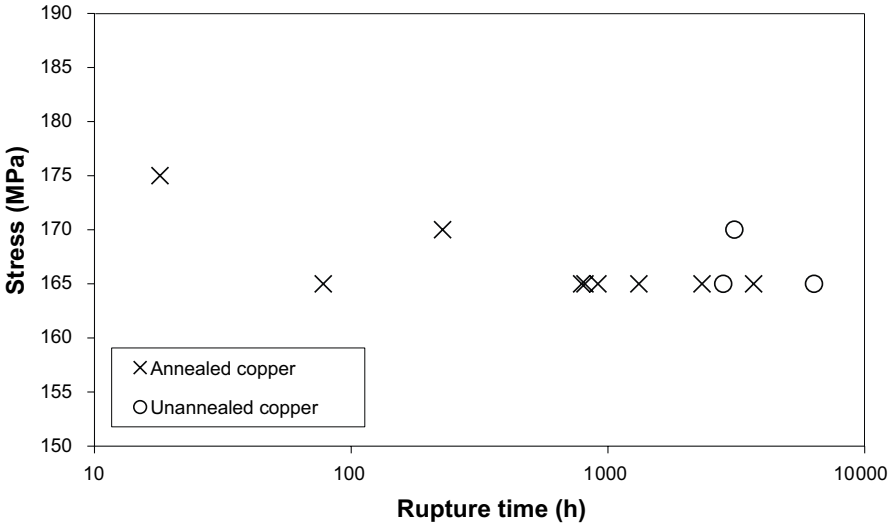

Figure 5-21. *Time to rupture plotted versus applied stress for the tests with varying loading times. In this graph, the time to rupture is the creep time without the loading time (Andersson-Östling and Sandström 2011).*

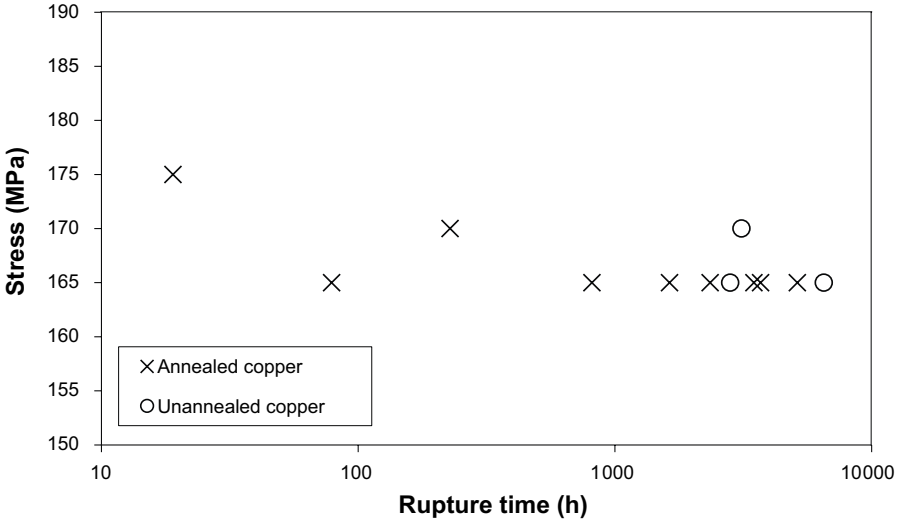

Figure 5-22. *Time to rupture plotted versus applied stress for the tests with varying loading times. In this graph, the rupture time is the time to rupture including the loading time (Andersson-Östling and Sandström 2011).*

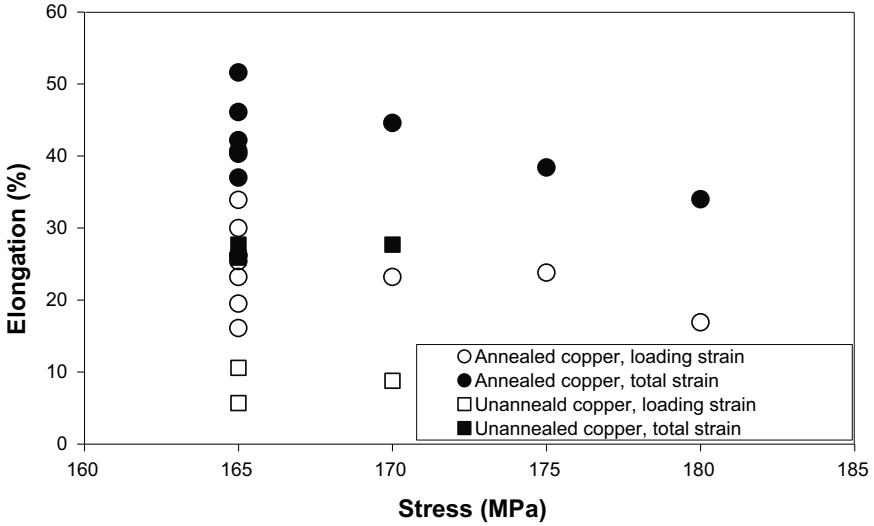

Figure 5-23. *The strain measured on the specimens during loading and after competed testing (Andersson-Östling and Sandström 2011).*

In 2014, a further study on the effect of the loading time on the creep properties was published (Mannesson and Andersson-Östling 2016). In this study, the specimen was slowly loaded but with hold steps at 80 %, 90 % and 100 % of the full load. The hold times were 168 and 1 000 hours in the creep test series. The results of these tests can be found in Table A4-11 and are presented in graphical form in Figure 5-24, Figure 5-25, Figure 5-26 and Figure 5-27. It is evident from an examination of the results that a stepwise loading is detrimental to the creep life, with a stronger effect obtained for longer hold steps. The total ductility is high for all tests. However, as in other investigations for which the new active control test rigs were used, the observed values were low since the specimens were all interrupted immediately prior to the final fracture. It was concluded from this investigation that the hold time decreases the creep life, while the load stages after the hold times give rise to a renewed primary creep stage in the creep curve. This is somewhat counterintuitive, and the development of the subgrain structure is the origin of this effect. However, a complete explanation was not found, and future studies were recommended.

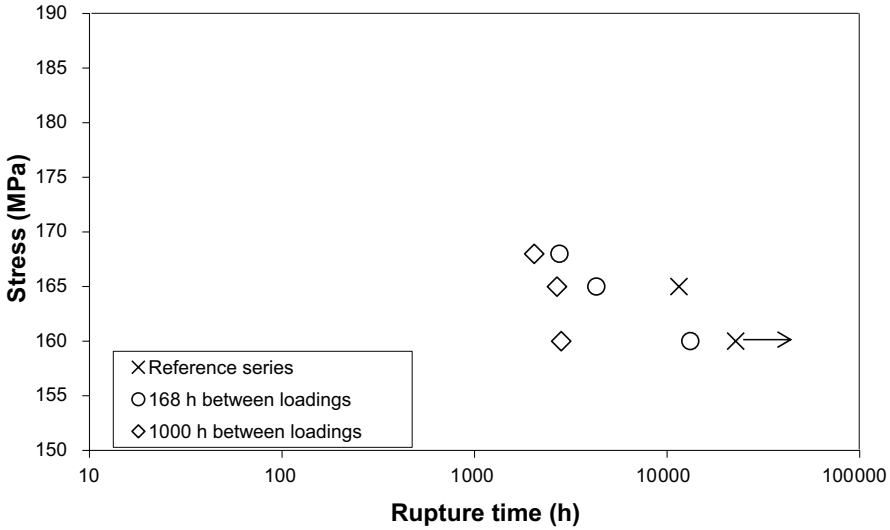

Figure 5-24. *Time to rupture against applied stress for the tests with varying loading times. In this graph, the time to rupture is the creep time including the loading time (Mannesson and Andersson-Östling 2016).*

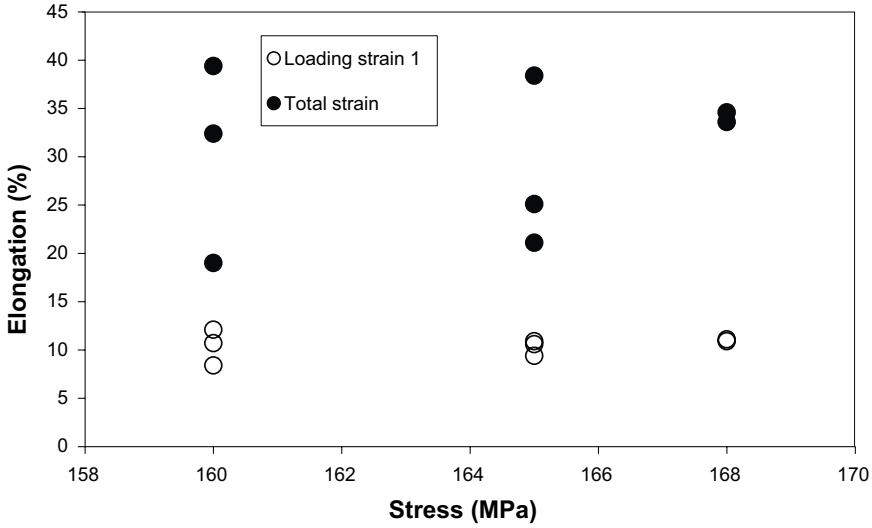

Figure 5-25. *The strain measured on the specimens during loading and after competed testing. Loading strain 1 is the initial loading strain, and the subsequent hold time strains and loading strains are included in the total strain (Mannesson and Andersson-Östling 2016).*

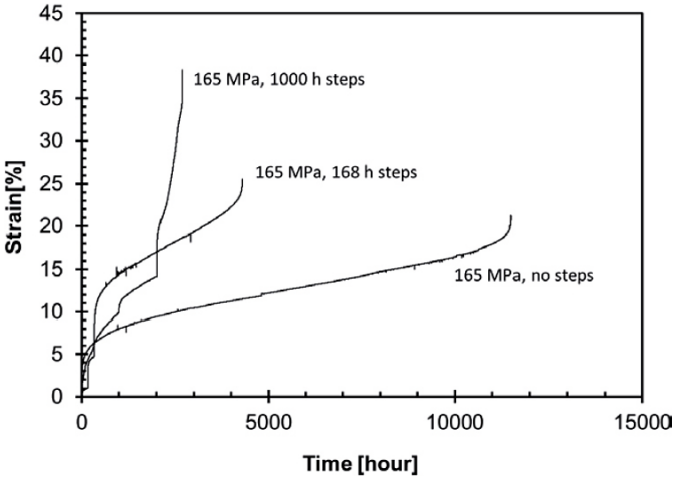

Figure 5-26. *Creep curves from the tests performed at 165 MPa and different loading steps (Mannesson and Andersson-Östling 2016).*

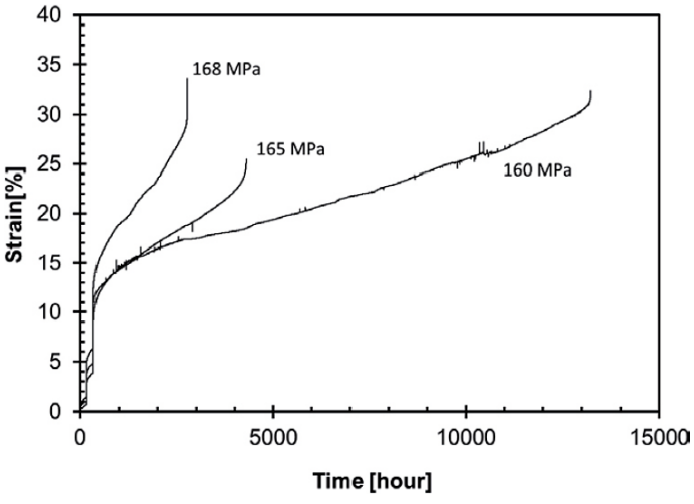

Figure 5-27. *Creep curves from the tests performed using 168 h steps at different stresses (Mannesson and Andersson-Östling 2016).*

5.6 Creep crack growth studies on Cu-OFP

Preliminary studies of the creep crack propagation (or growth, CCG) properties of Cu-OFP were performed in 1995 (*Henderson and Seitisleam 1995*, *Seitisleam and Henderson 1996*). In these studies, no crack propagation could be measured. This was mainly due to the high electrical conductivity of copper, which meant that potential drop measurements did not give sufficient resolution of any crack propagation. The specimen type and size used was compact tension with a characteristic size of 25 mm (CT-25).

New experiments were conducted in 2005 without any change in the results (*Andersson 2005*). This was despite the rapid development of the potential drop measurement methods in the intervening years. The specimen was still CT-25.

A larger study was initiated in 2010 where larger-sized specimens, CT-50, were used with even more developed measurement methods (Wu et al. 2011, Wu et al. 2013). A schematic drawing of the specimen is given in Figure 5-28. The specimens were extracted from bulk material. In these measurements, the potential drop signal was sufficiently clear to resolve the changes. Tests were conducted at 22, 75, 175 and 215 °C. An example of the resulting creep crack growth curves is given in Figure 5-29. It was concluded that some crack propagation could be observed at the higher temperatures (175 and 215 °C), but the results from the lower-temperature measurements were ambiguous. At the higher temperatures, crack propagation up to 10 mm was measured prior to the rapid final fracture. At the lower temperatures, the specimen deformed so much that the potential drop signal showed crack growth, but when the specimen was observed, it was found that this was most likely due to the deformation of the specimen in the crack propagation plane.

The main conclusion from the study is that the specimens tested at the lower temperatures do not show any brittle tendencies.

In 2017, a study examining the fracture surfaces from previous creep crack growth specimens and ruptured uniaxial specimens was carried out (Björkblad and Faleskog 2018). The examinations were performed using both light optical microscopy and scanning electron microscopy.

The main finding from this study was that at temperatures up to 75–125 °C, any flaw that develops into a crack will immediately blunt and disperse the stress concentration. The authors also found metallographical evidence for this effect in the similarity of the rupture surfaces in CCG and in uniaxial specimens from the tests that had resulted in large elongations.

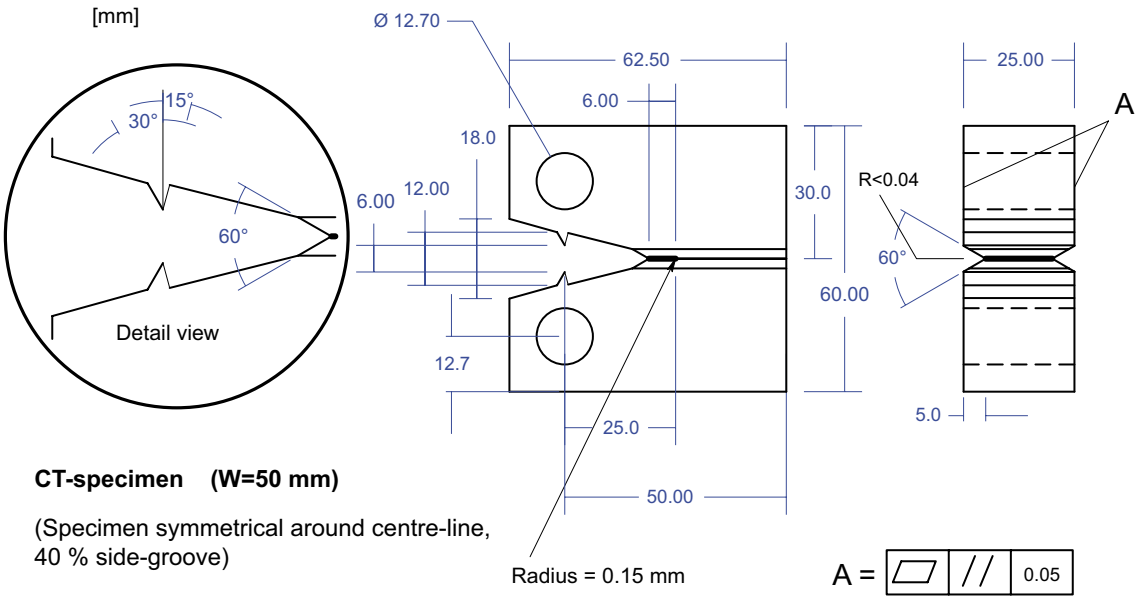

Figure 5-28. *Compact tension specimen with the characteristic size shown as W = 50 mm (CT-50) (Wu et al.2011).*

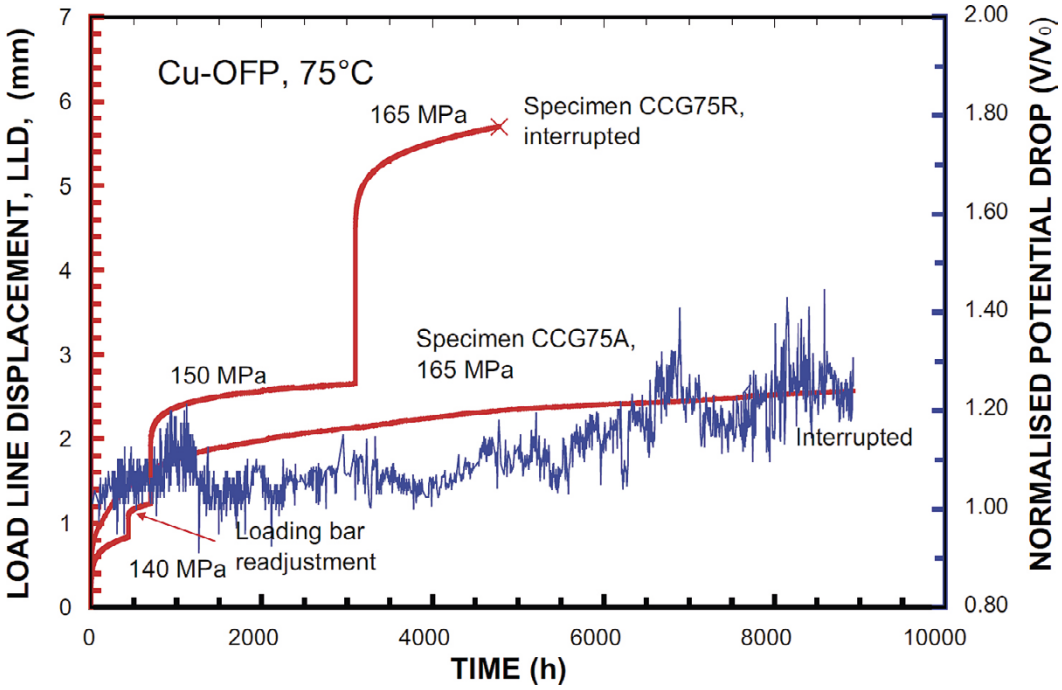

Figure 5-29. *Load line displacement (continuous line) and normalised potential drop signal (undulating line) as function of time for a test conducted at 75 °C (Wu et al. 2011).*

5.7 Multiaxial creep studies on Cu-OFP

In laboratory tests, uniaxial creep test specimens are most often used to obtain material characteristics and data. In a real-life situation, this does not provide the best representation of the situation. For most cases, loading can be decomposed into main stresses and strains, but several stress directions are often active at the same time. This is especially important in the case of crack formation, and both crack growth specimens (as used in creep crack growth studies) and multiaxial notched specimens are used to study the interaction of stresses. In 2009, a study was performed on Cu-OFP using notched specimens (Wu et al. 2009). In this study, several different aspect ratios notches were tested and compared to uniaxial results. The results from the study are given in Table A5-2 and in Figure 5-30.

The main finding from the study is that the investigated Cu-OFP is notch insensitive at 75 °C and that at this temperature, a sharper notch corresponds to a longer creep lifetime. The most likely interpretation of this result is that the sharp notches give rise to more localised strain and therefore greater strain hardening. The bluntest notches are most similar to a cylindrical uniaxial test, and the lifetime is similar. The sharpest notches exhibit more than 10^4 times the lifetime of the bluntest notches. A comprehensive finite element study is included in the report to better understand this phenomenon. It should also be mentioned that if effective stress is used for comparison rather than net section stress (as was used in the current study), the conclusion may be different, as some researchers have found in unpublished investigations.

In conclusion, in both creep crack growth studies and in multiaxial creep test studies, the homogenous Cu-OFP material was shown to be resistant to cracking in laboratory air at 75 °C. All of the formed cracks immediately become blunt and dissipate the stress concentration.

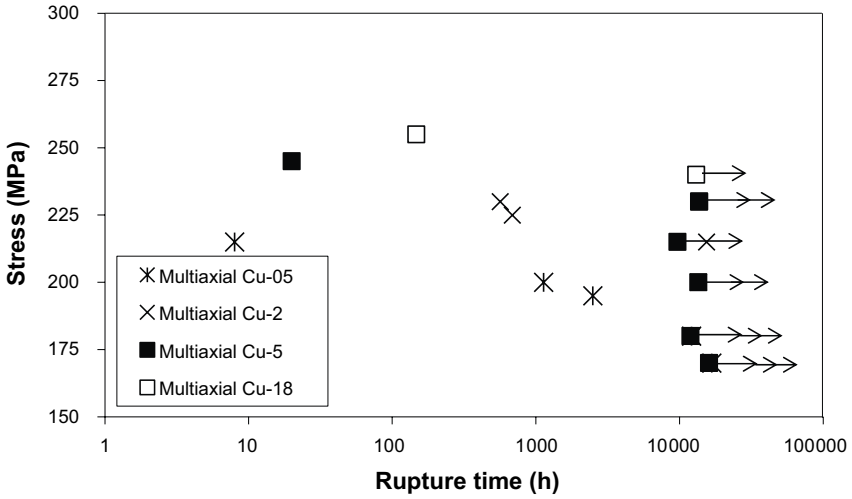

Figure 5-30. *Time to rupture versus applied stress for the multiaxial creep test specimens (Wu et al. 2009).*

5.8 Hydrogen content and creep of Cu-OFP

It is considered that in the repository, hydrogen gas can develop at the copper surface under certain conditions. For example, if water is trapped within the fuel rods, the water will eventually corrode the cast iron insert, and hydrogen gas will develop. This gas will be available for intrusion into both the cast iron and the copper. Therefore, several investigations have been carried out to study the penetration of hydrogen gas into copper and the creep properties of high-hydrogen Cu-OFP.

The first study was performed in 2012, when Cu-OFP blanks were subjected to hydrogen charging (Martinsson and Sandström 2012, later published as Martinsson et al. 2013). Thermal charging was avoided since the high temperatures associated such charging would promote grain growth, and electrochemical charging was used instead. Thin rod specimens with a diameter of 5 mm were used, and the depth of penetration was found to be approximately 50 µm for reasonable charging times. The bulk content was unaffected. In the affected surface layer, the hydrogen content was measurably increased, as evidenced by the hydrogen bubbles that formed close to the surface. These bubbles, which could be seen to contain gas at a high overpressure, were observed throughout the surface layer to the penetration depth. They were thought to most likely contain recombined hydrogen molecules because the penetration of hydrogen is carried out by individual hydrogen atoms rather than hydrogen molecules.

It should be mentioned here that it is known that hydrogen embrittles copper by the penetration of hydrogen, which forms water molecules by combining with oxygen in the material if oxygen is present, for example, in the form of oxides. Since the studied material is an oxygen-free copper, this embrittlement process cannot occur. Instead, individual hydrogen atoms traverse the copper until they reach an accumulation site such as a grain boundary, stacking faults and vacancies where they become trapped (Korzhavyi and Sandström 2014). When several atoms are accumulated at a single site, they recombine, and the resulting hydrogen gas bubble then functions as a trap for further hydrogen atoms and thereby grows in size. However, it should also be mentioned that if the oxygen-free copper has been friction stir welded, oxide particles will be present in the copper that can contribute to hydrogen embrittlement. The studied material had not been welded.

In 2014, a follow-up study was performed for the creep specimen with in situ charging during creep testing (*Leijon and Ahlström 2014*, followed by Leijon et al. 2018 with additional reference tests included). The work was partially inspired by publications by a Finnish research group reported two years earlier (Yagodzinsky et al. 2012). The Finnish group results showed cracking in the presence of hydrogen charging of copper under creep loads. In the study by Leijon et al. (2018), no cracks were found at the same stress and temperature as those used in the Finnish group experiments, but when the stress was increased, some structures appeared (Table 5-1). Whether these cracks had the same origin as those found by Yagodzinsky et al. is unknown. The cracks also were predominately formed at grain boundaries, and gas bubbles were observed ahead of the crack in the grain boundary.

In addition to the hydrogen charging studies performed on copper, similar studies were performed on nodular cast iron. These have been reported in Wu et al. (2015b).

Table 5-1. Test matrix with test parameters and amount of charged hydrogen in wt-ppm (Leijon et al. 2018).

Specimen	Temp.	Creep stress	Creep time	Hydrogen charging time	Pre-strain	Hydrogen avg.	Approx. crack
	degC	MPa	h	h	%	wtppm	µm
H-Creep-01	RT	140	92.5	95.5	0	3.8	0
H-Creep-02	RT	140	92	95	0	7.9	0
H-Creep-03	RT	140	100	103	0	7.9	0
H-Creep-04	50	185	3.3	16.7	0	1.6	0
H-Creep-05	RT	170	1 005.7	1 008.7	0	8.5	100
H-Creep-06	50	172	113.0	116.0	0	7.7	100
H-Creep-07	RT	175	94.6	97.6	10	3.8	0
H-Creep-08	50	172	114.5	117.5	10	8.0	30
H-Creep-09	50	172	168.5	171.5	20	4.8	20
H-Creep-10	75	172	168.8	171.8	20	9.2	20
H-Creep-11	75	176	97.9	100.9	10	9.0	30
H-Creep-12	RT	176	257.3	260.3	20	6.1	0
H-Creep-13	75	176	13.4	16.4	0	Measurement failed	
H-Creep_14	50	172	120	0	10	2.0	0
H-Creep_15	50	172	167	0	0	1.8	0
H-Creep_16	75	172	20	0	20	1.0	0

5.9 Electron beam and friction stir welds

For the studies described above, all testing was performed on electron beam welds and the base material. In the studies described below, friction stir welds (FSW) were included as well (Andersson et al. 2004, 2005). The creep test results are given in Table A4-6 and are presented in graphical form in Figure 5-31 to Figure 5-36.

All of the tests in this work show ductility values greater than 20 %, but the appearance of the specimens varied. The electron beam welds exhibit sufficient ductility, but the deformation is localised to the narrow weld metal, where the ductility is much higher locally. By contrast, the friction stir welds strain evenly over the whole gauge length, and necking appears in the middle of the specimen only in the last stage of the creep test. During service, such even creep deformation should provide better protection against cracking. The FSW welds show a creep ductility of 30 % or higher, which is quite satisfactory.

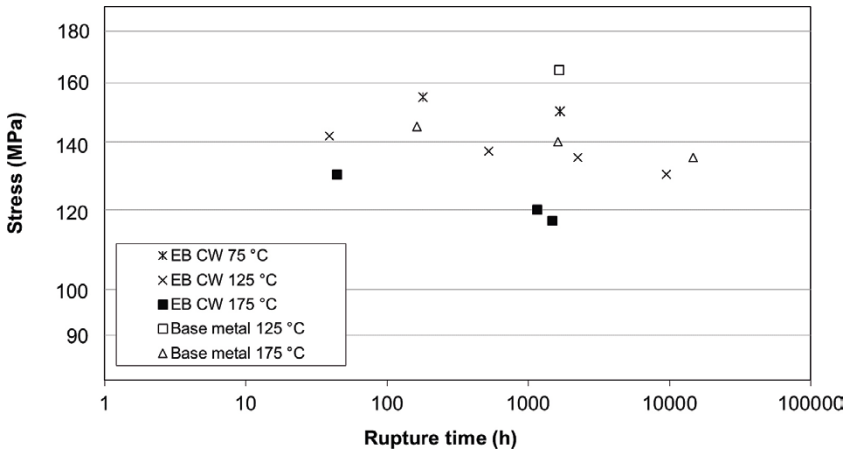

Figure 5-31. *Creep rupture time plotted against applied stress for base metal and electron beam weld specimens (Andersson et al. 2004, 2005).*

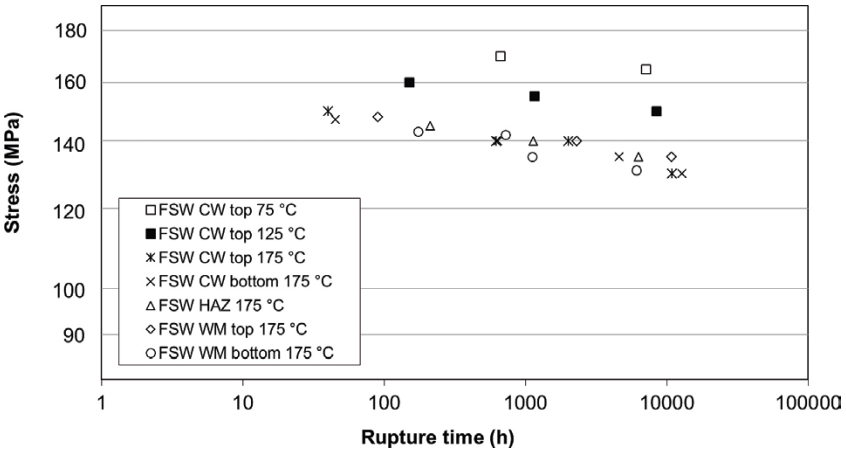

Figure 5-32. *Creep rupture time plotted against applied stress for friction stir weld specimens (Andersson et al. 2004, 2005).*

In addition, the electron beam welds have an average grain size of 2 000 µm compared to the 75 µm for the weld metal from the friction stir welds. If the low temperature is taken into account, the Petch-Hall effect contributes approximately 15 MPa to the strength of the weld, which is on the same order of magnitude as the difference in the rupture strength. Previous testing has also shown that large grain sizes are detrimental to the creep strength (Andersson et al. 1999).

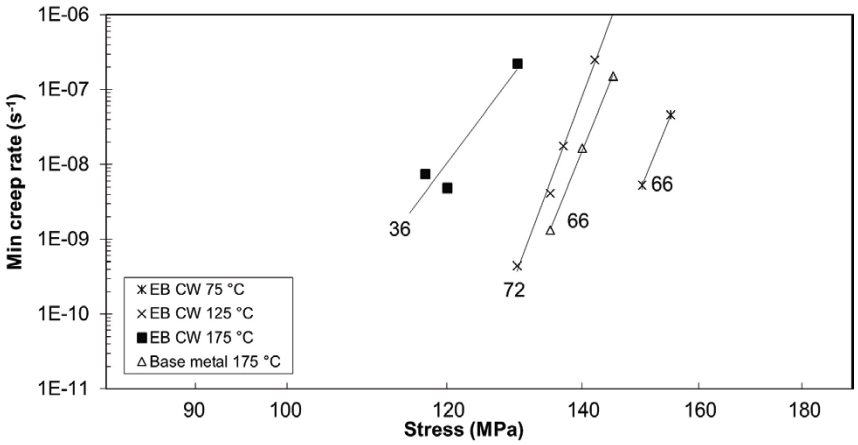

Figure 5-33. *Norton plot for electron beam welds. A comparison with the parent metal is made (Andersson et al. 2004, 2005). The Norton exponents are marked in the graph.*

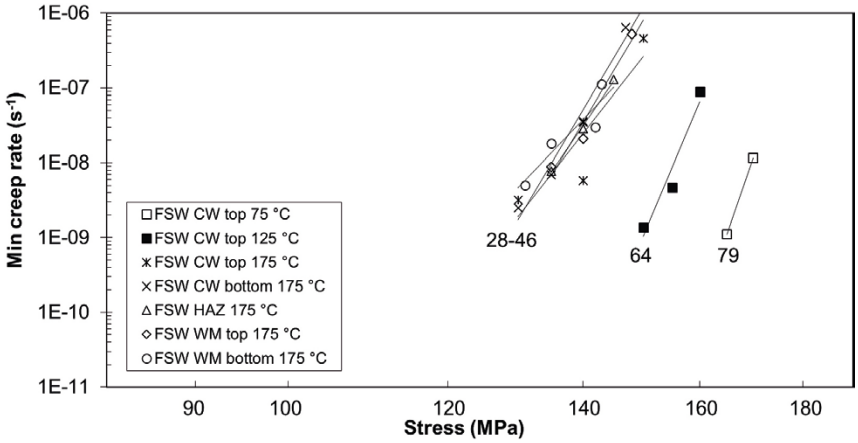

Figure 5-34. *Norton plot for friction stir weld specimens (Andersson et al. 2004, 2005). The Norton exponents are marked in the graph.*

To conclude, the results of this work show that friction stir welds are more suitable than electron beam welds for the canister weld, and the properties of the friction stir welds are adequate for this application.

In 2005, friction stir welding was chosen as the preferred welding method. By contrast, the previous study had used hot rolled plates, which had been rolled as the material in which the welds were performed. Since the extruded material was much more likely to be used as a canister material, a new project was initiated to study the creep response of thick wall FSW welds in extruded tubes. By this time, SKB had also accumulated experience in using the FSW welding machine at the Oskarshamn canister laboratory, and a real weld was used to extract the tested specimens (Andersson et al. 2007).

The specimen extraction diagram for the FSW welds has been presented in Figure 3-2, and base metal samples both from the lid and from the tube was tested along with the weld metal, HAZ and cross-weld specimens. For the EB welds, only cross-weld specimens were tested.

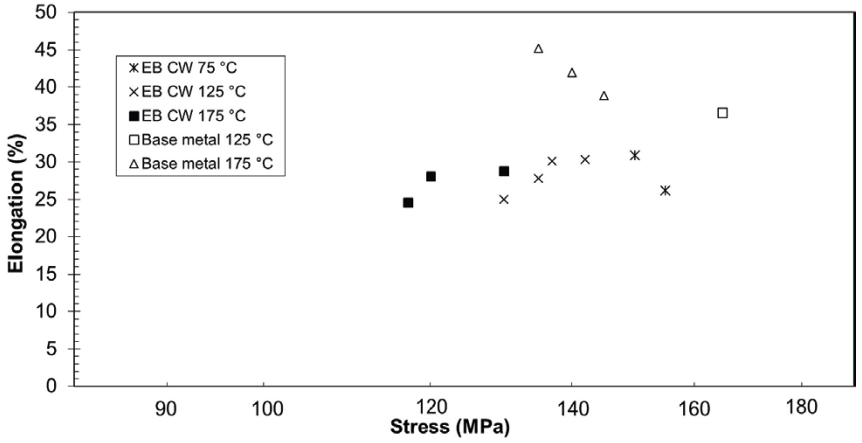

Figure 5-35. *Rupture elongation for the base metal and electron beam weld specimens (Andersson et al. 2004, 2005).*

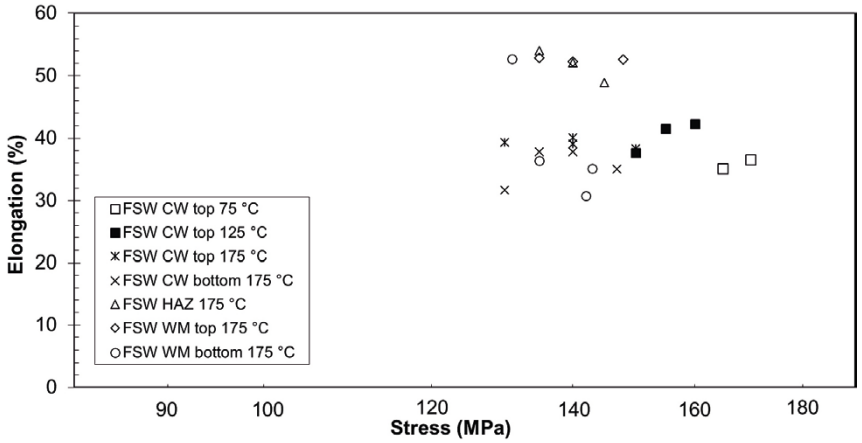

Figure 5-36. *Rupture elongation for the friction stir weld specimens (Andersson et al. 2004, 2005).*

The results in Figure 5-37 to Figure 5-39 show that the good ductility of phosphorus-alloyed copper is also observed at 75 °C. The creep ductility exceeds 40 %. The creep tests are well within the power-law breakdown regime with the Norton creep exponents in the range of 50–120. The procedure used to apply the load to the specimens also influences the obtained results. The loading time was varied for a number of specimens that were tested at the same stress/temperature, and it was found that the measured loading strains were significantly different. This prompted a follow-up project where the loading was varied further.

Either the HAZ or the intermixing zone, which has not received the same mixing as the weld metal but where the temperature is almost as high as in the weld metal, was found to be the weakest part of the frictions stir weld. In cross-weld specimens that contained the base metal, weld metal and two heat-affected zones, two areas of necking were observed. These two areas corresponded to the heat-affected zones: one of the necking areas contained the rupture, and the other area was on the verge of rupturing. Nevertheless, no large differences were observed between the creep results from the base metal, from the weld metal, or from the heat-affected zone specimens.

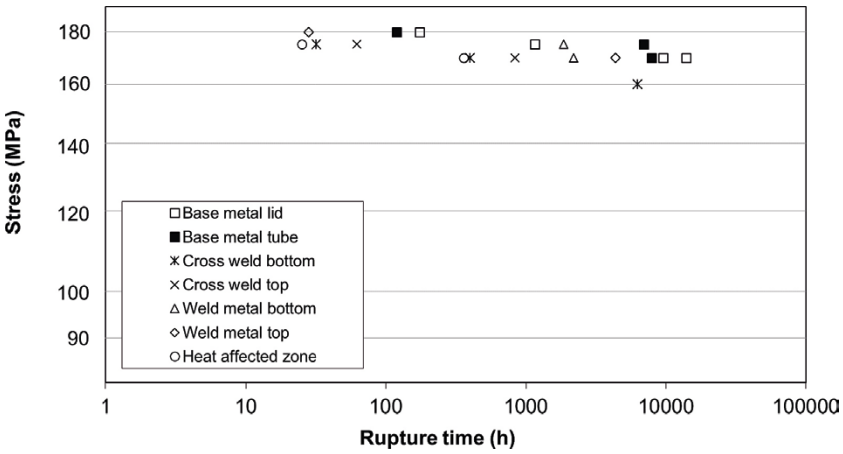

Figure 5-37. *Creep rupture time plotted against applied stress for the 2007 creep test study of friction stir welds (Andersson et al. 2007). All testing was performed at 75 °C.*

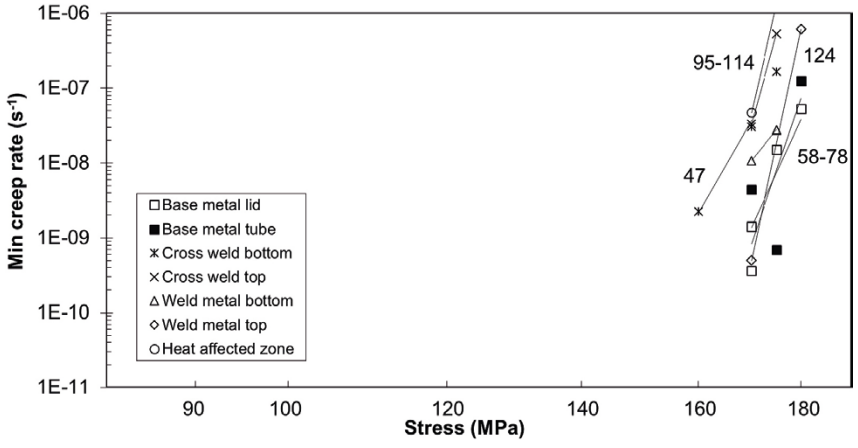

Figure 5-38. *Norton plot for friction stir welds at 75 °C (Andersson et al. 2007). The Norton exponents are marked in the graph.*

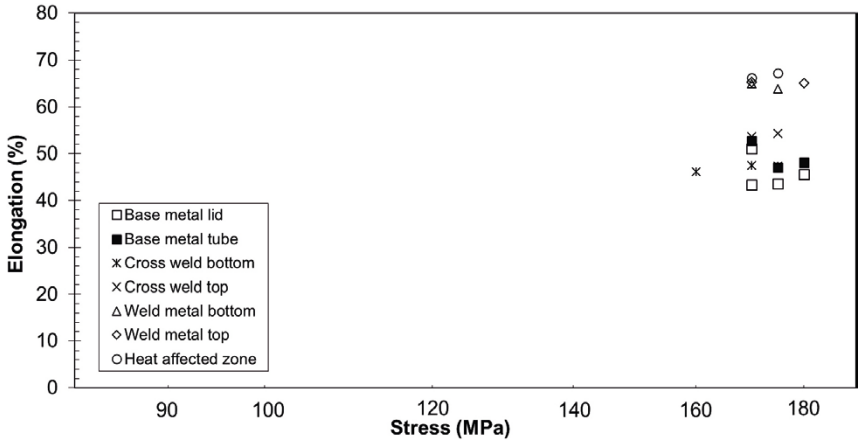

Figure 5-39. *Rupture elongation friction stir welds at 75 °C (Andersson et al. 2007).*

5.10 Weld creep strength reduction factors

A weld is often the weak part of a structure. Therefore, a weld reduction factor must be applied when designing a component. This factor is usually extracted from laboratory tests of the base and weld material. The weld reduction factor is then used for calculating the allowable stresses in the component along with a safety factor.

In the case of a spent nuclear fuel canister, the lid is welded to the tube to seal the canister. The bottom can also be welded but can be manufactured together with the tube. It has not yet been determined which of the two options will be used. In both cases, the weld is a part of the completed canister, and the design calculations must account for the reduced strength of the weld.

Two weld methods have been considered for the canister, and specimens cut from the test welds of both types have been creep tested (Andersson et al. 2004). While various temperatures were used for the tests, the majority of the tests have been performed at 75 °C or 175 °C. Since the creep response is different at the two temperatures, the weld reduction factor must be measured for each temperature. In Figure 5-40 and Figure 5-41, the weld test results were collected in the same graphs. It is observed that the cross-weld specimens require a lower stress to attain the same rupture time. The reduction in the rupture time can be converted to a weld creep strength reduction factor using Equation (5-1) (ECCC 2001).

$$SRF(t/T) = \frac{R_{u/t/T} - R_{u(w)/t/T}}{R_{u/t/T}} \tag{5-1}$$

where $R_{u/t/T}$ is the stress required to achieve a given rupture time of the base metal at a given temperature and $R_{u(w)/t/T}$ is the same for a weld specimen. The results for the welds are presented in Table 5-2. We note that the given factors are for the 1 000 h creep rupture, but since the curves are roughly parallel, the same factors are valid for a wider range of rupture times. An examination of the data presented in Table 5-2 shows that the weld reduction factors are modest, particularly for friction stir welds. For example, for creep resistant steels, values in the interval of 20–50 % are often found (ECCC 2001).

Table 5-2. Weld creep strength reduction factors for creep rupture after 1 000 h. From Andersson-Östling (2010).

Weld type	75 °C	125 °C	175 °C
Friction stir weld	5.7 %	6.1 %	2.1 %
Electron beam weld	14.2 %	12.1 %	16.3 %

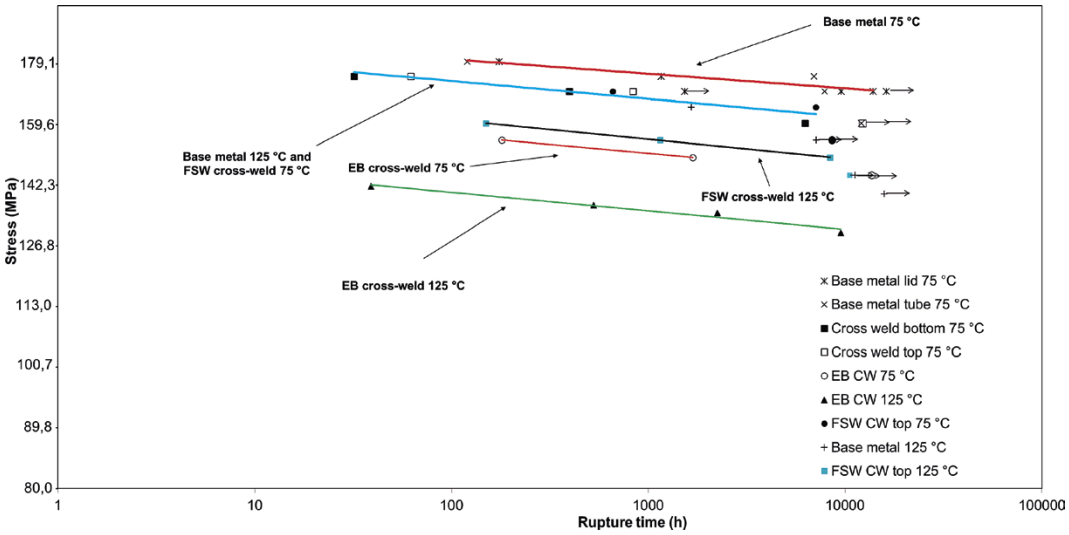

Figure 5-40. *Comparison of creep tests for the weld specimens performed at 75 and 125 °C. Base metal test results are included in the graph. Adapted from results in Andersson et al. (2004). Arrows indicate interrupted tests.*

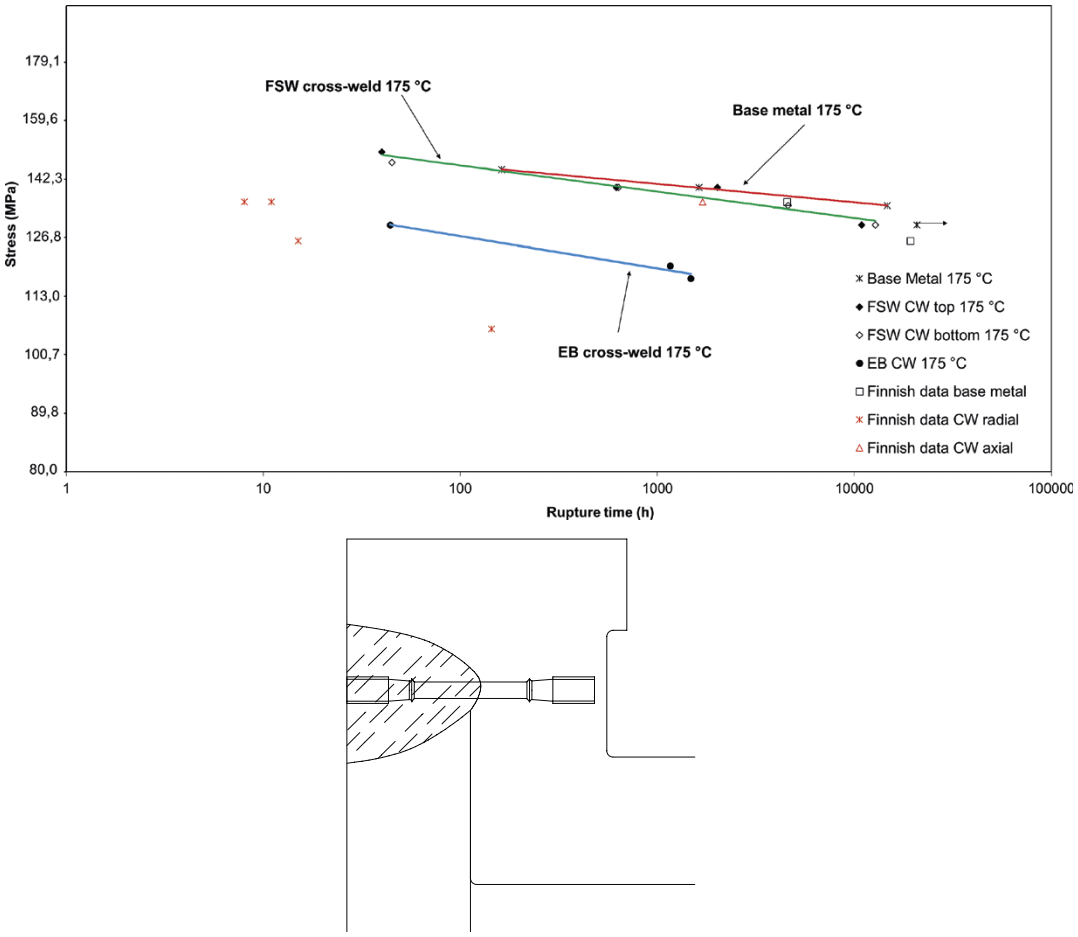

Figure 5-41. *a) Comparison of creep test results of the weld specimens performed at 175 °C. Base metal test results are included in the graph. Included are data from a Finnish study on FSW welds (Auerkari et al. 2009). b) Specimen extraction of radial cross-weld specimens.*

5.11 Oxide streaks, processing line inclusions

In Figure 5-41, the results from a study performed in Finland (Auerkari et al. 2009) are shown. In this study, which was performed on a similar material as that used in the studies in Sweden, it was found that the creep lives of base metal and cross-weld specimens taken in the axial direction are similar to the Swedish results. The Finnish study was performed at 175 °C. Included in the study were also specimens taken in a radial direction (Figure 5-41). It is known that the friction stir welds can sometimes contain a feature known as oxide trails (Savolainen et al. 2008). In the Finnish study, oxide trails or other defects had accumulated at the bottom of the weld. This was given as the reason why the radial cross-weld specimens showed reduced rupture times Figure 5-41). Oxide trails appear in all types of FSW, not only in copper. Further studies on oxide trails or processing line inclusions were published in 2011. The first (*Wu 2011a*) was a study giving guidelines for the observation of processing line inclusions and the related phenomenon of joint line hooking, which is when the slit on the other side of the weld bends along the advancing side of the weld (Figure 5-42).

The second study concentrated on the hot tensile and creep properties of the specimens taken across the weld in a cross-weld position (*Wu 2011b*). The results from the creep testing are tabulated in Table A4-10. The results show that the joint line hooking feature is simply unfused material, and when present in a specimen, it simply decreases the load bearing area. The processing line inclusion specimens show a slightly different behaviour. The specimens were designed to include a band of inclusions with a width of 2 mm, and defect-free specimens were also tested. The results are given in Table A4-10 and in Figure 5-43. Time to rupture results are plotted versus applied nominal stress. In this case, nominal stress means the stress without an adjustment for the processing line inclusions. The results show that the processing line inclusions have a detrimental effect on the creep properties for the higher temperatures, and the results at 75 °C are too ambiguous to allow a definite conclusion. The inclusions themselves were also analysed and were found to contain carbon, aluminium and oxygen.

As shown in Table A4-10, high rupture ductility was obtained, but the presence of processing line inclusions makes a direct comparison with homogenous specimens difficult. An example of the rupture surface is given in Figure 5-44. The flat surface that can be observed on the rupture surface is the processing line inclusion band. This has ruptured in a brittle manner, while the material on either side of the band has not.

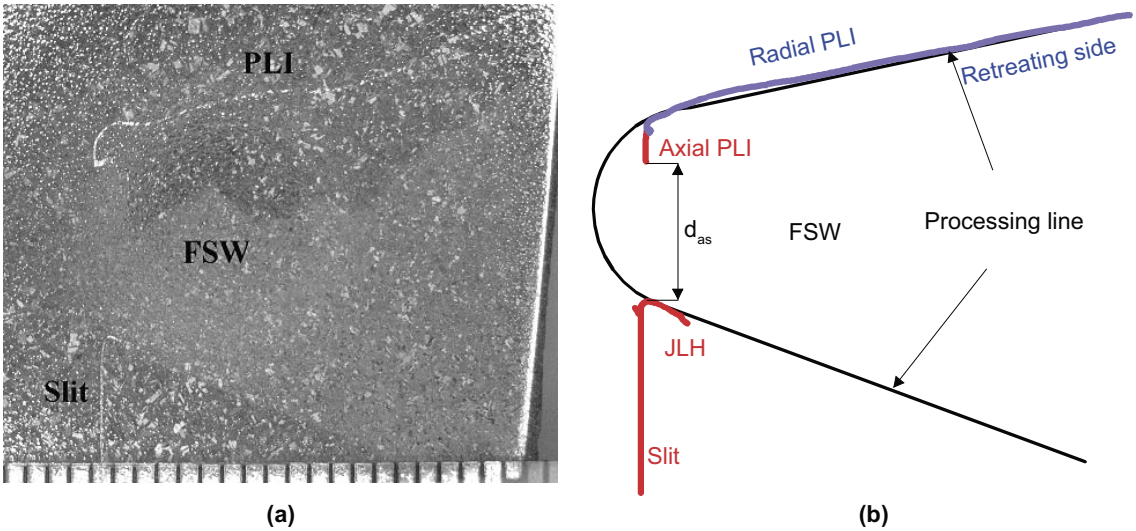

Figure 5-42. *(a) Processing line inclusions (PLI) in an FSW weld of Cu-OFP. (b) Schematic illustration of slit, joint line hooking (JLH), axial PLI and radial PLI. From Wu (2011b).*

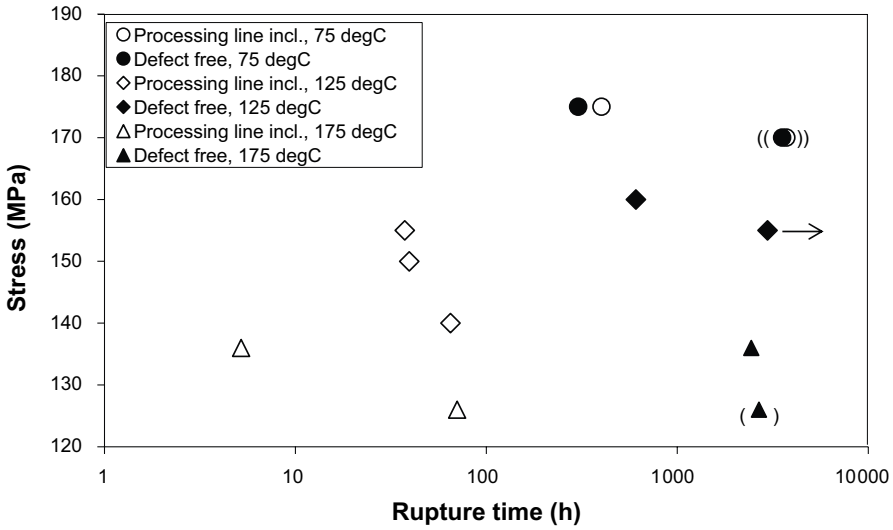

Figure 5-43. *Time to rupture versus applied and nominal stress for the creep tests with processing line inclusions. The results for the interrupted tests are shown in brackets, and the results of the running tests are denoted by the arrow (Wu 2011b).*

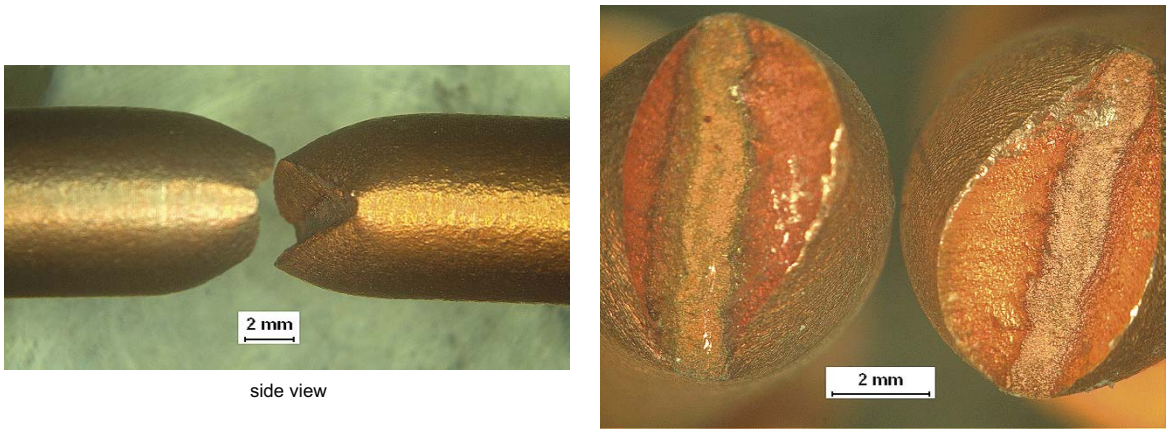

Figure 5-44. *The rupture surface of a processing line inclusion specimen from Wu (2011b). The specimen was tested at 150 MPa and 125 °C. The flat surface in the middle of the rupture is the processing line inclusion band in this specimen.*

The procedure used to extract the specimens in the 2011 study meant that the gauge length of the specimen contained both inclusions and defect-free material over the cross-section (Figure 5-44). In the next study on the phenomenon of oxide inclusions in welds (Björck et al. 2019), care was taken to design a specimen that contained only oxide particles, or processing line inclusions as they were previously called, over the whole gauge length cross-section. The specimen was also flat and had a short narrow gauge length that was placed just over the oxide particles (Figure 5-45). The oxide streaks emanate from the surface of the material before friction stir welding, and by varying the oxide thickness prior to welding, the amount of oxides present in the weld after welding can be controlled.

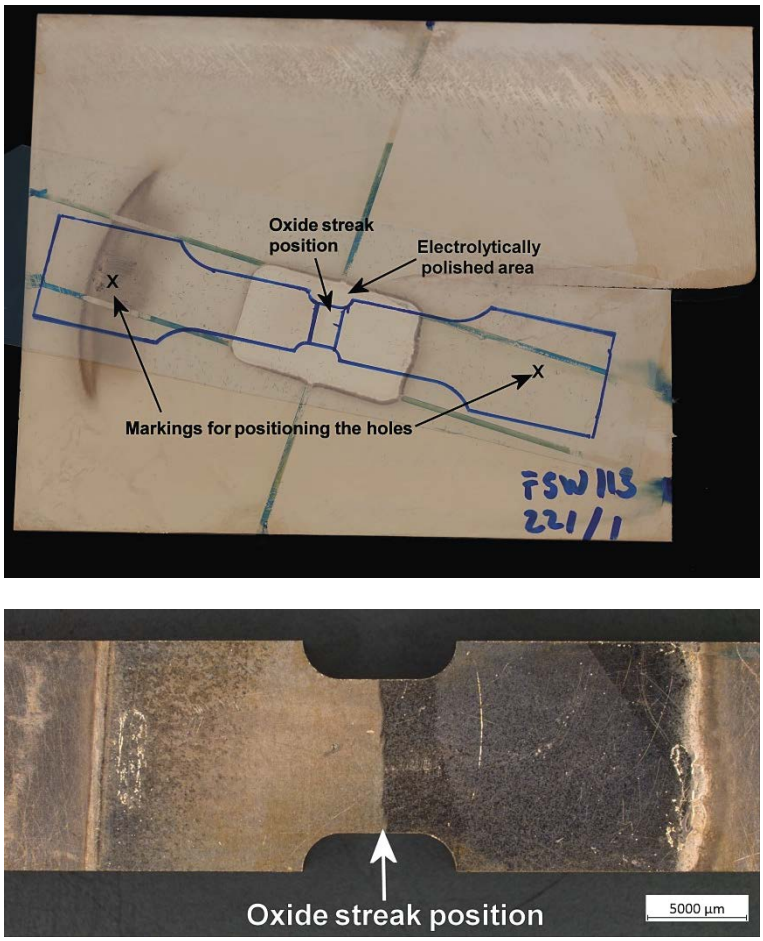

Figure 5-45. *Example of the positioning of the oxide streak in the specimen gauge section. a) A milled specimen is electrolytically polished in the region of oxide streak. Two markings are made to ensure the correct positioning and angle in WEDM-cutting of the specimens. b) A finished specimen with an oxide streak perpendicular to the loading direction (Björck et al. 2019).*

Six types of specimens were made, of which one was the reference material without any oxide streaks, and five specimens with oxide streaks were made from different pre-welding oxide thicknesses. The thicknesses used for these specimens are listed in Table 5-3.

Table 5-3. Initial oxide thicknesses and denotations used for the materials tested in Björck et al. (2019).

Material	Initial oxide layer thickness
Material 1	~1 µm
Material 2	6–11 µm
Material 3	0 µm
Material 4	Reference material
Material 5	1.5–1.7 µm
Material 6	0.1 µm

Both hot tensile tests and creep tests were performed on the specimens. The hot tensile testing showed brittle behaviour for the specimens with the initial oxide thickness of approximately 1 µm or higher. The creep test results are presented in Figure 5-46 and in Table A4-17. It is evident from the results that oxide thicknesses greater than approximately 1 µm show a more brittle-like rupture behaviour (area reduction in Table A4-17) and shorter creep life (Figure 5-46). Metallography of the fracture surfaces also shows that the rupture traverses the oxide streak in the specimens with heavier oxidation prior to welding. In addition to the special rectangular creep test specimens, a series of round cylindrical specimens were also tested. These were extracted in a cross-weld manner; inside the gauge length, the base material, the weld material and an intermixing region are found. The only oxide thickness studied this way is the 0 µm type, and the results for this specimen show both good ductility and long creep life. The rupture in this specimen that has already ruptured did not traverse the position of the oxide streak.

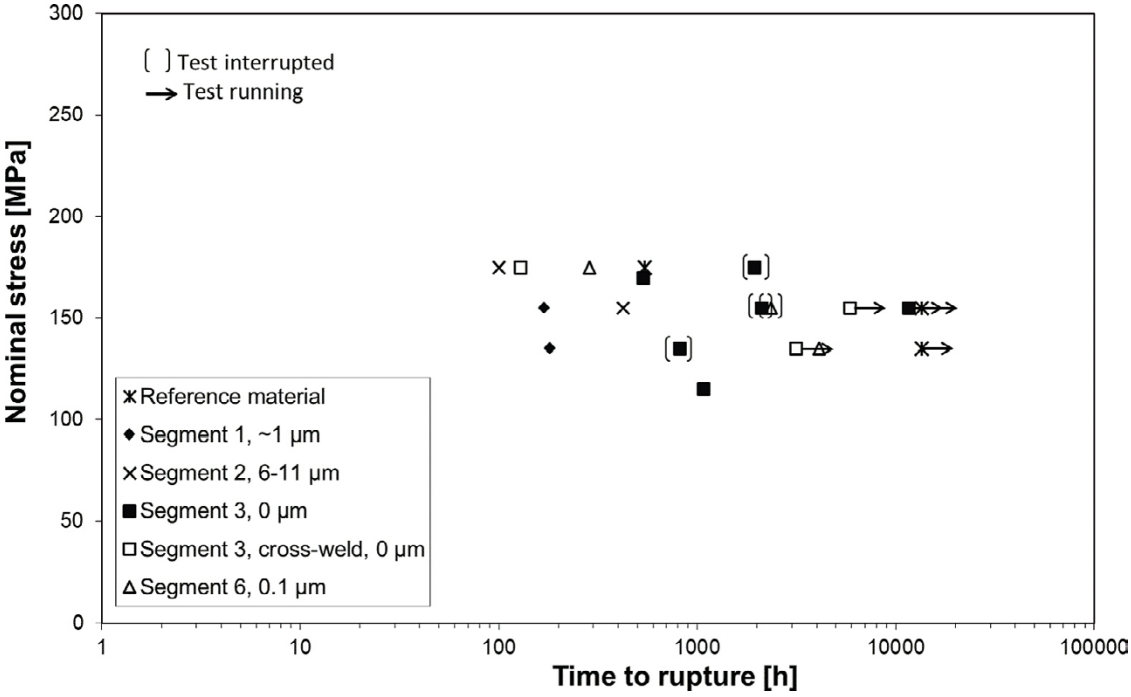

Figure 5-46. *Time to rupture versus nominal initial stress in the creep tests. A total of five tests are still running (indicated by à) at the time of this report. The tests that were interrupted due to problems with the testing or prior to final failure for microscopy are marked with parentheses (a total of four). From Björck et al. (2019).*

6 Influence of cold work on creep

6.1 Background

Starting from manufacturing to the final disposal in the repository, copper is subjected to handling that can introduce cold work into the material. Tools and other handling equipment can be pressed or punched into the canister material. Cold work has also been observed after forging in the lids. The machining of copper components is a potential source of cold work. Such cold work may influence the creep strength and ductility and thereby jeopardise the long-term safety of the canisters. Some information on fcc-alloys can be found in the literature; in particular, information on cold-drawn copper can be found in Davis (2001). With an increasing amount of cold work, the creep strength can increase (316, 17Cr12Ni2Mo, 650 °C, max 30 % cold work) (Furuta et al. 1973) or decrease (304, 18Cr10Ni, 677 and 760 °C, max 12 % cold work) (Ajaja and Ardell 1977). At the same time, the creep ductility is reduced (Savoliainen et al. 2008). The ductility can decrease by 75 % after 20 % cold work in comparison to solution heat-treated material.

The effect of cold work is influenced by the occurrence of either recovery or recrystallisation during creep. Some examples are the studies of 314 (25Cr20Ni) at 900 and 950 °C (Adelus et al. 1980). The influence of cold work disappears after long testing times and low stresses at these high temperatures. In Pilloni et al. (2000), it is demonstrated that the effect of cold work is reduced with decreasing stress for 347 (18Cr11NiNb) at 750 °C.

The above studies are all limited to test times shorter than 1 000 h, which means that the conclusions of these studies should be handled with some caution. None of the above studies examined cold work in compression.

The effect of cold work and back stress in multiaxial notched specimens has been studied and reported (Wu and Sandström 2018).

6.2 Cold work and the annealing of creep test specimens

Of special interest are the creep test specimens themselves. For soft materials, the turning operation on the lathe can introduce cold work into the material and more specifically into the gauge length. Early on in the creep testing of Cu-OFP, this was studied briefly and reported in a progress report (*Henderson and Lindblom 1995*)[4]. It was found that thin-diameter creep specimens were more affected than thick-diameter specimens, as presented in Table A4-3. The results of the relevant creep tests are given in Table 6-1. It can be seen from the results that the specimens with a diameter of 10 mm exhibit larger creep ductility than the specimens with a diameter of 5 mm. If the 5 mm diameter specimens are heat-treated for 5 minutes at 600 °C, the properties are restored to the same values as those of the 10 mm diameter specimens.

At the time, this was considered to be merely a detail because in any case, the 10 mm specimens were preferred for all tests. When it later became necessary to study smaller-diameter specimens, it was decided to anneal these specimens after their manufacturing to remove any cold work that could affect the creep result from the material. Eventually, all specimens of all diameters were annealed as a standard procedure, with the exception of the specimens where the as-received properties showed that no annealing was necessary.

[4] References given in *italics* do not meet SKB´s quality assurance requirements for public reports, see further Section 2.2. These references are presented in the Report list in Appendix 1.

Table 6-1. Comparison of the creep results from 5 mm and 10 mm diameter specimens (Henderson and Lindblom 1995).

Specimen	Temp °C	Stress MPa	Time to rupture h	Min creep rate h^{-1}	Elongation %	Area reduction %	Dia. (mm)
523	215	120	1 350	1.6×10^{-4}	54.5	59.9	10
524	250	120	53.2	3.7×10^{-3}	59.9	72.7	10
525	250	100	1 084	1.9×10^{-4}	47.5	51.8	10
501	215	120	2 133	8.4×10^{-5}	41.6	55.6	5
502	250	120	94	2.5×10^{-3}	45.3	75.5	5
504	250	100	883	2.2×10^{-4}	38.9	50.3	5
555*	215	120	894	2.4×10^{-4}	63.4	60.0	5
556*	250	120	48.4	4.1×10^{-3}	54.6	73.6	5

* Heat-treated for 5 min at 600 °C.

6.3 Creep tests of cold-worked materials

Creep tests have been performed for four types of cold work (Martinsson and Andersson-Östling 2009).

1. 12 % strain in tension
2. 24 % strain in tension
3. 12 % strain in compression
4. 15 % strain in compression perpendicular to the creep testing direction.

The influence of cold work on creep rupture is illustrated in Figure 6-1.

Cold working by 12 % in tension gives more than a 10 % increase in the creep rupture strength. The corresponding increase for 24 % cold work in tension is 25 %. In contrast, 12 % cold work in compression does not influence the rupture strength at all, and 15 % cold work in a direction perpendicular to the test direction gives approximately the same increase in the strength as the same strain in tension.

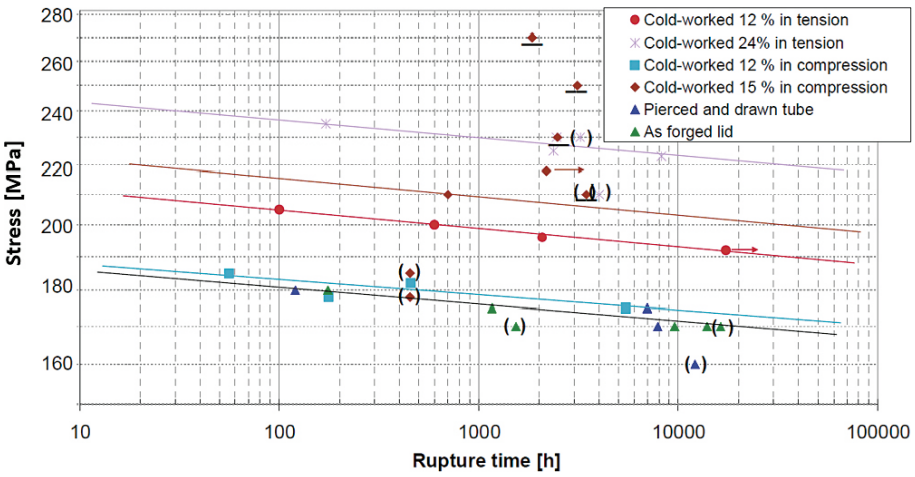

Figure 6-1. *Applied creep stress versus rupture time for cold-worked and reference material at 75 °C. → – still in test, ( ) – interrupted before fracture, _ – creep stress increased during testing. Four sets of cold-worked copper are included. The pierced and drawn tube and forged lid are reference materials without cold work (Martinsson and Andersson-Östling 2009).*

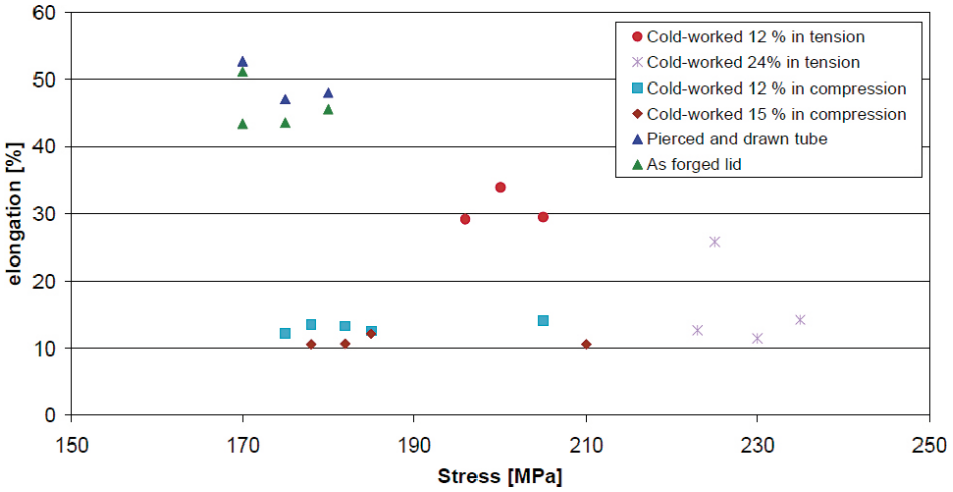

Figure 6-2. *Rupture elongation versus applied creep stress for cold-worked and reference materials at 75 °C. Four sets of cold-worked copper are included. The pierced and drawn tube and forged lid are reference materials without cold work (Martinsson and Andersson-Östling 2009).*

For the reference materials, the creep elongation is 30–50 %, as shown in Figure 6-2 and previous figures in this report. The 12 % cold-worked copper in tension has a high ductility of 30 %. For the other sets, the elongation is 10–15 %. It should also be noted that the initial strain on loading is below 2 % for practically all of the cold-worked specimens, whereas the initial strain is approximately 10 % for the reference materials. This extra ductility margin obviously disappears for cold-worked material. Surprisingly, cold working does not appear to influence the reduction in area. The area reduction is approximately 90 % for both the reference and the cold-worked materials. This is technically quite significant since this finding demonstrates that high strains can be allowed locally without the immediate occurrence of failure.

The test results can be qualitatively understood. With increasing cold deformation, an increase in creep strength can be expected as long as recovery and recrystallisation do not take place, and that is not the case for copper at 75 °C. If cold work in tension and compression are compared, compression will give a dislocation structure that can easily be overcome by creep strain in tension contrary to the cold work in tension. Cold work perpendicular to the creep direction will only be partially removed by creep in tension.

Cold work consumes some of the available straining capacity of the material. Thus, it is not surprising that the creep ductility is reduced after cold working. It is well-known that cold work increases the density of creep cavities, which contributes to a reduction in the rupture ductility. The mechanisms by which the cavitation increases are not well-known. One possible mechanism that has been proposed involves dislocations forming ledges at the grain boundaries, stimulating cavity nucleation. Another possible mechanism is the increased diffusion along dislocations that gives rise to more rapid cavity growth.

6.4 Effect of indentations

In the manufacturing and further handling of the canisters, cold work can be introduced by accidental indentation of the copper. Both experiments and FEM modelling of indentation with a sphere, cylinder and cone have been studied. The results were summarised by Unosson (2009). The results show that high strains up to 50 % can easily be reached. Such high cold work strains may jeopardise the canister integrity during creep.

To analyse this situation and to try to find a solution, new FEM simulations have been performed. The case considered is an indentation with a cylindrical punch with a diameter of 20 mm. The applied stress is 500 MPa. The results are illustrated in Figure 6-3 and Figure 6-4. The maximum plastic strain is 12 %, and the displacement is 1.1 mm. If the stress is increased to 600 and 700 MPa and the same computations are performed again, the plastic strain is raised to 23 and 53 %, respectively, and the depth of the indentation is increased to 2 and 3.9 mm, respectively. It is evident that an applied stress of 500 MPa gives an acceptable plastic strain, but a slightly higher stress of 700 MPa does not. To handle the canister, it is therefore essential to use tools made of soft materials such that a stress level of 500 MPa is not exceeded.

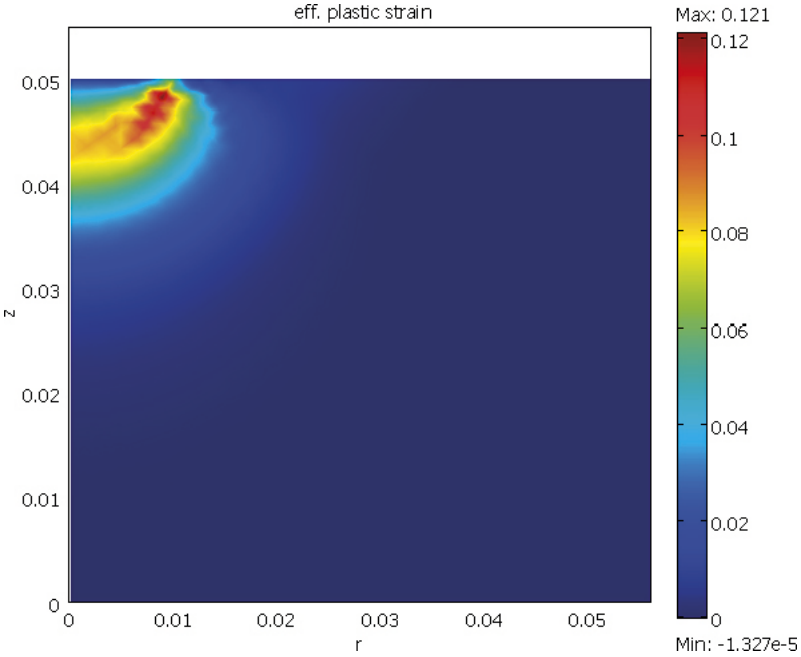

Figure 6-3. *Effective plastic strain below an applied punch of Ø 20 mm with a stress of 500 MPa and a load of 0.157 MN. From Andersson-Östling and Sandström (2009).*

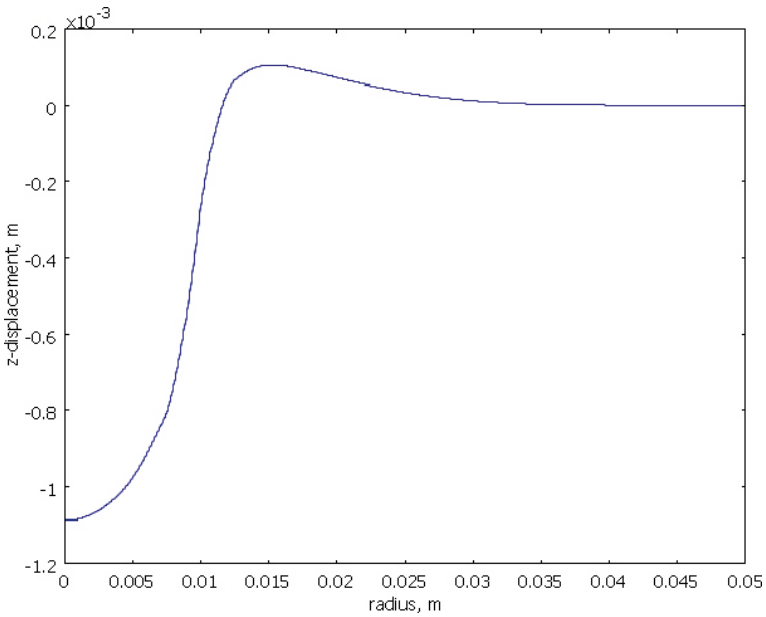

Figure 6-4. *Same as Figure 6-3 but showing the displacement below the punch. From Andersson-Östling and Sandström (2009).*

6.5 Creep testing of specimens with indentations

In Mannesson et al. (2013), rectangular specimens with conical indentations were creep tested at 75 °C. The results are given in Figure 6-5 and Table A4-10bis. The indentation depths used were 1 mm, 1.5 mm, 2 mm and finally 2 mm with an additional annealing performed after indenting the specimens. It is observed from the results that the indentation of the specimens has some effect, but this effect is limited, and most of the test results fall within the scatterband. It is noteworthy that since all specimens were annealed prior to testing, they were all creep-soft. However, the indenting process cold-worked a portion of the gauge length, making it harder for creep to occur and giving the deformation of the gauge length a double hourglass shape (Figure 6-6). In this study, only light optical microscopy was used, and no cracks were observed within or around the indentations.

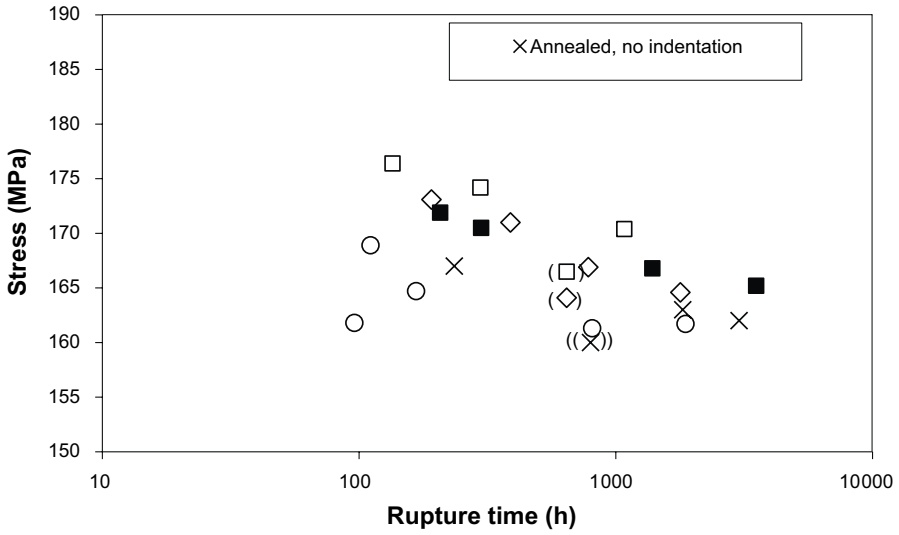

Figure 6-5. *Stress against rupture time for the creep test specimens with conical indentations. Values inside parentheses are for the interrupted tests. From Mannesson et al. (2013).*

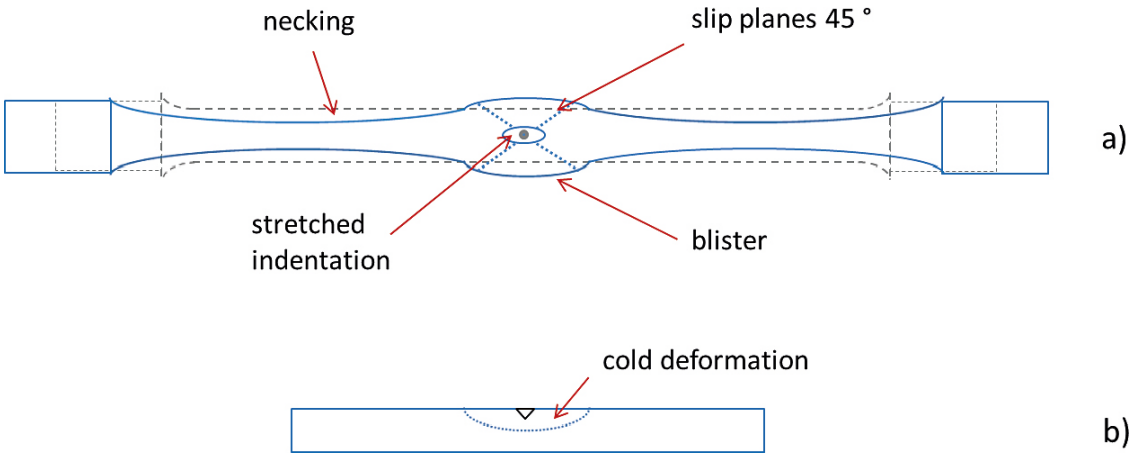

Figure 6-6. *a) Schematic drawing showing the necking, slip planes and blister; b) cold deformation "bubble". From Mannesson et al. (2013).*

A further study in 2014 developed the indentation concept further and used indentations on a wide rectangular-shaped gauge length. The main idea behind the specimen shape was that it should be a 1:10-scale version of an indentation on a real canister. The thickness of the specimen was thus chosen as 5 mm with the real canister being 50 mm thick. The indentations depths were chosen to be between 0.4 and 0.6 mm, translating to 4–6 mm in the real canister. The results from the creep testing are given in Table A4-13 and are presented in Figure 6-7. Two different temperatures (75 and 125 °C) were used, and the results from the testing showed that all of the indentation shapes had the same creep properties and that the properties were comparable to the unindented material.

In this study, scanning electron microscopy (SEM) was also used in addition to light optical microscopy for the metallographical studies. In SEM images, small cracks were observed around and inside the cylindrical-shaped impressions (Figure 6-8). The cracks are shallow, as can be seen from Figure 6-9, where a cross-section of an indentation is shown. At the time of writing, it is not known whether cracks form in all Cu-OFP impressions or whether they are associated with the spark erosion process used to produce the specimens. Spark erosion leaves a thin layer of heat-affected material on the surface of the specimen and this may have different cracking properties than the underlying base material.

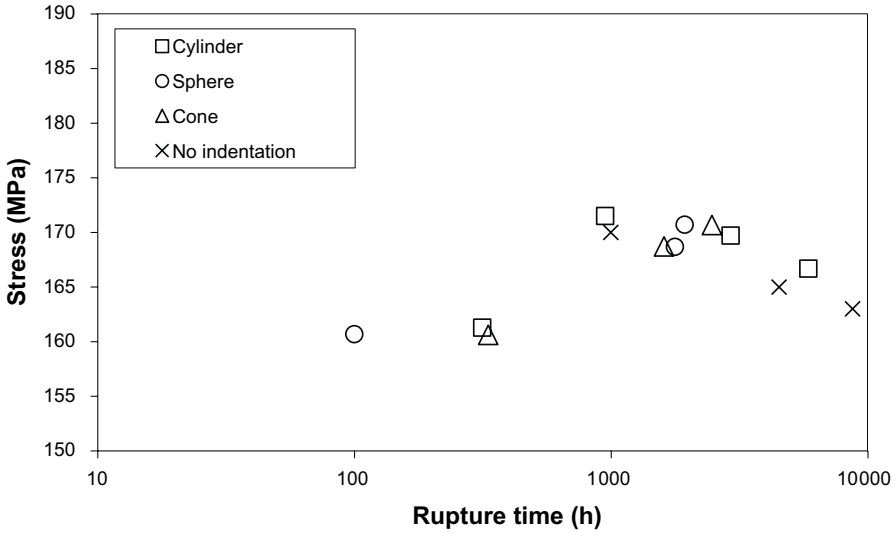

Figure 6-7. *Stress against rupture time for the creep test specimens with indentations: the 125 °C specimens are grouped on the left side, and the 75 °C specimens are grouped on the right side. From Mannesson and Andersson-Östling (2014b).*

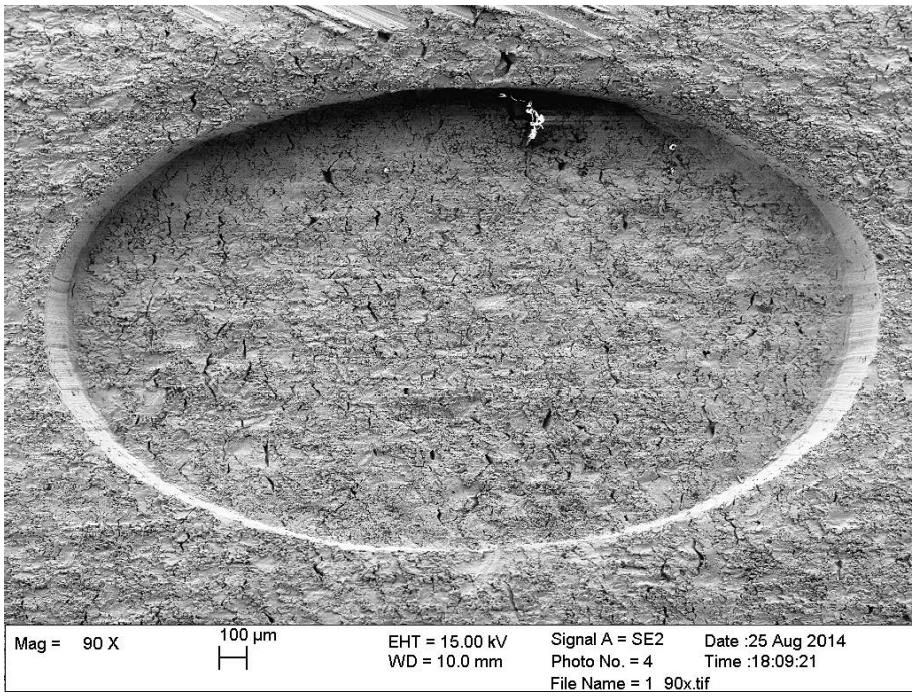

Figure 6-8. *SEM image of a cylindrical indentation after creep testing. Note the abundance of small cracks that are all transverse to the loading direction. From Mannesson and Andersson-Östling (2014b).*

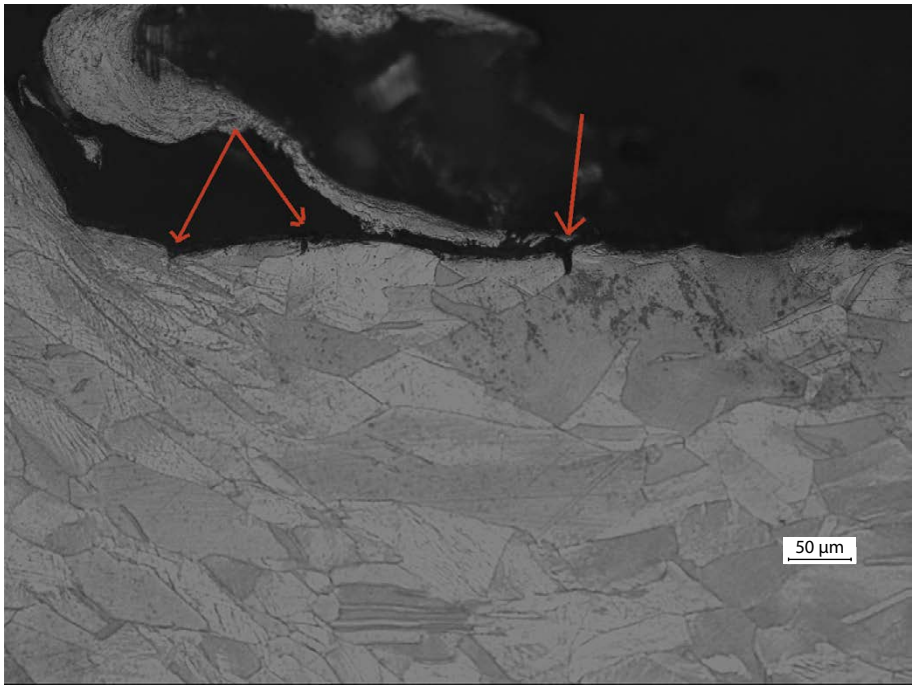

Figure 6-9. *Light optical image of a cut, ground and polished section through the indentation. Note the small cracks in the grain boundaries marked by arrows. The crack depth is approximately 20 µm. The structure above the surface is composed of swarf from the cutting and polishing and is not a surface defect. From Mannesson and Andersson-Östling (2014b).*

6.6 Grain boundary sliding in Cu-OFP

In 2015, a study was initiated and executed where two specially designed specimens was used to evaluate the amount of grain boundary sliding occurring during creep testing at 125 °C (Wu et al. 2015a, Sandström et al. 2016). Two standard round specimens were machined to include two wide flat faces that were then highly polished. After polishing, a pattern was inscribed into the polished surfaces. The polishing and the inscription of the pattern were performed because if a scribed line traversed a grain boundary and the grain boundary then experienced sliding during creep, the amount of sliding could afterwards be metallographically measured on the surface.

The specimens were creep tested at 125 °C, and after testing, they were studied by SEM and electron backscatter diffraction (EBSD). Only a few instances of grain boundary sliding were observed, mostly due to experimental difficulties. An example of sliding is shown in Figure 6-4. Very few instances of grain boundary sliding were observed, but those that were recorded had slid 20–60 µm, which is comparable to the results reported in the literature.

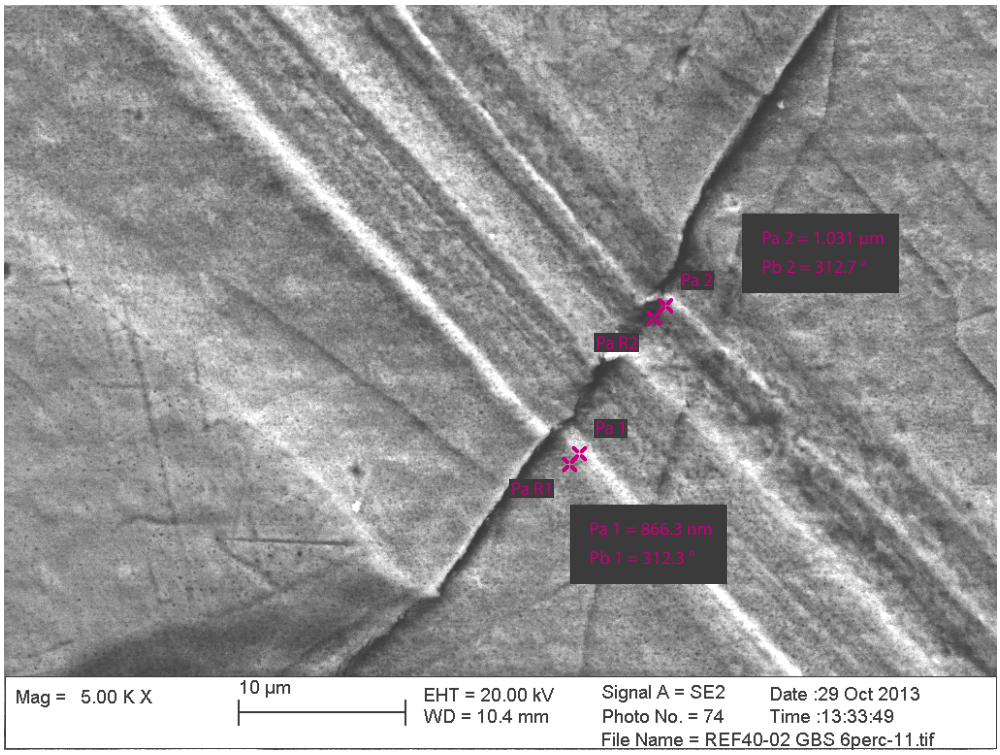

Figure 6-10. *Grain boundary sliding on the surface of a specimen. The inscribed line has been bisected by a sliding grain boundary, and measurements were carried out. From Wu et al. (2015a).*

6.7 Subcell/subgrain structures and their development

It is well-known that dislocation movement during plastic deformation forms cells and subgrains in many alloys. The cells are built up by nearly dislocation-free regions that are separated by loosely knit tangles of dislocations. On the other hand, subgrains are separated by boundaries of sets of parallel dislocations.

It is well-established that the subgrain size that is developed during creep is frequently inversely proportional to the creep stress σ (Sikka et al. 1975). In some cases, a stronger stress dependence is observed at higher stresses (Sherby et al. 1977). In stress dip tests where the creep stress is suddenly reduced and the microstructure is unchanged, it has been found that the creep rate is proportional to the cube of the subgrain size. A survey of these studies can be found in Sherby et al. (1977). Thus, it appears that the control of the subgrain size will be a powerful method for improving the creep strength. However, the subgrain size is not stable, and as pointed out above, the subgrain is generally controlled by the creep stress. To exploit the increased creep strength due to a fine subgrain size, the subgrain size must be stabilised. This is well established for 9–12 % Cr-steels, where the carbides are stabilising the subgrain size (Magnusson and Sandström 2007).

In 2014, a project was initiated where cold-worked and creep-tested material was studied by transmission electron microscopy (TEM). The aim of the project was to study the subgrain size and shape. It was found that the subgrain size was inversely dependent on the amount of deformation to which the material had been subjected (Figure 6-11). It was also found that the wall thickness of the subgrains increased with increasing creep deformation if the prestraining was performed in tension rather than in compression. An example of the TEM images analysed in the project is given in Figure 6-12. The work was further analysed and a model was extracted (Sandström 2016b, 2017).

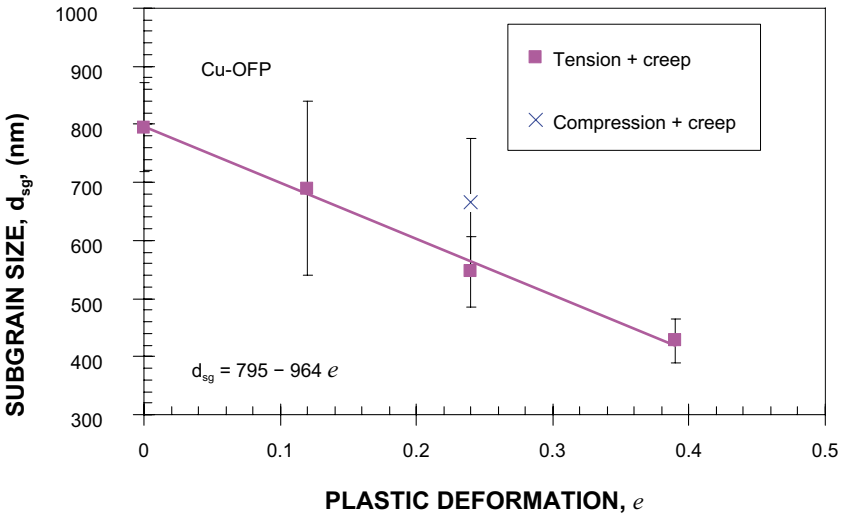

Figure 6-11. *Subgrain size as a function of plastic deformation (cold work in tension/compression with or without creep). × refers to total plastic deformation in which compression and creep deformation are added. The 95 % standard deviation range is included. From Wu et al. (2014).*

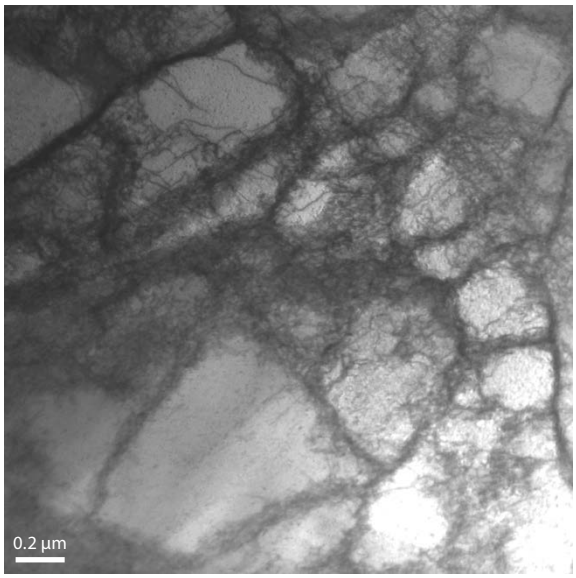

Figure 6-12. *An example TEM image showing dislocation and subgrain structures in cold-worked material. From Wu et al. (2014).*

7 Slow strain rate tensile tests

After disposal in the repository, copper canisters for spent fuel can be exposed to temperatures close to 100 °C. The external pressure from the surrounding bentonite and the ground water will reach approximately 15 MPa after a period that can take many years (Hökmark and Fälth 2003). Slow plastic deformation will occur due to the external pressure and increased temperature, and the gap between the canister and the insert will gradually close.

To model the deformation in the copper canisters, accurate data for creep and plastic deformation must be available. The generation of creep data has been described above in this report. In the present chapter, slow strain rate tensile tests will be summarised for phosphorus-alloyed pure copper. The copper must have good ductility properties to avoid crack formation during the deformation. The ductility behaviour can be studied both with traditional creep tests and slow strain rate tensile tests.

The first slow strain rate tensile tests for Cu-OFP were performed for cold-worked material (Yao and Sandström 2000). The tests were carried out at 20 to 175 °C for strain rates between 10^{-7} and 10^{-3}. Two examples of the results are shown in Figure 7-1. In terms of engineering stresses, the results have a simple form. After the elastic region, the curves become essentially flat. A stationary value is reached. At 20 °C, a slight work hardening is present that does not appear at higher temperatures. The behaviour of the curves is what would be expected at higher temperatures when the deformation is climb-controlled. In terms of true stress, linear work hardening is observed at all investigated conditions.

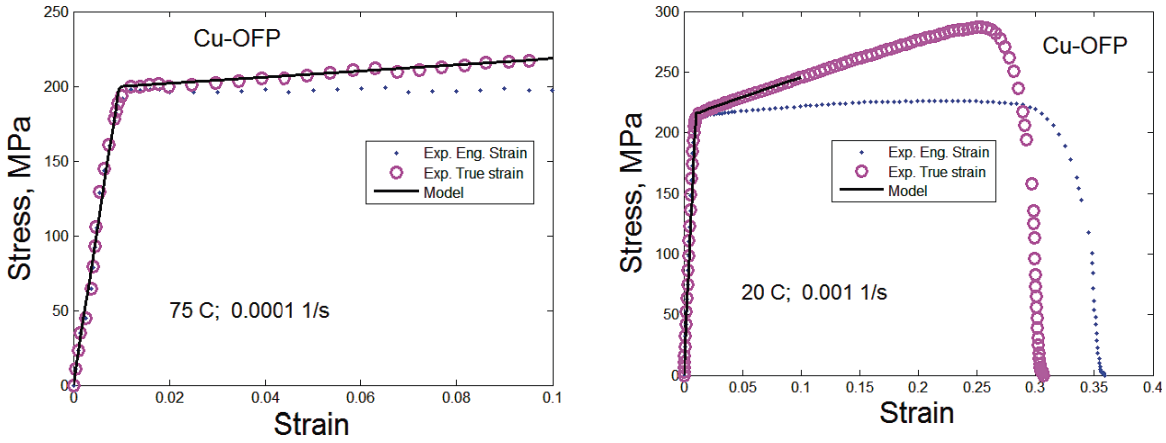

Figure 7-1. *Slow rate tensile tests for cold-worked Cu-OFP at 75 °C, 0.0001 1/s, and at 20 °C, 0.001 1/s (Yao and Sandström 2000).*

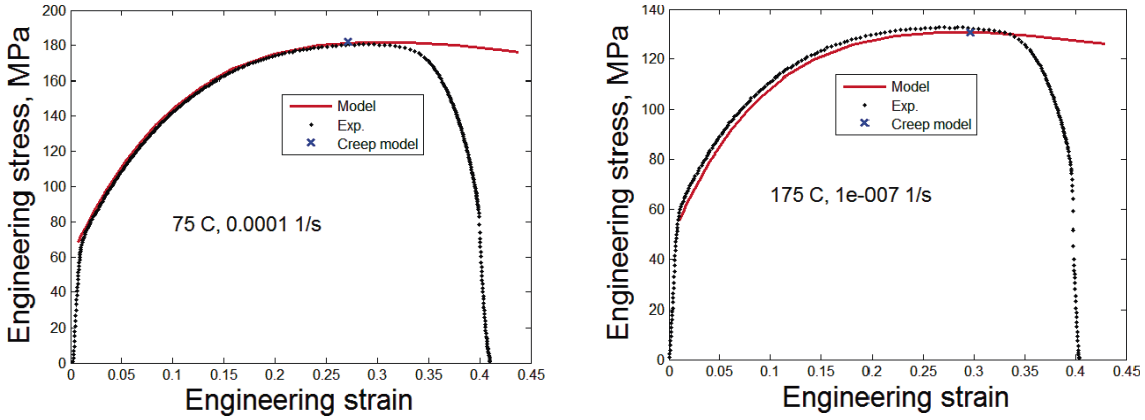

Figure 7-2. *Slow rate tensile tests for annealed Cu-OFP at 75 °C, 10^{-4} 1/s, and at 175 °C, 10^{-7} 1/s (Sandström et al. 2009).*

The amount of cold work that the copper was exposed to is not known. The material is taken from a rolled formed canister cylinder. Roll forming for such a component should in principle give a modest cold deformation, but the actual cold deformation is quite significant considering the appearance of the stress strain curves.

More recently, annealed copper has been studied. Temperatures in the range of 20–175 °C and strain rates between 10^{-7} and 10^{-4} 1/s were examined (Sandström et al. 2009). The results have also been reported in Sandström and Hallgren (2012). Two examples of the obtained curves are shown in Figure 7-3.

It is immediately apparent that the curves for annealed copper are quite different from those of the cold-worked material. A significant work hardening is observed, and the "flat" region is much less pronounced. However, it is still assumed that the maximum value in the "flat" region represents a stationary value.

In Figure 7-3, the stationary values from the cold-worked and the annealed materials are compared. In addition, the available creep data at 75 and 175 °C are included. The SSR data for the cold-worked material are close to the minimum strain rates in the creep tests. The strain rates for the annealed material are higher. The dislocation barriers that are built up in the two types of tests can be expected to be different. It is likely that the dislocation barriers are broken down more efficiently in the strain-controlled tests than in the stress-controlled creep test. The difference in the stationary stress level was found to be 10 %.

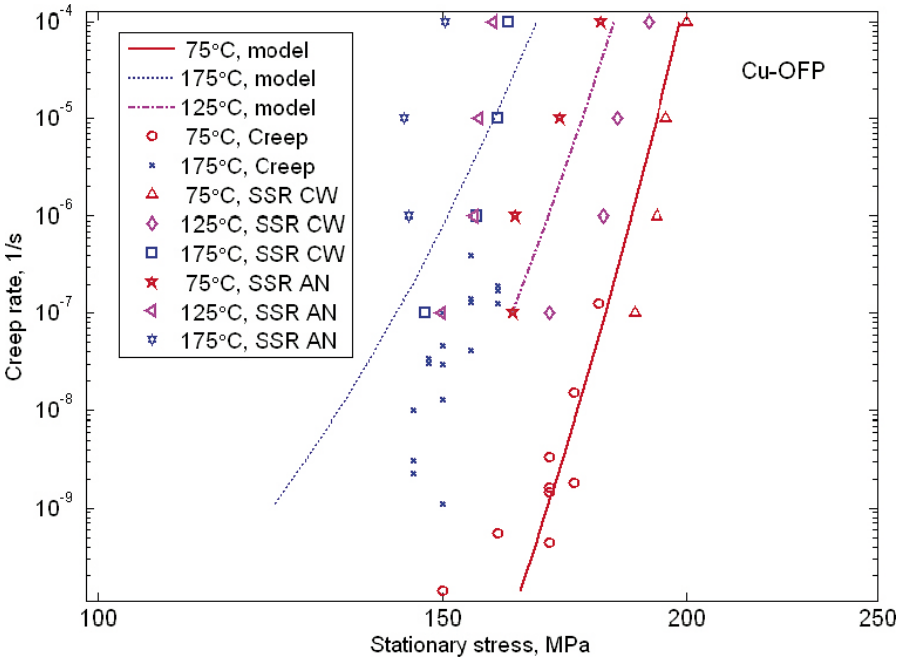

Figure 7-3. *Comparison between the minimum creep rates at 75 and 175 °C and stationary stress in slow strain rate (SSR) tensile tests at 75, 125 and 175 °C. For each temperature and strain rate, two SSR values are given. The value at the lower stress is for the annealed material (SSR AN), and the value at the higher stress is for the cold-worked material (SSR CW). The model values for creep are discussed in Chapter 11.2. From Andersson-Östling and Sandström (2009).*

Further work on slow strain rate testing was published in Sui and Sandström (2016). In this study, round notched specimens were used. Notch acuity ratios 0.5, 2 and 5 were used in the testing. The main result from the testing was that the presence of a notch decreased the tensile strength, the elongation and the reduction in the area compared to the un-notched specimens. A sharper notch corresponded to lower ductility.

A comprehensive study on slow strain rate testing performed on Cu-OFP where a model of the characteristics after testing was developed was published in 2017 (Sandström et al. 2017).

Recently, a study was performed to investigate the SSRT behaviour of copper with and without phosphorus (Josefsson and Andersson-Östling 2019). In this study, four different copper samples were investigated. Two of these were of Cu-OF type (Cu-6N and Cu-OF), and two were of Cu-OFP type (Cu-H and Cu-OFP). The SSRT testing was performed at three temperatures, 75, 125 and 175 °C. The results are given in Figure 7-4, Figure 7-5 and Figure 7-6. The strain rate used was close to 1×10^{-7} s^{-1}, which is comparable to that used in the previous studies. The results show good ductility for all materials at 75 °C, but the non-phosphorus-doped materials exhibited significantly lower ductility at 125 and 175 °C. The reason for this behaviour is not immediately clear at the moment.

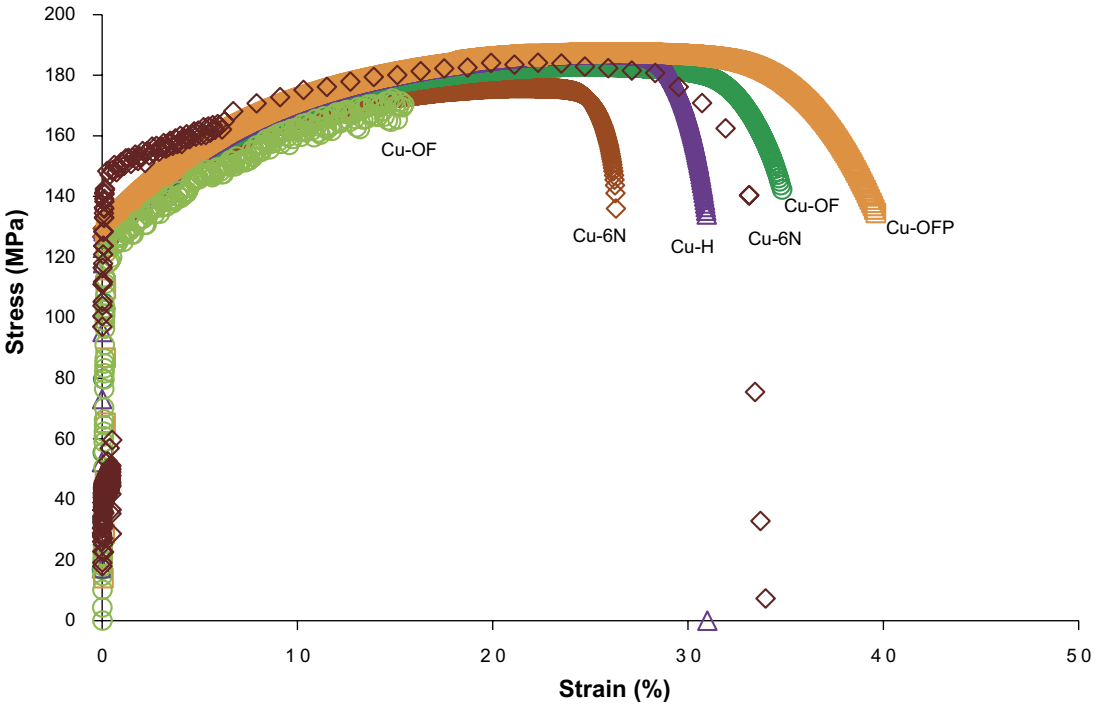

Figure 7-4. *Comparison between the minimum creep rates at 75 and 175 °C and the stationary values. From Josefsson and Andersson-Östling (2019).*

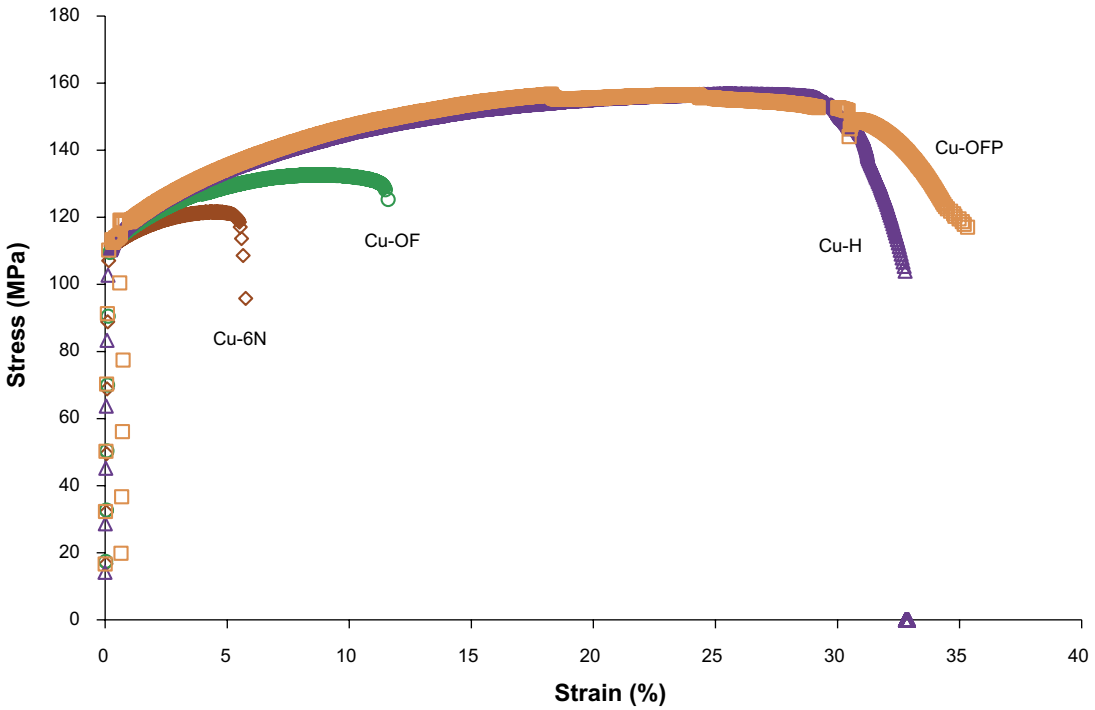

Figure 7-5. *Comparison between minimum creep rates at 75 and 175 °C and the stationary values. From Josefsson and Andersson-Östling (2019).*

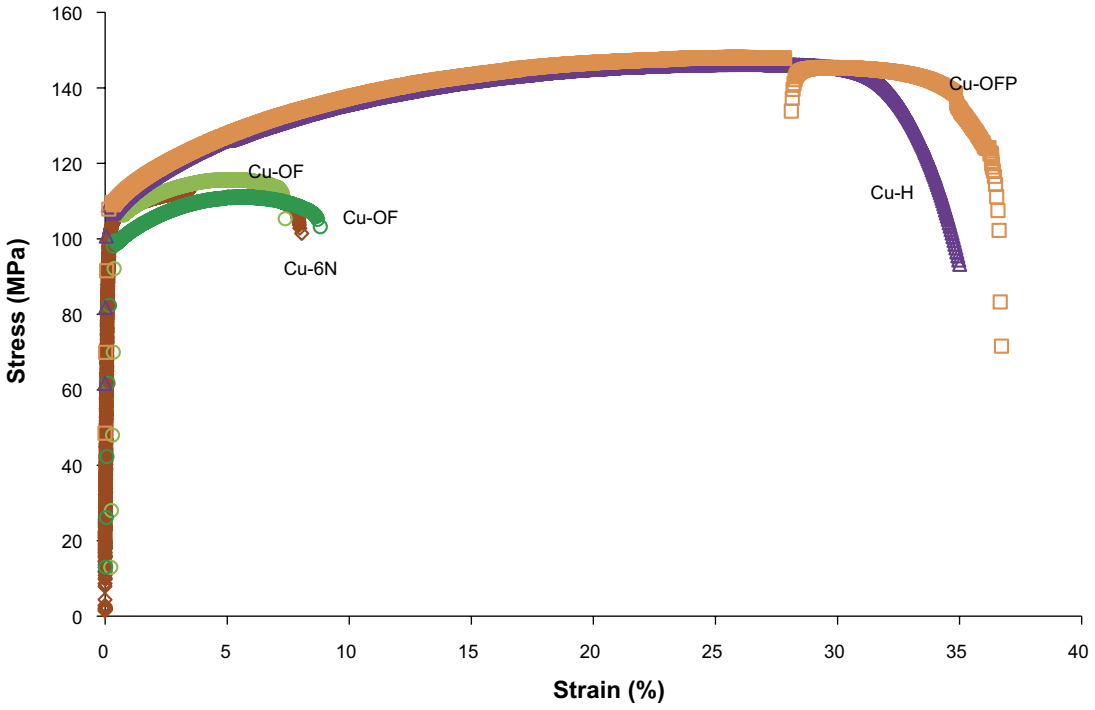

Figure 7-6. *Comparison between minimum creep rates at 75 and 175 °C and the stationary values. From Josefsson and Andersson-Östling (2019).*

8 Creep of cast iron

The inner load bearing part of the canister is made from nodular cast iron. The iron also becomes hot during the initial time after disposal, and thus, it is necessary to consider whether this creep behaviour has been studied. The first two studies, namely, *Martinsson and Larsson (2009)*[5] and Martinsson et al. (2010), concentrated on hot tensile testing and creep testing, respectively. The results can be found in Appendices A6-1 and A6-2.

Nodular cast iron has sufficient strength in compression at room temperature to withstand the expected stresses. The effect of elevated temperatures is less well-known. The results for creep testing at very high temperatures (over 500 °C) have been reported, but the results for the creep testing at lower temperatures (below 300 °C) have not been published. The aim of the project was to evaluate the creep properties at 100 and 125 °C. The testing was performed in tension since no equipment was available for testing in compression. For an additional series at room temperature, acoustic emission monitoring methods were used to further study the creep behaviour.

The results from the testing show that the specimens most likely entered logarithmic creep for all tested stresses. Logarithmic creep means that the creep rate decreases logarithmically until it approaches zero. No further creep strain will result after this threshold has reached, even on a repository time scale. An example of the creep results from 100 °C is given in Figure 8-1. One specimen ruptured during loading, but a metallographic examination indicated that this specimen ruptured due to the amount of graphite nodules present in the gauge length of this specific specimen.

In addition to the hydrogen charging studies performed on copper, similar studies were performed on nodular cast iron. These have been reported in Wu et al. (2015b). It was found that hydrogen readily diffuses in and out of the cast iron.

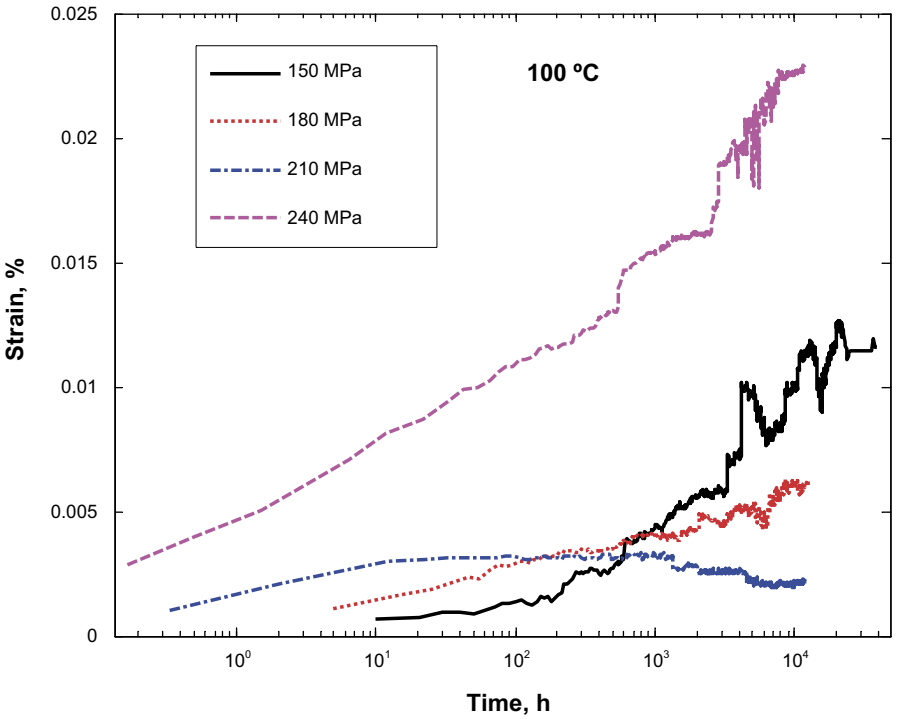

Figure 8-1. *Creep curves for the 100 °C specimens. The creep strain is plotted versus time on the logarithmic scale. Insert cast ID I30. From Martinsson et al. (2010).*

[5] References given in *italics* do not meet SKB´s quality assurance requirements for public reports, see further Section 2.2. These references are presented in the Report list in Appendix 1.

9 Conclusions

From the research presented in this work, a number of conclusions can be drawn. These conclusions are general conclusions; for specific details, the reader is referred to the respective publications. The conclusions are listed below under their respective heading:

Cu-OF, non-phosphorus-doped oxygen-free copper

Cu-OF generally shows brittle behaviour during creep at temperatures from 75 to 450 °C, and a particularly low creep ductility has been observed between 180 and 250 °C. Creep ductility including loading strain often stays well below 20 %. The creep ductility of Cu-OF is generally lower than that of Cu-OFP.

Cu-OFP, phosphorus-doped oxygen-free copper, general comment

Phosphorus-doped copper show high creep ductility at temperatures between 75 and 450 °C, higher than that of Cu-OF. This is valid for at least 20 years, since the longest-running tests are of this duration. Once the influence of phosphorus on ductility is established for long times, predictions about creep ductility can be made.

Cu-OFP, grain size effect on creep

The creep results show that only for the very largest grain size tested (2 000 μm) are the creep properties negatively affected.

Cu-OFP, effects of sulphur on creep

The creep results show that 6 or 12 ppm sulphur has no effect on the creep properties for the two test series that were tested.

Cu-OFP, effects of loading rate on creep

Creep tests show that the loading rate has an effect on the creep strain. However, the total experienced strain, loading plus creep strain, tends to remain constant for all tested loading times.

Cu-OFP, creep crack growth studies

The results from the testing show that it is very difficult to achieve any creep crack propagation in Cu-OFP. This is particularly true at the lower tested temperatures of approximately 75 °C. The material is not notch sensitive at 75 °C.

Cu-OFP, effects of multiaxial stress states on creep

Multiaxial creep tests show the same general tendencies as the creep crack propagation tests. The material is not notch sensitive.

Cu-OFP, hydrogen content effect on creep

In the studies presented in this report, the hydrogen content does not have a significant effect on the creep properties of Cu-OFP. In the case of creep testing of welds that contain oxide inclusions, the results are not clear.

Cu-OFP, electron beam welding (EBW) vs. friction stir welding (FSW)

Creep testing of electron beam welds and friction stir welds show that the latter have generally better creep characteristics that are often undistinguishable from those of the base metal. Because of their much lower hardness, electron beam welds concentrate all deformation to a very narrow band, and the overall properties are thus worse than those of the friction stir welds, which have a hardness like the base material.

Cu-OFP, creep strength weld reduction factors

Creep strength weld reduction factors have been obtained for use in canister design calculations.

Cu-OFP FSW, oxide streaks, processing line inclusions

Oxide streaks can result from the welding process. If these are sufficiently large, the presence of oxide streaks can have a detrimental effect on the creep properties.

Cu-OFP, effects of cold working on creep

General cold working exhausts some of the ductility potential of the material. When this is taken into consideration, the creep properties in the cold-worked material are comparable to those of the non-cold-worked material even if the creep ductility alone is reduced in the cold-worked material.

Cu-OFP, effects of local cold work and indentations on creep

In the performed tests, the performed indentations do not have a strong effect on the creep properties of the specimen as a whole. No large cracks have been found in conjunction with the impressions, but smaller cracks have been found. The extent of these cracks and their long-term effect have not yet been studied.

Cu-OFP, grain boundary sliding

Grain boundary sliding has been observed in Cu-OFP. This phenomenon is difficult to study experimentally, and only limited data from experiments are available.

Cu-OFP, subgrain/subcell structures

The subgrain structures in creep tested material have been studied, and correlations between deformation and subgrain size and shape have been noted.

Slow strain rate tests (SSRT)

Slow strain rate tests have been performed on both Cu-OF and Cu-OFP. SSRT can potentially be used to test material batches in shorter timeframes than proper creep tests.

Creep of cast iron

Cast iron from the proposed cast iron inserts to the canisters has been tested. No significant creep has been noted at 75 and 125 °C.

Acknowledgement

The financial support from the Swedish Nuclear Fuel and Waste Management Co (SKB) is greatly acknowledged. SKB is also thanked for providing test material.

References

SKB's (Svensk Kärnbränslehantering AB) publications can be found at www.skb.com/publications. SKBdoc documents will be submitted upon request to document@skb.se.

References written in italics are not included in this reference list, these can be found in Appendix 1 (for more information see Section 2.2).

Adelus J L, Guttmann V, Scott V D, 1980. Effect of prior cold working on the creep of 314 alloy steel. Materials Science and Engineering 44, 195–204.

Ajaja O, Ardell A J, 1977. Microstructural parameters and steady-state creep. Scripta Metallurgica 11, 1089–1093.

Andersson H, Seitisleam F, Sandström R, 1999. Influence of phosphorous and sulphur as well as grain size on creep in pure copper. SKB TR-99-39, Svensk Kärnbränslehantering AB.

Andersson H C M, Seitisleam F, Sandström R, 2001. Influence of phosphorous on creep in pure copper. In Nuclear waste containment materials. Papers related to the SKB waste disposal programme presented at the Materials Research Society Spring Meeting, April 19, 2001 MRS Spring Meeting, San Francisco, 16–20 April 2001. SKB TR-01-25, Svensk Kärnbränslehantering AB, 41–46.

Andersson H C M, Seitisleam F, Sandström R, 2004. Creep testing of thick-wall copper electron beam and friction stir welds. In Hanchar J M, Stroes-Gascoyne S, Browning L (eds). Scientific Basis for Nuclear Waste Management XXVIII: symposium held in San Francisco, California, USA, 13–16 April 2004. Warrendale, PA: Materials Research Society. (Materials Research Society Symposium Proceedings 824), 51–56.

Andersson H C M, Seitisleam F, Sandström R, 2005. Creep testing of thick wall copper electron beam and friction stir welds at 75, 125 and 175 °C. SKB TR-05-08, Svensk Kärnbränslehantering AB.

Andersson H C M, Seitisleam F, Sandström R, 2007. Creep testing and creep loading experiments on friction stir welds in copper at 75 °C. SKB TR-07-08, Svensk Kärnbränslehantering AB.

Andersson-Östling, H C M, 2010. Mechanical properties of welds at creep activation temperatures. PhD thesis. KTH Royal Institute of Technology, Stockholm.

Andersson-Östling H C M, Sandström R, 2009. Survey of creep properties of copper intended for nuclear waste disposal. SKB TR-09-32, Svensk Kärnbränslehantering AB.

Andersson-Östling H C M, Sandström R, 2011. Effect of loading rate on creep of phosphorous doped copper. SKB TR-11-09, Svensk Kärnbränslehantering AB.

Andersson-Östling H C M, Hagström J, Danielsson M, 2018. Phosphorus in copper intended for nuclear waste disposal. SKB R-17-19, Svensk Kärnbränslehantering AB.

Auerkari P, Rantala J, Salonen J, Laukkanen A, Holmström S, Kinnunen T, 2009. Effects of defects on low temperature creep of OFP copper. In Shibli I A, Holdsworth S R. Creep & Fracture in High Temperature Components – Design & Life Assessment Issues, ECCC Creep Conference, Zürich, 21–23 April 2009, 287–297. DEStech Publications, 287–297.

Björck M, Taxén C, Vuoristo T, Elger R, Zavalis T, Wikström L, Sparr M, 2019. Embedded oxide particles in Friction Stir Welds. Effect on creep and corrosion properties. Posiva SKB Report 10, Posiva Oy, Svensk Kärnbränslehantering AB.

Björkblad A, Faleskog J, 2018. Evaluation of Cu-OFP creep crack growth and theoretical fracture models for Cu-OFP. Posiva SKB Report 03, Posiva Oy, Svensk Kärnbränslehantering AB.

Danielsson M, Andersson-Östling H C M, 2018. Creep testing of Cu-OF. Swerea KIMAB. SKBdoc 1668100 ver 1.0, Svensk Kärnbränslehantering AB.

Davis J R, 2001. Copper and copper alloys. Materials Park, OH: ASM International. (ASM specialty handbook.)

ECCC, 2001. ECCC recommendations, volume 2 part IIb (issue 2), Brite-Euram thematic network BET2-0509 Weld-Creep. European Creep Collaborative Committee.

Frost H F, Ashby M F, 1983. Deformation-mechanism maps. Oxford: Pergamon Press.

Furuta T, Kawasaki S, Nagasaki R, 1973. The effect of cold working on creep rupture properties for helium-injected austenitic stainless steel. Journal of Nuclear Materials 47, 65–71.

Gifkins R C, 1994. Grain-boundary participation in high-temperature deformation: an historical review. Materials Characterization 32, 59–77.

Henderson P J, Sandström R, 1998. Low temperature creep ductility of OFHC copper. Materials Science and Engineering A 246, 143–150.

Henderson P J, Werme L, 1996. Creep testing of copper for radwaste canisters. In Proceedings of EUROMAT 96 – Materials and Nuclear Power, Bournemouth, UK, 21–23 October 1996. Institute of Materials, 227–234.

Henderson P J, Österberg J O, Ivarsson B, 1992. Low temperature creep of copper intended for nuclear waste containers. SKB TR 92-04, Svensk Kärnbränslehantering AB.

Hökmark H, Fälth B, 2003. Thermal dimensioning of the deep repository. Influence of canister spacing, canister power, rock thermal properties and nearfield design on the maximum canister surface temperature. SKB TR-03-09, Svensk Kärnbränslehantering AB.

Ivarsson B, Sandstrom R, 1980. Creep deformation and rupture of butt welded tubes of cold worked AISI 316 steel. Metals Technology 7, 440–448.

Ivarsson B, Österberg J-O, 1988. Creep properties of welded joints in OFHC copper for nuclear waste containment. SKB TR 88-20, Svensk Kärnbränslehantering AB.

Ivarsson B, Österberg J O, Sandström R, Werme L, 1989. Creep properties of welded joints in copper canisters for nuclear waste containment. In Lutz W, Ewing R C (eds). Scientific basis for nuclear waste management XII: Pittsburgh, PA: Materials Research Society. (Materials Research Society Symposium Proceedings 127), 397–402.

Josefsson J, Andersson-Östling H C M, 2019. SSRT testing of Cu. SKB R-18-09, Svensk Kärnbränslehantering AB.

Korzhavyi P A, Sandström R, 2014. Monovacancy in copper: Trapping efficiency for hydrogen and oxygen impurities. Computational Materials Science 84, 122–128.

Leijon G, Ahlström J, Andersson-Östling H C M, 2018. In situ hydrogen charging of OFP copper under creep. SKB R-17-17, Svensk Kärnbränslehantering AB.

Magnusson H, Sandström R, 2007. Creep strain modeling of 9 to 12 pct Cr steels based on microstructure evolution. Metallurgical and Materials Transactions A 38, 2033–2039.

Mannesson K, Andersson-Östling H C M, 2014a. Creep of copper with different NDT sound attenuation. KIMAB-2013-124, Swerea KIMAB. SKBdoc 1411196 ver 1.0, Svensk Kärnbränslehantering AB.

Mannesson K, Andersson-Östling H C M, 2014b. Creep of indented copper – cone, sphere and cylinder. KIMAB-2014-114, Swerea KIMAB. SKBdoc 1442561 ver 1.0, Svensk Kärnbränslehantering AB.

Mannesson K, Andersson-Östling H C M, 2016. Stress application and the effect on creep of copper. SKB R-14-31, Svensk Kärnbränslehantering AB.

Mannesson K, Andersson-Östling H C M, Sandström R, 2013. Influence of local cold work in creep failure of phosphorus doped oxygen free copper. SKB R-13-32, Svensk Kärnbränslehantering AB.

Martinsson Å, Andersson H C M, 2009. The effect of cold work on the creep properties of copper. MRS Proceedings 1193. doi:10.1557/PROC-1193-521

Martinsson Å, Sandström R, 2012. Hydrogen depth profile in phosphorus-doped, oxygen-free copper after cathodic charging. Journal of Materials Science 47, 6768–6776.

Martinsson Å, Andersson-Östling H C M, Seitisleam F, Wu R, Sandström R, 2010. Creep testing of nodular iron at ambient and elevated temperatures. SKB R-10-64, Svensk Kärnbränslehantering AB.

Martinsson Å, Sandström R, Lilja C, 2013. Hydrogen in oxygen-free, phosphorus-doped copper: charging techniques, hydrogen contents and modelling of hydrogen diffusion and depth profile. SKB TR-13-09, Svensk Kärnbränslehantering AB.

Pilloni G, Quadrini E, Spigarelli S, 2000. Interpretation of the role of forest dislocations and precipitates in high-temperature creep in a Nb-stabilised austenitic stainless steel. Materials Science and Engineering A 279 52–60.

Sandström R, 1999. Extrapolation of creep strain data for pure copper. Journal of Testing and Evaluation 27, 31–35.

Sandström R, 2012. Basic model for primary and secondary creep in copper. Acta Materialia 60, 314–322.

Sandström R, 2016a. Influence of phosphorus on the tensile stress strain curves in copper. Journal of Nuclear Materials 470, 290–296.

Sandström R, 2016b. The role of cell structure during creep of cold worked copper. Materials Science and Engineering: A 674, 318–327.

Sandström R, 2017. Formation of a dislocation back stress during creep of copper at low temperatures. Materials Science and Engineering: A 700, 622–630.

Sandström R, 2018. Fundamental models for the creep of metals. In Tanski T, Sroka M Zieliński A (eds). Creep. IntechOpen. doi:10.5772/intechopen.70726

Sandström R, Andersson H C M, 2008a. The effect of phosphorus on creep in copper. Journal of Nuclear Materials 372, 66–75.

Sandström R, Andersson H C M, 2008b. Creep in phosphorus alloyed copper during power-law breakdown. Journal of Nuclear Materials 372, 76–88.

Sandström R, Hallgren J, 2012. The role of creep in stress strain curves for copper. Journal of Nuclear Materials 422, 51–57.

Sandström R, Jin L-Z, 2008. Creep of copper canisters in power-law breakdown. Computational Materials Science 43, 403–416.

Sandström R, Wu R, 2013. Influence of phosphorus on the creep ductility of copper. Journal of Nuclear Materials 441, 364–371.

Sandström R, Hallgren J, Burman G, 2009. Stress strain flow curves for Cu-OFP. SKB R-09-14, Svensk Kärnbränslehantering AB.

Sandström R, Wu R, Hagström J, 2016. Grain boundary sliding in copper and its relation to cavity formation during creep. Materials Science and Engineering: A 651, 259–268.

Sandström R, Waqas Ahmad S, Pasupuleti K T, Mahdavi Shahri M, 2017. Slow strain rate tensile testing of friction stir welded Cu-OFP. Constitutive equations for creep. SKB R-13-33, Svensk Kärnbränslehantering AB.

Savolainen K, Saukkonen T, Mononen J, Hänninen H, 2008. Entrapped oxide particles in friction stir welds of copper. Material Flow during Friction Stir Welding of Copper, 7th International Symposium on Friction Stir Welding, Awaji Island, Japan.

Sherby O D, Klundt R H, Miller A K, 1977. Flow stress, subgrain size, and subgrain stability at elevated temperature. Metallurgical Transactions A 8, 843–850.

Sikka V K, Nahm H, Moteff J, 1975. Some aspects of sub-boundary and mobile dislocations during high temperature creep of AISI 316 and 304 stainless steels. Materials Science and Engineering 20, 55–62.

Sui F, Sandström R, 2016. Slow strain rate tensile tests on notched specimens of copper. Materials Science and Engineering: A 663, 108–115.

Unosson M, 2009. Intryck i koppar. SKBdoc 1205273 ver 2.0, Svensk Kärnbränslehantering AB. (In Swedish.)

Wu R, Sandström R, 2015. Effect of phosphorus content on creep properties of Cu-OFP at 75 and 125 °C. Swerea KIMAB. SKBdoc 1449099, ver 1.0, Svensk Kärnbränslehantering AB.

Wu R, Sandström R, 2018. Influence of cold work and notches on creep failure of Cu-OFP. SKB R-15-04, Svensk Kärnbränslehantering AB.

Wu R, Seitisleam F, Sandström R, 2009. Creep properties of phosphorus alloyed oxygen free copper under multiaxial stress state. SKB R-09-41, Svensk Kärnbränslehantering AB.

Wu R, Seitisleam F, Sandström R, Jin L-Z, 2011. Creep crack growth in phosphorus alloyed oxygen free copper. SKB R-11-11, Svensk Kärnbränslehantering AB.

Wu R, Sandström R, Jin L-Z, 2013. Creep crack growth in phosphorus alloyed oxygen free copper. Materials Science & Engineering A 583, 151–160.

Wu R, Pettersson N, Martinsson Å, Sandström R, 2014. Cell structure in cold worked and creep deformed phosphorus alloyed copper. Materials Characterization 90, 21–30.

Wu R, Hagström J, Sandström R, 2015a. Grain boundary sliding in phosphorus alloyed oxygen-free copper under creep. SKB R-15-14, Svensk Kärnbränslehantering AB.

Wu R, Ahlström J, Magnusson H, Frisk K, Martinsson Å, 2015b. Charging, degassing and distribution of hydrogen in cast iron. SKB R-13-45, Svensk Kärnbränslehantering AB.

Yagodzinsky Y, Malitckii E, Saukkonen T, Hänninen H, 2012. Hydrogen-enhanced creep and cracking of oxygen-free phosphorus-doped copper. Scripta Materialia 67, 931–934.

Yao X, Sandström R, 2000. Study of creep behaviour in P-doped copper with slow strain rate tensile tests. SKB TR-00-09, Svensk Kärnbränslehantering AB.

Appendix 1

References given in *italics* do not meet SKB´s quality assurance requirements for public reports and are not included in the Reference list. These references are instead presented in the Report list below, see further Section 2.2.

Table A1-1. Report list for copper research preformed at Swerim AB, previously SIMR (Swedish Institute for Metals Research) and Swerea KIMAB.

Author(s), title, year	Source*	Alternate version	Content
Andersson H C M, 2001. *Superalloy friction stir welding materials.*	SIMR, IM-2001-815		Several candidate tool materials for the FSW welding is studied.
Andersson H C M, 2005. *Creep crack propagation in pure copper at 75 °C.*	Swerea KIMAB Technical report KIMAB-2008-128		Creep crack propagation study on Cu-OFP using new digitalised potential drop collection methods. Work first published in 2005 but the report was renumbered in 2008.
Andersson H C M, Lindblom J, 2005. *Loading test rig for creep machines.*	SIMR, IM-2005-130		New design for creep test rigs with longer stroke than dead weight lever designs.
Andersson H , Seitisleam F, Sandström R, 1999. Influence of phosphorous and sulphur as well as grain size on creep in pure copper.	SKB TR-99-39		Creep of Cu-OFP and Cu-OF. The effect of sulphur content, phosphorus content and grain size on the creep properties are studied.
Andersson H C M, Seitisleam F, Sandström R, 2001. Influence of phosphorous on creep in pure copper.	Proc. of MRS Spring Meeting, San Francisco, 16–20 April 2001	SKB TR-01-25	Abridged version of Andersson et.al (1999) containing only the phosphorus variation.
Andersson H C M, Seitisleam F, Sandström R, 2004. Creep testing of thick-wall copper electron beam and friction stir welds.	Proc. of MRS Spring Meeting, San Francisco, 12–16 April, Mat. Res. Soc. Symp. Proc. Vol. 824, 51–56		Published version of Andersson et al. (2004).
Andersson H C M, Seitisleam F, Sandström R, 2004. Creep testing of thick wall copper electron beam and friction stir welds at 75, 125 and 175 °C.	SKB TR-05-08	Swedish Institute for Metals Research, IM-2004-110	Cu-OFP. Creep test studies of friction stir welds and electron beam welds. Electron beam welds are shown to exhibit poor mechanical properties.
Andersson H C M, Seitisleam F, Sandström R, 2007. Creep testing and creep loading experiments on friction stir welds in copper at 75 °C.	SKB TR-07-08		Creep studies of Cu-OFP welds. The effect on the creep results of the creep loading time is studied. Loading times up to 6 months are included.
Andersson-Östling H C M, 2009. *High speed tensile testing of annealed copper from the lid TX184.*	Swerea KIMAB Technical report KIMAB-268013		High speed tensile testing of Cu-OFP. Strain rates used varied from 0.1 %/s to 1 000 %/s.
Andersson-Östling H C M, 2010. Mechanical properties of welds at creep activation temperatures.	Doctoral thesis		Doctoral thesis by Andersson-Östling on welds in copper intended for spent nuclear fuel disposal canisters.
Andersson-Östling H C M, 2013. *Measurements of hardness and P, S and O levels in copper.*	Swerea KIMAB Technical report, KIMAB-2013-123		Measurements of P, S and O in test specimens from Mannesson and Andersson-Östling (2014) and Martinsson and Andersson Östling (2009).

Table A1-1. Continued.

Author(s), title, year	Source*	Alternate version	Content
Andersson-Östling H C M, Sandström R, 2009. Survey of creep properties of copper intended for nuclear waste disposal.	SKB TR-09-32		Overview of all testing performed up to 2008. All results are presented and conclusions made. Modelling and constitutive equations.
Andersson-Östling H C M, Sandström R, 2011. Effect of loading rate on creep of phosphorous doped copper.	SKB TR-11-09	Swerea KIMAB technical report KIMAB-2010-134	First study on effect of the rate of load application. The time of application was varied between 1 hour and 6 months. One finding was that the total strain measured on the specimen was roughly constant but that the strain shifted from creep strain towards more loading strain as the loading time was increased.
Andersson-Östling H C M, Hagström J, Danielsson M, 2018. Phosphorus in copper intended for nuclear waste disposal.	SKB R-17-19	Swerea KIMAB technical report KIMAB-2016-105	An overview of creep in copper with phosphorus. The grains size distribution of Cu-OFP is modelled and also studied by EBSD microscopy. A small number of creep tests has also been included. The main conclusion from the study is that the phosphorus effect of increasing creep ductility is present at short term creep tests, up to 20 years. If the surrounding copper matrix around the phosphorus atoms is not changed at the temperatures of the repository, it is likely that the properties stays the same during the same during the repository of the canisters.
Björck M, Elger R, Vuoristo T, Cederqvist L, 2019. Embedded oxide particles in Friction Stir Welds. Effect on creep and corrosion properties.	Posiva SKB Report 10		Specimens cut from welds prepared using materials with different levels of oxidation prior to welding are studied. Creep test specimens are cut from the welds in a consistent manner perpendicular to the welds. The results show acceptable creep properties for specimens cut from weld with 0 and 0.1 µm oxides. Thicker oxides yield unacceptable creep properties.
Björkblad A, Faleskog J, 2018. Evaluation of Cu-OFP creep crack growth and theoretical fracture models for Cu-OFP.	Posiva SKB Report 03		Studies of fracture surfaces from previous experiments, mainly from Wu et.at. (2013) and Andersson (2005). A literature survey of the area is included and the main conclusion from the study is that cracks formed in any way during creep is immediately blunted and the stress concentration diminished.
Danielsson M, Andersson-Östling H C M, 2018. Creep testing of Cu-OF.	SKBdoc 1668100 ver 1.0		A repeat study of old Cu-OF tests from Henderson and Sandström (1998) using modern dynamic creep test equipment and procedures. The low ductility at 2015 and 175 °C remains in this study.
Engberg G, Karlsson S, von Walden E, 1986. *Creep and elevated tensile properties of Cu-Zr and Cu-Zr-P alloys with high electrical conductivity. Revised version of IM-1921.*	SIMR, IM-2099		Study aimed at the copper manufacturers. Zirconium alloying to increase strength. Tensile and hot tensile tests. Creep tests up to 0.1 %.
Henderson P J, 1994. *Creep of copper.*	KASAM/SKI International Seminar on Design and Manufacturing of Copper Canisters for Nuclear Waste, Sollentuna, Sweden, 27–28 April		Highly abridged version of Henderson et al. (1992).
Henderson P J, Lindblom J, 1995. *Results of round-robin tensile testing and effect of specimen diameter on the tensile and creep properties of high-purity copper.*	SIMR, Progress Report 95-2		Internal progress report. Contains a study on the effect of cold deformation in 5 and 10 mm diameter specimens. The conclusion is that annealing is required if the diameter is smaller than 10 mm.

Author(s), title, year	Source*	Alternate version	Content
Henderson P J, Seitisleam F, 1995. *Creep crack growth in oxygen-free phosphorous copper, Cu-OFP.*	SIMR, Progress report for SKB	KIMAB-2008-129	Creep crack propagation study. No crack propagation measured. 215 °C.
Henderson P J, Werme L, 1996. Creep testing of copper for radwaste canisters.	Proc EUROMAT 96 – Materials and Nuclear Power, Bournemouth, United Kingdom, 21–23 October, 227–234	IM-3374	Overview of testing up to 1995. Contains results from IM-3327 and IM-3506.
Henderson P J, Sandström R, 1998. Low temperature creep ductility of OFHC copper.	Materials Science and Engineering A 246, 143–150		Creep studies of Cu-OFHC. Results from the earliest studies published around 1985–1992.
Henderson P J, Österberg J O, Ivarsson B, 1992. Low temperature creep of copper intended for nuclear waste containers.	SKB TR 92-04		Five materials studied. Grain size, silver content and oxygen content studied in creep testing.
Ivarsson B, Österberg J O, 1988. Creep properties of welded joints in OFHC copper for nuclear waste containment.	SKB TR 88-20	IM-2384	Creep of copper at 75, 110 and 145 °C. Electron beam welds where PM, HAZ and CW were tested. Component testing of containers with internal pressure.
Ivarsson B, Österberg J O, Sandström R, Werme L, 1989. Creep properties of welded joints in copper canisters for nuclear waste containment.	Scientific basis for nuclear waste management XII: Pittsburgh, PA: Materials Research Society. (Materials Research Society Symposium Proceedings 127), 397–402	IM-2478	Abridged version of IM-2384 containing only uniaxial creep.
Josefsson J, Andersson-Östling H C M, 2019. SSRT testing of Cu.	SKB R-18-09		SSRT testing of Cu-OF and Cu-OFP. A methodology for short term testing of different grades of copper has been produced and tested. The results confirm previous results where Cu-OF exhibit lower ductility than Cu-OFP.
Leijon G, Ahlström J, 2014. *In situ hydrogen charging of OFP copper under creep.*	Swerea KIMAB Technical report, KIMAB-2014-108		As a follow-up to the studies on hydrogen charging of copper experiments was conducted on copper being charged during creep testing The work is concluded in Leijon et al. (2018).
Leijon G, Ahlström J, Andersson-Östling H C M, 2018. In situ hydrogen charging of OFP copper under creep.	SKB R-17-17		Leijon and Ahlström (2014) is updated by the inclusion of reference tests without in situ hydrogen charging.
Lindblom J, Henderson P J, Seitisleam F, 1992. *Creep, stress relaxation and tensile testing of oxygen free phosphorous copper (Cu-OFP) intended for nuclear waste containment*.	SIMR, IM-2936		Version of Henderson et al. (1992). A few extra results.
Lindblom J, Henderson P J, Seitisleam F, 1995. *Creep testing of oxygen-free phosphorous copper and extrapolation of the results.*	SIMR, IM-3197		Large creep study with extrapolation of the results. Cu-OFP tensile tested and creep tested. Temperatures from 75 to 600 °C but mostly 200–300 °C.

Table A1-1. Continued.

Author(s), title, year	Source*	Alternate version	Content
Mannesson K, Andersson-Östling H C M, 2014a. Creep of copper with different NDT sound attenuation.	SKBdoc 1411196 ver 1.0		A study of extruded tube materials that exhibit different sound attenuation when ultrasound inspected after manufacturing. This difference in sound attenuation is likely due to differences in grain size in the material. The differences studied were not found to have any significant effect on the creep properties.
Mannesson K, Andersson-Östling H C M, 2014b. Creep of indented copper – cone, sphere and cylinder.	SKBdoc 1442561 ver 1.0	Swerea KIMAB technical report KIMAB-2014-114	The second study on the effect of local cold deformation in annealed Cu-OFP. In this study smaller indentations of three different shapes were used. Shallow cracks in the surface region of the indentations were found.
Mannesson K, Andersson-Östling H C M, 2016. Stress application and the effect on creep of copper.	SKB R-14-31	Swerea KIMAB technical report KIMAB-2014-112	Continuation of the work in Andersson-Östling and Sandström (2011). It is found that a stepwise loading of a creep test yields a decreased creep life when compared to a instantaneously loaded specimen at the same final load.
Mannesson K, Andersson-Östling H C M, Sandström R, 2013. Influence of local cold work in creep failure of phosphorus doped oxygen free copper.	SKB R-13-32		The first study on the effect of local cold deformation in annealed Cu-OFP. In this study the cold deformation was found to increase the creep strength of the material around the impression but not induce any cracks.
Martinsson Å, Andersson H C M, 2009. The effect of cold work on the creep properties of copper.	MRS Proceedings, 1193. doi:10.1557/PROC-1193-521		Published version of Martinsson and Andersson-Östling (2009). Peer reviewed conference proceedings.
Martinsson Å, Andersson-Östling H C M, 2009. *Effect of cold work on creep properties of oxygen-free copper.*	Swerea KIMAB Technical report KIMAB-2009-109		Creep specimens with a defined degree of cold work either in tension or compression are creep tested. The results show that overall ductility is affected roughly the same amount as the pre-testing cold working.
Martinsson Å, Larsson M, 2009. *Hot tensile testing of nodular cast iron.*	Swerea KIMAB Technical report KIMAB-264016		Hot tensile testing of cast iron cut from a canister insert.
Martinsson Å, Sandström R, 2012. Hydrogen depth profile in phosphorus-doped, oxygen-free copper after cathodic charging.	Journal of Materials Science 47, 6768–6776		A study on the penetration of hydrogen into copper and the depth of penetration. No practical creep experiments but forms the basis for Martinsson et al. (2013) and subsequently the experiments in Leijon and Ahlström (2014) and Leijon et al. (2018).
Martinsson Å, Andersson-Östling H C M, Seitisleam F, Wu R, Sandström R, 2010. Creep testing of nodular iron at ambient and elevated temperatures.	SKB R-10-64	Swerea KIMAB technical report KIMAB-2009-131	Creep testing of nodular cast iron intended for the cast iron insert in the canisters. Test specimens extracted from different positions in the cast insert. The spread of the results is large but in essence the properties are such that the insert can be expected to withstand the estimated loads of the repository.
Martinsson Å, Sandström R, Lilja C, 2013. Hydrogen in oxygen-free, phosphorus-doped copper: charging techniques, hydrogen contents and modelling of hydrogen diffusion and depth profile.	SKB TR-13-09		The published version of Martinsson and Sandström (2012). It is found that it is difficult to charge copper with hydrogen and that as soon as the charging is stopped the amount of hydrogen in the copper decreases rapidly.
Sandström R, 1999. Extrapolation of creep strain data for pure copper.	Journal of Testing and Evaluation. 27, 31–35		Study on the extrapolation of creep results to long times.

Author(s), title, year	Source*	Alternate version	Content
Sandström R, 2012. Basic model for primary and secondary creep in copper.	Acta Materialia 60, 314–322		Modelling paper where a creep model is evaluated against experiments on austenitic stainless steels and Cu-OFP. The copper experiments are reported in Andersson et al. (2007) and Andersson-Östling and Sandström (2009).
Sandström R, 2016a. Influence of phosphorus on the tensile stress strain curves in copper.	Journal of Nuclear Materials 470, 290–296		A modelling study on the creep curves obtained from Cu-OF and Cu-OFP. The cavitation model is shown to be able to adequately describe the differences.
Sandström R, 2016b. The role of cell structure during creep of cold worked copper.	Materials Science and Engineering: A 674, 318–327		The role of the cell structure and its development during creep is studied. Extended version of the analytical and modelling part of Wu et al. (2014).
Sandström R, 2017. Formation of a dislocation back stress during creep of copper at low temperatures.	Materials Science and Engineering: A 700, 622–630		Modelling of creep curves. The basic model and experiments are taken from Sandström (2012).
Sandström R, Andersson H C M, 2008a. The effect of phosphorus on creep in copper.	Journal of Nuclear Materials 372, 66–75		Reassessments of creep tests presented in Henderson and Sandström (1998), Andersson et al. (1999), Henderson and Werme (1996) and Sandström (1999). The effect of phosphorus on the creep properties is studied.
Sandström R, Andersson H C M, 2008b. Creep in phosphorus alloyed copper during power-law breakdown.	Journal of Nuclear Materials 372, 76–88		Reassessments of creep tests presented in Lindblom et al. (1992), Seitisleam et al. (1995), Henderson and Werme (1996) and Andersson et al. (1999). Also included are slow strain rate tests from 2000. Extensive modelling of the results.
Sandström R, Hallgren J, 2012. The role of creep in stress strain curves for copper.	Journal of Nuclear Materials 422, 51–57		Evaluation and modelling study on slow strain rate tests on Cu-OFP.
Sandström R, Jin L-Z, 2008. Creep of copper canisters in power-law breakdown.	Computational Materials Science 43, 403-416		Finite element modelling of the copper canister.
Sandström R, Wu R, 2007. Origin of the extra low creep ductility of copper without phosphorus.	SKB TR-07-02	KIMAB-2007-101	The early experiments (1985–1992) of Cu-OF are studied and new metallography has been presumed. A model using the cavitation properties is developed.
Sandström R, Wu R, 2013. Influence of phosphorus on the creep ductility of copper.	Journal of Nuclear Materials 441, 364–371		Modelling study on creep properties of Cu-OFP. Cavitation studies on Cu-OF and Cu-OFP tested at 215 °C. The Cu-OFP material come from Henderson et.al (1992) and from Andersson-Östling and Sandström (2009).
Sandström R, Wu R, Hagström J, 2016. Grain boundary sliding in copper and its relation to cavity formation during creep.	Materials Science and Engineering A 651, 259–268		The published version of Wu et al. (2015a).
Sandstrom R, Waqas Ahmad S, Pasupuleti K T, Mahdavi Shahri M, 2017. Slow strain rate tensile testing of friction stir welded Cu-OFP. Constitutive equations for creep.	SKB R-13-33		Extensive study on slow strain rate testing of Cu-OFP performed at the Royal Institute of Technology. Modelling of creep behaviour included.

Table A1-1. Continued.

Author(s), title, year	Source*	Alternate version	Content
Seitisleam F, Henderson P J, 1996. *Creep of copper for nuclear waste containment – Results of testing performed in 1996.*	SIMR, IM-3506		Continuation of the work presented in IM-3327. Diffusion creep testing and creep crack propagation testing of Cu-OFP.
Seitisleam F, Henderson P J, Lindblom J, 1995. *Creep of copper for nuclear waste containment – Results of creep and tensile tests on Cu-OF, Cu-OFP cathode copper and welded joints.*	SIMR, IM-3327		Large report on both Cu-OF and Cu-OFP. Creep testing and tensile testing. Electrolytic copper dismissed as a candidate material.
Sui F, Sandström R, 2016. Slow strain rate tensile tests on notched specimens of copper.	Materials Science and Engineering: A 663, 108–115		Slow strain rate testing at 10^{-6} and 10^{-7} s^{-1} at 75 and 125 °C. The results are modelled and the lack of observed cavitied commented. The results show no significant difference for specimens conducted at either strain rate.
Wu R, 2011a. *Guideline and procedure for evaluating processing line inclusions in friction stir welded copper canister – in combination with case study.*	Swerea KIMAB Technical report, KIMAB-2011-105		A study on the metallographic methods of evaluating processing line inclusions. It is stated that hydrogen annealing is not always needed to examine the inclusions.
Wu R, 2011b. *Processing line inclusion (PLI) and joint line hooking (JLH) in Cu-OFP friction stir weld – part 2: hot tensile and creep properties.*	Swerea KIMAB Technical report KIMAB-2011-114		Processing line inclusions study. Hot tensile and creep tests on a Cu-OFP weld.
Wu R, 2011c. *Processing line inclusion (PLI) and joint line hooking (JLH) in Cu-OFP friction stir weld – part 1: metallographic examinations.*	Swerea KIMAB Technical report KIMAB-2011-111		Metallography part of the processing line inclusions study. Cu-OFP welds.
Wu R, Sandström R, 2015. Effect of phosphorus content on creep properties of Cu-OFP at 75 and 125 °C.	SKBdoc 1449099, ver 1.0	Swedish Institute for Metals Research Technical Report, KIMAB-2015-102	Creep experiments on Cu-OFP with different grains sizes and phosphorus content. The copper materials studied were lab charges. The results are not conclusive and could be connected to the material being produced in an unconventional way from all other creep tests performed at the institute. The total ductility was above 30 % for all specimens though.
Wu R, Sandström R, 2018. Influence of cold work and notches on creep failure of Cu-OFP.	SKB R-15-04		Creep experiments using uniaxial, compact tension, notched and plate shear specimens of Cu-OFP. The actual failure mode of the specimen is given attention and the cavity formation close to the fracture is identified.
Wu R, Seitisleam F, Sandström R, 2009. Creep properties of phosphorus alloyed oxygen free copper under multiaxial stress state.	SKB R-09-41	Swerea KIMAB technical report KIMAB-2009-119	Multiaxial stress state creep study. The used specimen was a notched variant of the standard uniaxial creep specimen. Several different notch acuilies was studied.
Wu R, Seitisleam F, Sandström R, Jin L-Z, 2011. Creep crack growth in phosphorus alloyed oxygen free copper.	SKB R-11-11	Swerea KIMAB technical report KIMAB-2010-102	Creep crack growth study on Cu-OFP the studies main conclusion is that whatever the crack propagation properties are the failure is not brittle. Problems with the test setup and the result evaluation was encountered. A chapter on modelling of the results is included.
Wu R, Sandström R, Jin L-Z, 2013. Creep crack growth in phosphorus alloyed oxygen free copper.	Materials Science & Engineering A 583, 151–160		Published version of Wu et al. (2011), SKB Report, R-11-11.

Author(s), title, year	Source*	Alternate version	Content
Wu R, Pettersson N, Martinsson Å, Sandström R, 2014. Cell structure in cold worked and creep deformed phosphorus alloyed copper.	Materials Characterization 90, 21–30		Transmission electron microscopy studies on material from Martinsson and Andersson-Östling (2009) and Martinsson and Andersson (2009). Special emphasis is placed on the development of the sub cell structure with the amount of strain in the material.
Wu R, Hagström J, Sandström R, 2015. Grain boundary sliding in phosphorus alloyed oxygen-free copper under creep.	SKB R-15-14		Experiments aimed at identifying the amount of grain boundary sliding in Cu-OFP. Only one or two instances of sliding was found in any specimen. Results inconclusive as a result.
Wu R, Ahlström J, Magnusson H, Frisk K, Martinsson Å, 2015. Charging, degassing and distribution of hydrogen in cast iron.	SKB R-13-45		Companion study to Martinsson et.al (2013) but on nodular cast iron. It is found that hydrogen readily diffuses in and out of the cast iron.
Yngrén L, 1985. *Konstitutiva ekvationer för krypning hos renkoppar. (In Swedish.)*	SIMR, IM-1970		Literature survey regarding creep of copper studies pre 1985. Contains some modelling and extrapolation of the results found. Cu-OFHC, Cu-OF and Cu-O.

* Swerim AB was previously called Swedish Institute for Metals Research (SIMR) and Swerea KIMAB. The current address is Swerim AB, Box 7047, 164 40, Kista, Sweden.
** SKB reports and technical reports may be downloaded on https://www.skb.se/publikationer/

Appendix 2

Table A2-1. Chemical compositions where known for the reports in Appendix 1.

Material	Ag	Al	As	Bi	Cd	Co	Cr	Fe	H	Hg	Mn	Ni	O	P	Pb	S	Sb	Se	Si	Sn	Te	Zn	Zr	Reference
Published data (1)								< 3				< 5			< 1							< 10		*Yngrén (1985)*
Published data (2)	1		< 1					< 1				1			< 1	1	1							*Yngrén (1985)*
Published data (3)																								*Yngrén (1985)*
Published data (4)	< 1		< 1					4				< 1	2		< 1	< 1		< 1						*Yngrén (1985)*
Published data (5)	< 1		< 1															< 1		< 1				*Yngrén (1985)*
Published data (6)	2							< 1				2	31		< 1	1		< 1			< 1			*Yngrén (1985)*
Published data (7)													25	5										*Yngrén (1985)*
Published data (8)	< 2							1				1		8										*Yngrén (1985)*
Published data (9)																								*Yngrén (1985)*
Published data (10)			< 10					< 10				< 10		20						< 1		< 10		*Yngrén (1985)*
Published data (11)			< 10									< 10		20						< 1		< 10		*Yngrén (1985)*
Published data (12)								< 2				< 2			< 1					< 1				*Yngrén (1985)*
Batch 000	20	1	2	0.4	< 1	< 10	< 3	6	0.16	< 1	2	3	1.2	2	0.5	10	< 3	< 1	< 1	< 3	< 3	9	< 3	Henderson and Sandström (1998)
Batch 100	16	1.5	3	0.3	< 1	< 10	< 3	5	0.69	< 1	2	3	1.6	2	0.5	10	3	< 1	< 1	< 3	< 3	< 1	< 3	Henderson and Sandström (1998)
Batch 200	10	< 1	< 1	< 1	< 1	< 10	< 3	2	< 0.10	< 1	< 1	< 3	1.1	< 1	1	6	< 3	< 1	< 1	< 3	< 3	< 1	< 3	Henderson and Sandström (1998)
Batch 300	1500	1	< 1	< 1	< 1	< 10	< 3	2	0.1	< 1	< 1	3	0.9	< 1	< 1	6	< 3	< 1	< 1	< 3	< 3	< 1	< 3	Henderson et al. (1992)
Batch 400 (IM)	9.6	9.5	1.4		< 0.1	< 0.1				< 0.1		3.3		59	0.7		1.8				0.6	0.1	< 0.1	*Lindblom et al. (1995)*
Batch 500 (IM)	15	9	1.1		< 0.1	< 0.1				< 0.1		0.8	0.9	54	0.8		1.9				0.2	< 0.1	< 0.1	*Lindblom et al. (1995)*
Batch 600 weld	47	1	4	4	3		2	4			2	3	1.3	3	3	3	3	1	4	3	< 10	< 1		*Seitisleam et al. (1995)*
Batch 700 plate left	12	< 1	3	3	< 1		< 1	3			2	1	1.4	68	3	3	1	1	4	3	< 10	< 1		*Seitisleam et al. (1995)*
Batch 700 plate right	12	< 1	3	2	2		1	4			2	< 1	1.4	66	4	3	2	1	4	1	< 10	< 1		*Seitisleam et al. (1995)*
Batch 700 weld bottom	12	< 1	< 1	3	1		2	4			2	3	1.3	66	4	3	< 1	< 1	4	2	< 10	< 1		*Seitisleam et al. (1995)*
Batch 700 weld top	12	< 1	4	3	2		< 1	5			2	2	1.1	64	3	3	1	1	3	2	< 10	< 1		*Seitisleam et al. (1995)*

Table A2-1. Continued.

Material	Ag	Al	As	Bi	Cd	Co	Cr	Fe	H	Hg	Mn	Ni	O	P	Pb	S	Sb	Se	Si	Sn	Te	Zn	Zr	Reference
Batch 720 cylinder	13	< 1	5	2	2		2					< 1	1.7	58	1	2	< 1	< 2	2	< 1	< 10	< 1		*Seitisleam and Henderson (1996)*
Batch 720 lid	12	< 1	7	1	2		< 1					< 1	1.7	46	4	3	1	< 2	2	1	< 10	1		*Seitisleam and Henderson (1996)*
Batch 800 cathode	12	< 1	5	< 1	2		< 1	3			2	3	7	4	3	< 1	2	1	3	< 1	< 10	< 1		*Seitisleam and Henderson (1996)*
Batch 820 cathode	1	< 1	8	1	2		1					< 1	51	< 1	< 1	< 1	< 1	< 2	2	< 1	< 10	< 1		*Seitisleam and Henderson (1996)*
Cu65_450_S12									< 0.5				1.1	67		12								Andersson et al. (1999)
CuP0_300									< 0.5				1.1	< 1		6								Andersson et al. (1999)
CuP105_450									< 0.5				1.1	106		6								Andersson et al. (1999)
CuP30_450									< 0.5				1.2	29		6								Andersson et al. (1999)
CuP60_100									< 0.5					58		6								Andersson et al. (1999)
CuP60_2000									< 0.5				1.3	62		6								Andersson et al. (1999)
CuP60_350									< 0.5				1.1	58		6								Andersson et al. (1999)
CuP60_800									< 0.5				1.6	57		6								Andersson et al. (1999)
Lid L21/TX104 cast L760	13		< 1	< 1	< 1	< 1	< 1	2			< 0.5	2	1–2	45–60	< 1	5	1	< 1		< 0.5	< 1	< 1		Andersson-Östling and Sandström (2011)
T48-R2	13.5		0.82	0.12	< 0.003			1.5	0.5		< 0.1	0.9	0.8–1.5	72	0.28	4.4	0.06	< 0.09		0.07	0.05	< 0.1		Mannesson et al. (2013)
T58													3.2	54		< 5								*Andersson-Östling (2013)*

Material	Ag	Al	As	Bi	Cd	Co	Cr	Fe	H	Hg	Mn	Ni	O	P	Pb	S	Sb	Se	Si	Sn	Te	Zn	Zr	Reference
M1LP									0.56				6.9	32		11.6								Wu and Sandström (2015)
M2HP									0.52				7.3	113		12.3								Wu and Sandström (2015)
Ref phosporus variation									0.58				3.1	65		3								Wu and Sandström (2015)
04 G221 OF1	16		1	0.5	0.5	0.5	0.5	3			0.5	1	1	1	1	2	2	< 1		1	< 1	1		Daniels-son and Andersson-Östling (2018)

* Chemical data from Yngrén, 1985 are from the literature survey. 1: Burghoff, Blank 1947, 2: Schwope, Smith, Jackson 1949, 3: Jenkins, Digges 1950, 4: Feltman, Meakin 1959, 5: Barrett, Sherby 1964, 6: Schwope, Smith, Jackson 1949, 7: Bowers, Lushey 1978, 8: Burghoff, Blank 1947 and 1945, 9: Kouta, Webster 1981, 10 and 11: Drefahl, Kleinau 1982, 12: Burghoff, Blank 1947

Table A2-2. Copper type and material format for the tested materials.

Material	Copper type	As received format	Lid, weld or tube number if applicable	Grain size (µm)	Reference
Batch 000	Cu-OF	100 x 100 mm forged bars		60	*Henderson (1994)*, Henderson and Sandström (1998)
Batch 100	Cu-OF	Edge of 100 x 100 forged bars EB-welded together		370	*Henderson (1994)*, Henderson and Sandström (1998)
Batch 200	Cu-OF	10 mm diameter hot extruded (800 °C) bars		45	*Henderson (1994)*, *Henderson and Lindblom (1995),* Henderson and Sandström (1998)
Batch 300	Cu-OFS	10 mm diameter extruded bars		35	Henderson (1994), *Henderson and Lindblom (1995), Seitisleam et al. (1995)*
Batch 400 (IM)	Cu-OFP	10 mm diameter extruded bars		45	Henderson (1994), *Lindblom et al. (1995)*, Henderson and Werme (1996)
Batch 500 (IM)	Cu-OFP	30 mm hot rolled plate		115	*Lindblom et al. (1995), Henderson and Lindblom (1995), Seitisleam et al. (1995), Seitisleam and Henderson (1996)*, Henderson and Werme (1996)
Batch 600 weld	Cu-OF	Weld	Block reference 5E1307	variable	*Seitisleam et al. (1995)*, Henderson and Werme (1996)

Table A2-2. Continued.

Material	Copper type	As received format	Lid, weld or tube number if applicable	Grain size (µm)	Reference
Batch 700 plate left	Cu-OFP	Hot-worked blocks EB-welded together to one block 115 x 95 x 165 mm		238	*Seitisleam et al. (1995), Seitisleam and Henderson (1996)*, Henderson and Werme (1996)
Batch 700 plate right	Cu-OFP			345	
Batch 700 weld bottom	Cu-OFP			variable	
Batch 700 weld top	Cu-OFP			variable	
Batch 720 cylinder	Cu-OFP	Welded joint	Lid W92, 5E1585	variable	*Seitisleam et al. (1995), Seitisleam and Henderson (1996)*, Henderson and Werme (1996)
Batch 720 lid	Cu-OFP	Welded joint	Lid W92, 5E1585	variable	
Batch 800 cathode	Cu-cathode	18 x 74 x 180 mm cathode		anisotropic	*Seitisleam et al. (1995), Seitisleam and Henderson (1996)*, Henderson and Werme (1996)
Batch 820 cathode	Cu-cathode	Cathode tube length 70 mm, 30 mm diam, 5 mm thickness		anisotropic	
Cu65_450_S12	Cu-OFPS	20 mm diameter hot extruded bar		450	Andersson et al. (1999)
CuP0_300	Cu-OF			300	
CuP105_450	Cu-OFP			450	
CuP30_450	Cu-OFP			450	
CuP60_100	Cu-OFP			100	
CuP60_2000	Cu-OFP			2 000	
CuP60_350	Cu-OFP			350	
CuP60_800	Cu-OFP			800	
Lid L21/TX104 cast L760	Cu-OFP	Forged lid	Lid L21/TX104 cast L760		Andersson-Östling and Sandström (2011)
T48-R2	Cu-OFP	extruded tube	T48-R2		Mannesson et al. (2013)
T58	Cu-OFP	extruded tube	T58	198	*Andersson-Östling (2013)*
M1LP	Low P copper	Test cast	111025101	420	Wu and Sandström (2015)
M2HP	High P copper	Test cast	111032101	600	
Ref phosporus variation	Cu-OFP	Test cast	111027101	150	
04 G221 OF1	Cu-OF	extruded rods	04 G221 OF1		Danielsson and Andersson-Östling (2018)

Appendix 3

Table A3-1. Tabulated data points for tensile tests in the reports in Appendix 1, round specimens.

Specimen ID	Copper batch	Temp. (°C)	Anneal. time (min)	Anneal. temp (°C)	Strain rate (s^{-1})	Rp0.2 (MPa)	Rm (MPa)	Elong. (%)	Area red. (%)	Reference
Batch 000 average	Batch 000	22	0							Henderson et al. (1992)
Batch 100 average	Batch 100	22	0							Henderson et al. (1992)
Batch 200 average	Batch 200	22	0			50	234	61		Henderson et al. (1992)
Batch 300 average	Batch 300	22	0			57	246	59		Henderson et al. (1992)
Batch 400 average	Batch 400	22	0			46	239	60		Henderson et al. (1992)
Ref_11_400 ref	Batch 400	22	0							*Lindblom et al. (1995)*
Ref_11_1	Batch 400	26	0		0.0001	97	243	46	94	*Lindblom et al. (1995)*
Ref_11_2	Batch 400	100	0		0.0001	93	212	43	92	*Lindblom et al. (1995)*
Ref_11_3	Batch 400	150	0		0.0001	67	196	44	92	*Lindblom et al. (1995)*
Ref_11_4	Batch 400	200	0		0.0001	84	183	44	88	*Lindblom et al. (1995)*
Ref_11_5	Batch 400	250	0		0.0001	67	165	52	90	*Lindblom et al. (1995)*
Ref_11_6	Batch 400	300	0		0.0001	82	155	50	94	*Lindblom et al. (1995)*
Ref_11_7	Batch 400	400	0		0.0001	46	101	62	99	*Lindblom et al. (1995)*
Ref_11_8	Batch 400	500	0		0.0001	34	63	56	100	*Lindblom et al. (1995)*
Ref_11_9	Batch 400	600	0		0.0001	21	33	63	100	*Lindblom et al. (1995)*
Ref_11_500ref	Batch 500	22	0							*Lindblom et al. (1995)*
Ref_11_10	Batch 500	26	0		0.0001	93	202	42	76	*Lindblom et al. (1995)*
Ref_11_11	Batch 500	100	0		0.0001	95	180	47	87	*Lindblom et al. (1995)*
Ref_11_12	Batch 500	150	0		0.0001	86	165	40	81	*Lindblom et al. (1995)*
Ref_11_13	Batch 500	200	0		0.0001	81	149	48	78	*Lindblom et al. (1995)*
Ref_11_14	Batch 500	250	0		0.0001	70	138	46	76	*Lindblom et al. (1995)*
Ref_11_15	Batch 500	300	0		0.0001	66	124	51	83	*Lindblom et al. (1995)*
Ref_11_16	Batch 500	400	0		0.0001	54	92	59	86	*Lindblom et al. (1995)*
Ref_11_17	Batch 500	500	0		0.0001	27	54	64	98	*Lindblom et al. (1995)*
Ref_11_18	Batch 500	600	0		0.0001	16	30	90	99	*Lindblom et al. (1995)*

Table A3-1. Continued.

Specimen ID	Copper batch	Temp. (°C)	Anneal. time (min)	Anneal. temp (°C)	Strain rate (s^{-1})	Rp0.2 (MPa)	Rm (MPa)	Elong. (%)	Area red. (%)	Reference
RR 1	Batch 500	22	0		0.017	53	219	51	90	*Henderson and Lindblom (1995)*
RR 2	Batch 500	22	0		0.017	53	219	51	91	*Henderson and Lindblom (1995)*
RR 3	Batch 500	22	0		0.017	54	219	51	91	*Henderson and Lindblom (1995)*
RR 4	Batch 500	22	0		0.017	53	219	50	90	*Henderson and Lindblom (1995)*
FIN-1	Batch 500	22	0		0.017	55	218	54	91	*Henderson and Lindblom (1995)*
FIN-2	Batch 500	22	0		0.017	56	218	52	89	*Henderson and Lindblom (1995)*
200-1	Batch 200	22	0		0.0001	106	244	60	86	*Henderson and Lindblom (1995)*
200-2	Batch 200	22	0		0.0001	47	236	48	85	*Henderson and Lindblom (1995)*
200-3	Batch 200	22	0		0.0001	46	234	46	82	*Henderson and Lindblom (1995)*
300-1	Batch 300	22	0		0.0001	119	250	60	93	*Henderson and Lindblom (1995)*
300-2	Batch 300	22	0		0.0001	109	251	56	87	*Henderson and Lindblom (1995)*
300-3	Batch 300	22	0		0.0001	111	250	56	88	*Henderson and Lindblom (1995)*
300-4	Batch 300	22	0		0.0001	72	245	50	92	*Henderson and Lindblom (1995)*
500-1	Batch 500	22	0		0.0001	93	202	42	76	*Henderson and Lindblom (1995)*
500-2	Batch 500	22	0		0.0001	74	215	56	87	*Henderson and Lindblom (1995)*
553	Batch 500	22	0	0	0.0001	94	215	56	91	*Henderson and Lindblom (1995)*
550	Batch 500	22	5	600	0.0001	30	211	58	91	*Henderson and Lindblom (1995)*
551	Batch 500	22	10	600	0.0001	31	210	58	91	*Henderson and Lindblom (1995)*
552	Batch 500	22	30	600	0.0001	22	210	60	91	*Henderson and Lindblom (1995)*
602T	Batch 600	22	0		0.0001	134	189	40	86	*Seitisleam et al. (1995)*
612L	Batch 600	22	0		0.0001	134	199	32	89	*Seitisleam et al. (1995)*
702CW	Batch 700	22	0		0.0001	102	185	32	82	*Seitisleam et al. (1995)*
712L	Batch 700	22	0		0.0001	107	192	44	79	*Seitisleam et al. (1995)*
803T	Batch 800	22	0		0.0001	137	262	44	73	*Seitisleam et al. (1995)*
813L	Batch 800	22	0		0.0001	136	266	44	71	*Seitisleam et al. (1995)*
Ref_18_1	CuP0_300	22	0			62	228	45		Andersson et al. (1999)
Ref_18_2	CuP30_450	22	0							Andersson et al. (1999)
Ref_18_3	CuP60_350	22	0			52	225	45		Andersson et al. (1999)
Ref_18_4	CuP105_450	22	0			51	224	46		Andersson et al. (1999)
Ref_18_5	Cu65_450_S12	22	0			52	231	45		Andersson et al. (1999)
Ref_18_6	CuP60_100	22	0			56	231	46		Andersson et al. (1999)
Ref_18_7	CuP60_800	22	0			53	225	46		Andersson et al. (1999)
Ref_18_8	CuP60_2000	22	0			55	244	37		Andersson et al. (1999)

Specimen ID	Copper batch	Temp. (°C)	Anneal. time (min)	Anneal. temp (°C)	Strain rate (s^{-1})	Rp0.2 (MPa)	Rm (MPa)	Elong. (%)	Area red. (%)	Reference
Batch 500 average	Batch 500	22	0				215	56		Henderson and Werme (1996)
Batch 600 average	Batch 600	22	0				194	40		Henderson and Werme (1996)
Batch 700 plate average top	Batch 700	22	0				189	38		Henderson and Werme (1996)
Batch 800 plate average	Batch 800	22	0				264	44		Henderson and Werme (1996)
High speed tensile tests	TX184	22	5	500	10	43	234	60.5		*Andersson-Östling (2009)*
High speed tensile tests	TX184	22	5	500	10	43	235	59.3		*Andersson-Östling (2009)*
High speed tensile tests	TX184	22	5	500	1	37	226	57.0		*Andersson-Östling (2009)*
High speed tensile tests	TX184	22	5	500	1	37	225	58.7		*Andersson-Östling (2009)*
High speed tensile tests	TX184	22	5	500	0.1	53	217	57.0		*Andersson-Östling (2009)*
High speed tensile tests	TX184	22	5	500	0.1	39	217	58.1		*Andersson-Östling (2009)*
High speed tensile tests	TX184	22	5	500	0.001	57	206	59.3		*Andersson-Östling (2009)*
High speed tensile tests	TX184	22	5	500	0.001	37	205	57.0		*Andersson-Östling (2009)*
112A_Dfr	FSWL08/KL059	75			0.001	97	197	47.0		*Wu (2011a)*
43C_Pli	FSWL08/KL059	75			0.001	98	195	47.9		*Wu (2011a)*
338A_JLH	FSWL08/KL059	75			0.001	85	159	24.9		*Wu (2011a)*
112B_Dfr	FSWL08/KL059	175			0.001		168	40.8		*Wu (2011a)*
43D_Pli	FSWL08/KL059	175			0.001	93	165	31.9		*Wu (2011a)*
338B_JLH	FSWL08/KL059	175			0.001	75	129	21.0		*Wu (2011a)*
Hot_tens_3_5 CW	FSW113 – 0 µm cross weld	75					195		0.87	Björck et al. (2019)
Hot_tens_3_6 CW	FSW113 – 0 µm cross weld	175					166		0.88	Björck et al. (2019)
Cu-OF-1	04 G221 OF1	215	10	600	0.0001	28	138	45		Danielsson and Andersson-Östling (2018)
Cu-OFP-1	LID L21/TX104	215	10	600	0.0001	57	147	56		Danielsson and Andersson-Östling (2018)

Table A3-2. Tabulated data points for tensile tests in the reports in Appendix 1, square specimens.

	Specimen ID	Temp. (°C)	Width (mm)	Thickness (mm)	Ext. gauge length (mm)	Rm (MPa)	Area red (%)	Reference
Hot_tens_4_1	FSW113 Ref material	175	8	8	4	172	0.86	Björck et al. (2019)
Hot_tens_4_2	FSW113 Ref material	75	8	8	4	198	0.87	Björck et al. (2019)
Hot_tens_1_1	FSW – 1 µm	75	8	8	4	198	0.69	Björck et al. (2019)
Hot_tens_1_2	FSW – 1 µm	75	8	8	4	200	0.66	Björck et al. (2019)
Hot_tens_1_3	FSW – 1 µm	175	8	8	4	167	0.34	Björck et al. (2019)
Hot_tens_2_1	FSW113 – 6–11 µm	75	8	8	4	200	0.44	Björck et al. (2019)
Hot_tens_2_2	FSW113 – 6–11 µm	75	8	8	4	199	0.43	Björck et al. (2019)
Hot_tens_2_3	FSW113 – 6–11 µm	175	8	8	4	167	0.33	Björck et al. (2019)
Hot_tens_2_4	FSW113 – 6–11 µm	175	8	8	4	168	0.47	Björck et al. (2019)
Hot_tens_3_1	FSW 113 – 0 µm	75	8	8	4	201	0.89	Björck et al. (2019)
Hot_tens_3_2	FSW 113 – 0 µm	75	8	8	4	196	0.9	Björck et al. (2019)
Hot_tens_3_3	FSW 113 – 0 µm	175	8	8	4	169	0.85	Björck et al. (2019)
Hot_tens_3_4	FSW 113 – 0 µm	175	8	8	4	169	0.86	Björck et al. (2019)
Hot_tens_6_1	FSW – 0.1 µm	75	8	8	4	194	0.9	Björck et al. (2019)
Hot_tens_6_2	FSW – 0.1 µm	75	8	8	4	195	0.9	Björck et al. (2019)
Hot_tens_6_3	FSW – 0.1 µm	175	8	8	4	167	0.87	Björck et al. (2019)

Appendix 4

Tabulated data points for creep tests in the reports in Appendix 1

Table A4-1. Creep test results from pilot creep study, Ivarsson and Österberg (1988).

Test ID	Copper batch	Struct.	Temp. (°C)	Stress (MPa)	Rupt. time (h)	Min creep rate (s^{-1})	Elong. (%)	Red. in area (%)	Dia. (mm)	Gauge length (mm)	PLM (10^3)	n $d\varepsilon/dt = B*\sigma^n$
2	Cu-OF	PM	75	140	6300	2.4E−09	20	31	5	50	8.28	27
3				145	7840	8.9E−10	18	33			8.32	
4				150	1697	4.4E−09	13	33			8.08	
5				160	464	3.1E−08	28	42			7.89	
6				170	110	2.2E−07	36	45			7.67	
26	Cu-OF	CW	110	60	3866				5	50	9.03	
27				80	510						8.70	
29				100	223						8.56	
28				100	445						8.67	
30				120	36	6.1E−08					8.26	
7	Cu-OF	PM	110	100	7000	1.3E−09	11	25	5	50	9.13	13
8				110	5890	1.9E−09	9.8	23			9.10	
9				120	1430	5.6E−09	15	27			8.87	
10				130	661	1.5E−08	17	36			8.74	
11				140	168	6.1E−08	21	36			8.51	
12				150	60	1.9E−07	15	36			8.34	
23	Cu-OF	Sim HAZ	110	120	14523	5.6E−10	4.4	29	5	50	9.25	18
24				135	2105	3.9E−09	6.8	26			8.93	
25				150	408	3.3E−08	14	31			8.66	
19	Cu-OF	WM	110	80	16605	5.6E−11	2.7	18	5	50	9.28	18
20				100	2065	3.1E−09	5.8	25			8.93	
21				110	456	8.6E−09	9.5	39			8.68	
22				120	30	1.1E−07	9.5	42			8.23	

Table A4-1. Continued.

Test ID	Copper batch	Struct.	Temp. (°C)	Stress (MPa)	Rupt. time (h)	Min creep rate (s^{-1})	Elong. (%)	Red. in area (%)	Dia. (mm)	Gauge length (mm)	PLM (10^3)	n $d\varepsilon/dt = B*\sigma^n$
13	Cu-OF	PM	145	75	5356	7.8E−10	4.9	23	5	50	9.92	10
14				85	1775	1.4E−09	4.4	15			9.72	
15				90	735	6.4E−09	6	12			9.56	
16				100	650	1.2E−08	11	26			9.54	
17				110	265	3.1E−08	13	21			9.37	
18				120	110	9.7E−08	16	27			9.21	

Table A4-2. Creep test results from the 1992 study of series 000, 100, 200 and 300, Henderson et al. (1992).

Test ID	Copper batch	Struct.	Temp. (°C)	Stress (MPa)	Rupt. time (h)	Min creep rate (s^{-1})	Elong (%)	Dia. (mm)	Gauge length (mm)	PLM (10^3)	n $d\varepsilon/dt = B*\sigma^n$
31	000 Cu-OF	PM	180	60	2247	4.0E−10	0.9	5	50	10.58	5
32				80	373	1.2E−09	0.3			10.22	
33				100	102	4.6E−09	0.3			9.97	
41	000 Cu-OF	PM	215	40	4623	1.5E−10	0.8	5	50	11.55	5
42				60	754	8.1E−10	0.3			11.16	
43				80	86	4.8E−09	0.3			10.70	
52	000 Cu-OF	PM	250	40	1660	5.7E−10	0.7	5	50	12.14	4
53				60	175	3.0E−09	0.4			11.63	
102	100 Cu-OF	PM	215	55	250		0.2	5	50	10.93	4
101				45	684	5.6E−10	0.6			11.14	
103				70	84	5.0E−09	0.3			10.70	
104				85	33	7.2E−09	0.3			10.50	
203	200 Cu-OF	PM	215	70	5058	4.0E−09	12	5	50	11.57	7
204				85	1030	1.7E−08	11			11.23	
205				100	330	5.6E−08	10			10.99	

Table A4-3. Creep test results from the 1995 study of series 400 and 500, *Lindblom et al. (1995)*.

Test ID	Copper batch	Struct.	Temp. (ºC)	Stress (MPa)	Rupt. time (h)	Min creep rate (s^{-1})	Plastic strain on loading (%)	Elong. (%)	Red. in area (%)	Dia. (mm)	Gauge length (mm)	$t_{1\%}$ (h)	$t_{2\%}$ (h)	$t_{5\%}$ (h)	$t_{10\%}$ (h)	PLM (10^3)	n $d\varepsilon/dt = B*\sigma^n$
401	400 Cu-OFP	PM	215	120	7848	7.7E−09	0.2	36	64	5	50	7	85	533	1907	11.66	17
402				140	1447	1.4E−08	0.2	39	78			5	18	67	245	11.30	
406				160	52	8.3E−07		32	83					-	1	10.60	
407				150	192	3.3E−07		41	85					0.07	2	10.87	
410	400 Cu-OFP	PM	300	100	220	3.0E−07		39	76	5	50			15	55	12.80	8
415				90	622	1.1E−07		47	42					23	103	13.06	
416				80	1374	4.7E−08		49	54					81	315	13.26	
417				70	3635	1.7E−08		31	48					646	1494	13.50	
411	400 Cu-OFP	PM	450	30	195	2.5E−07		44	45	5	50			34	92	16.12	
412	400 Cu-OFP	PM	250	100	4796	9.9E−09		42	39	5	50			92	547	12.39	15
413				120	656	1.5E−07		58	57					3	42	11.93	
414				110	2768	2.4E−08		51	62					57	348	12.26	
424	400 Cu-OFP	PM	350	70	194	3.6E−07		80	90	5	50			7	35	13.89	7
426				40	4704	8.1E−09		24	39			299		1597	2894	14.75	
427	400 Cu-OFP	PM	400	40	469	9.7E−08		23	4.2	5	50			110	222	15.26	6
428				30	1558	1.9E−08		17	19					674	1189	15.61	
514	500 Cu-OFP	PM	200	120	3272	1.6E−08		44	40	5	50			0.05	17	11.12	
501	500 Cu-OFP	PM	215	120	2133	2.3E−08		42	56	5	50			-	11	11.38	9
509				110	2646	2.0E−08		39	49	5				0.02	55	11.43	
510				100	5125	5.4E−09		29	64	5				7	401	11.57	
523				120	1350	4.4E−08		54.5	59.9	10						11.29	
502	500 Cu-OFP	PM	250	120	94	6.9E−07		45	76	5	50			-	0.1	11.49	14
503				110	361	1.7E−07		46	65	5				-	1	11.80	
504				100	883	6.1E−08		39	50	5				-	22	12.00	
505				90	2895	1.5E−08		37	30	5				15	238	12.27	
524				120	53.2	1.0E−06		59.9	72.7	10						11.36	
525				100	1084	5.3E−08		47.5	51.8	10						12.05	
506	500 Cu-OFP	PM	275	100	295	2.1E−07		41	54	5	50			-	6	12.31	10
507				90	714	7.2E−08		34	50					0.6	37	12.52	
508				80	2142	2.1E−08		33	32					12	232	12.79	

Table A4-3. Continued.

Test ID	Copper batch	Struct.	Temp. (ºC)	Stress (MPa)	Rupt. time (h)	Min creep rate (s^{-1})	Plastic strain on loading (%)	Elong. (%)	Red. in area (%)	Dia. (mm)	Gauge length (mm)	$t_{1\%}$ (h)	$t_{2\%}$ (h)	$t_{5\%}$ (h)	$t_{10\%}$ (h)	PLM (10^3)	n $d\varepsilon/dt = B*\sigma^n$
512	500 Cu-OFP	PM	300	70	1218	3.9E−08		32	35	5	50			22.6	191	13.23	6
513			300	60	2426	1.3E−08		20	16					370	1398	13.40	
518			300	80	683	7.8E−08		37	38					6	63	13.08	
519	500 Cu-OFP	PM	325	50	1357	6.9E−09		14	13	5	50			983	1345	13.83	
516	500 Cu-OFP	PM	350	50	577	6.9E−08		22	22	5	50			105	305	14.18	5
517			350	40	1105	2.4E−08		14	19					560	1050	14.36	
527	500 Cu-OFP	PM	600	2	25873	1.4E−10	0.8	9.8	0.2	10	50	13296	23670	25100		21.31	
528			600	3	16769	1.4E−10	0.2	12.6				9356	16656	16756	16764	21.15	
555	500 Cu-OFP	PM*	215	120	894	6.7E−08		63	60	5	50					11.20	
556	500 Cu-OFP	PM*	250	120	48.4	1.1E−06		55	74	5	50					11.34	

Table A4-4. Creep test results from the 1996 study of series 600, 700 and 800, *Seitisleam et al. (1995), Seitisleam and Henderson (1996)*.

Test ID	Copper batch	Struct.	Temp. (ºC)	Stress (MPa)	Rupt. time (h)	Min creep rate (s^{-1})	Plastic strain on loading (%)	Elong. (%)	Red. in area (%)	Dia. (mm)	Gauge length (mm)	$t_{1\%}$ (h)	$t_{2\%}$ (h)	$t_{5\%}$ (h)	$t_{10\%}$ (h)	PLM (10^3)
614 L	600 Cu-OF	WM	215	70	17			9	9	5	50					10.36
604 T	600 Cu-OF	WM	215	70	49			4.1	13	5	50					10.58
603 T				30	4702	1.9E−10		2.1	1.3							11.55
605 T	600 Cu-OF	WM	250	120	0.08			7.9	37	5	50					9.89
703 CW	700 Cu-OFP	CW bottom	215	120	7	3.1E−06	7.9	29	75	5	35					10.17
706 CW				100	408	4.3E−08	2.0	22	65					15	192	11.03
709 CW	700 Cu-OFP	CW bottom	250	90	163	1.2E−07	0.8	28	48	5	35			28		11.62
705 CW	700 Cu-OFP	CW middle	215	100	592	2.7E−08	3.1	20	67	5	35			2	209	11.11
708 CW	700 Cu-OFP	CW middle	250	90	174	7.5E−08	1.8	17	53	5	35			15	125	11.63

Test ID	Copper batch	Struct.	Temp. (ºC)	Stress (MPa)	Rupt. time (h)	Min creep rate (s^{-1})	Plastic strain on loading (%)	Elong. (%)	Red. in area (%)	Dia. (mm)	Gauge length (mm)	$t_{1\%}$ (h)	$t_{2\%}$ (h)	$t_{5\%}$ (h)	$t_{10\%}$ (h)	PLM (10^3)
704 CW	700 Cu-OFP	CW top	215	100	604	1.6E−08	1.2	16	38	5	35			130	590	11.12
701 CW				70	5718	6.1E−10	0.2	8.9	37			2326	4920			11.59
707 CW	700 Cu-OFP	CW top	250	90	191	7.4E−08	0.5	17	40	5	35			15	197	11.65
714 L	700 Cu-OFP		215	100	1115	2.1E−08		27	43	5	35			18	378	11.25
720A long	720 Cu-OFP	WM top	215	100	1192	1.8E−08	1.5	24	52	5	35			217		11.26
720B long				110	105	1.3E−07	5.7	26	47					7	62	10.75
720C long				90	2112		1.1	28	41					158		11.38
720E long		WM bottom		100	531	4.4E−08	4.2	24	45					71	346	11.09
721 CW	720 Cu-OFP	CW	215	110	41			47	83	5	15					10.55
723 CW				100	699	1.8E−08	2.3	36	57				29	387		11.15
724 CW				90	1003			27	52							11.22
726 CW				70	6072			22	22							11.61
722 CW	720 Cu-OFP	CW	250	90	163			28	48	5	15					11.62
725 CW				70	543			26	38							11.89
727 CW				50	1748			12	5.5							12.16
731 trans	720 Cu-OFP	WM trans	215	100	122		0.0	35	70	5	35			5		10.78
732 trans				70	3140		0.2	17	45			7	98	1100		11.47
733 trans				90	678	3.8E−08	3.2	25	47					61	400	11.14
801 T	800 cathode Cu	Anisotrop	215	100	0.43			2.4	5.5	5	35					9.58
802 T				30	1212	3.9E−09	0.3	4.7	3.6				474			11.26
811 L	800 cathode Cu	Anisotrop	215	100	0.85			5.5	3.2	5	35					9.73
812 L				30	1468			6.3	0.8		35					11.31
821 L				50	0.23			1.5	1		30					9.45
822 L				30	581			4.4	0.5		30					11.11
824 L				40	18			3.5	0.1		30					10.37

Table A4-5. Creep test results from the 1999 study of creep tests with varying sulphur and phosphorus content and different grain sizes, Andersson et al. (1999), Andersson et al. (2001).

Test ID	Copper batch	Struct.	Temp. (ºC)	Stress (MPa)	Rupt. time (h)	Min creep rate (s^{-1})	Plastic strain on loading (%)	Elong. (%)	Red. in area (%)	Dia. (mm)	Gauge length (mm)	$t_{1\%}$ (h)	$t_{2\%}$ (h)	$t_{5\%}$ (h)	$t_{10\%}$ (h)	PLM (10^3)	n $d\varepsilon/dt = B*\sigma^n$
CuP0_300_1Lb	CuP0_300	PM	175	110	675	7.2E−09	4.7	14	30	10	75	7	200	8.8		10.23	20
CuP0_300_1Jb				120	315	1.5E−08	5.3	12	36			51	223	315		10.08	
CuP0_300_1Kb				130	116	5.0E−08	6.3	14	18			20	80			9.88	
CuP0_300_1N				130	29	1.9E−07	8.8	16.6	36.0				6	29		9.62	
CuP0_300_1M				135	24	5.6E−07	9.4	19	30					18		9.58	
CuP0_300_1K				140	27	2.1E−07	9.1	17.3	35.9					27		9.60	
CuP0_300_1J				150	4.6	4.1E−06	12.6	23.0	43.4					3.7		9.26	
CuP105_450_4N	CuP105_450	PM	175	145	3169	1.0E−08	11.2	39	69	10	75		58	408	1497	10.53	39
CuP105_450_4J				150	677	4.6E−08	12.3	39.2	80.7					34	249	10.23	
CuP105_450_4L				155	215	1.3E−07	13.5	39.3	75.3					10	86	10.00	
CuP30_450_2L	CuP105_450	PM	175	145	11086	2.3E−09	8.8	35	56	10	75		6	300	3493	10.77	37
CuP30_450_2N				147.5	676	3.4E−08	11.3	46	70					13	122	10.23	
CuP30_450_2J				150	147	1.0E−07	7	44.0	79.9					3	45	9.93	
CuP30_450_2K				160	92	1.9E−07	13.3	45.0	77.8					3	18	9.84	
CuP60_100_6J	CuP60_100	PM	175	150	1486	2.9E−08	11	48.4	75.4	10	75			9	102	10.38	27
CuP60_100_6L				155	949	4.2E−08	11.2	49.5	69.1					7	99	10.29	
CuP60_100_6K				160	242	1.7E−07	7.9	48.6	84.7					3.3	32	10.03	
CuP60_2000_8J	CuP60_2000	PM	175	120	5012	1.2E−09	6.5	15.8	57.3	10	75	26	768	4996		10.62	14
CuP60_2000_8M				145	67	1.1E−07	9.8	19.7	76.6					53		9.78	
CuP60_2000_8N				150	2138	4.8E−09	8.3	16	44				391	1978		10.45	
CuP60_2000_8L				155	84	1.2E−07	11.4	23.4	61.9					52	84	9.82	
CuP60_2000_8K				160	39	6.9E−08	13.3	23.1	49.3					39		9.67	
CuP60_350_3N	CuP60_350	PM	175	147.5	1173	3.1E−08	11.4	39.9	71.4	10	75			39	459	10.34	30
CuP60_350_3J				150	2351	1.3E−08	11.1	43.2	71.4					94	863	10.47	
CuP60_350_3L				155	103	3.9E−07	14.3	44.3	75.6					8	34	9.86	
CuP60_350_3M				155	231	1.4E−07	17.5	42.5	80.6					82	154	10.02	
CuP60_350_3K				160	240	1.3E−07	5.5	41.9	94.7					53	164	10.03	

Test ID	Copper batch	Struct.	Temp. (ºC)	Stress (MPa)	Rupt. time (h)	Min creep rate (s^{-1})	Plastic strain on loading (%)	Elong. (%)	Red. in area (%)	Dia. (mm)	Gauge length (mm)	$t_{1\%}$ (h)	$t_{2\%}$ (h)	$t_{5\%}$ (h)	$t_{10\%}$ (h)	PLM (10^3)	n $d\varepsilon/dt = B*\sigma^n$
CuP60_800_7J	CuP60_800	PM	175	150	8997	9.4E−10	9.4	30	46	10	75		16	614	6545	10.73	74
CuP60_800_7M				152	510	4.2E−08	12.4	37.6	65.8				14	83	346	10.17	
CuP60_800_7L				155	283	8.1E−08	12.1	39.2	73.9					25	131	10.06	
CuP60_800_7K				160	60	2.5E−07	14.4	39.5	95.6					7	44	9.76	
CuP65_450_S12_5N	CuP65_450_S12	PM	175	145	6414	4.2E−09	9.8	37	61	10	75		11	859	2588	10.67	
CuP65_450_S12_5J				150	1032	1.7E−08	11.7	36.1	74.5					45	527	10.31	46
CuP65_450_S12_5L				155	116	2.2E−07	14	43.8	84.0					7	38	9.88	
CuP65_450_S12_5K				160	171	2.6E−07	11.4	41.1	83.1					11	74	9.96	

Table A4-6. Creep test results from the 2004 study of creep tests on material from FSW and EB welds, Andersson et al. (2004), Andersson et al. (2005).

Test ID	Struct.	Temp. (ºC)	Stress (MPa)	Rupt. time (h)	Min creep rate (s^{-1})	Plastic strain on loading (%)	Elong. (%)	Red. in area (%)	Dia. (mm)	Gauge length (mm)	$t_{1\%}$ (h)	$t_{2\%}$ (h)	$t_{5\%}$ (h)	$t_{10\%}$ (h)	PLM (10^3)	n $d\varepsilon/dt = B*\sigma^n$
2-120-A	EB CW	125	130	9514	4.4E−10	7.1	25	67	10	50			145	8505	9.54	72
2-100-B			135	2251	4.2E−09	8.5	27.8	67					97	2150	9.29	
2-005-D			137	527	1.8E−08	10.3	30.1	87					43	511	9.04	
2-170-C			142	39	2.5E−07	9.9	30.3	88					6		8.59	
3-230-D	EB CW	175	117	1474	7.5E−09	7.5	24.6	65	10	50		3	224	1402	10.38	36
3-310-C			120	1158	4.9E−09	7.8	28.1	71					49	1028	10.31	
3-290-B			130	44	2.2E−07	9.1	28.8	84					12		9.70	
1-C-3	EB CW	75	150	1688	5.3E−09	11.7	30.9	78	10	50			134	1622	8.08	66
1-A-1			155	180	4.6E−08	10.1	26.2	81					56		7.74	
5-1-B		175	130	12787	2.5E−09	4.7	31.7	41	10	80			195	1941	10.80	46
5-3-C	FSW CW bottom		135	4606	6.9E−09	6.7	37.8	75					127	800	10.60	
5-2-A			140	635	3.6E−08	8.3	37.8	79					10	92	10.22	
5-4-D			147	45	6.4E−07	10.1	35	86				2	5	22	9.70	
6-5-A	FSW CW top	125	150	8430	1.4E−09	9.5	37.6	85	10	80			52	1112	9.52	64
6-3-C			155	1150	4.7E−09	12.4	41.5	86					5	75	9.18	
6-1-D			160	150	8.9E−08	13.5	42.3	88					5	27	8.83	

Table A4-6. Continued.

Test ID	Struct.	Temp. (ºC)	Stress (MPa)	Rupt. time (h)	Min creep rate (s^{-1})	Plastic strain on loading (%)	Elong. (%)	Red. in area (%)	Dia. (mm)	Gauge length (mm)	$t_{1\%}$ (h)	$t_{2\%}$ (h)	$t_{5\%}$ (h)	$t_{10\%}$ (h)	PLM (10^3)	n $d\varepsilon/dt = B*\sigma^n$
4-3-D	FSW CW top		130	10 875	3.2E−09	8.5	39.3	73	10	80			97	1 294	10.77	35
4-8-C		175	140	619	3.5E−08	10.1	39.1	81					9	100	10.21	
4-2-B			140	2 016	5.8E−09	9.3	40.1	81				20	152	568	10.44	
4-1-A			150	40	4.7E−07	12.0	38.3	88					2	20	9.68	
7-2-B	FSW CW top	75	165	7 122	1.1E−09	11.0	35.1	87	10	80			67	1 168	8.30	79
7-3-C			170	660	1.2E−08	11.7	36.5	87				1	26	790	7.94	
8-2-A	FSW HAZ	175	135	6 272	7.8E−09	9.0	54.1	81	10	80			25	485	10.66	39
8-3-B			140	1 133	2.9E−08	10.7	52.1	85					52	236	10.33	
8-4-C			145	211	1.3E−07	13.1	48.9	89					5	51	10.00	
10-3-B	FSW WM bottom	175	131	6 106	5.0E−09	8.9	52.7	69	10	80			40	361	10.66	28
10-2-A			135	1 113	1.8E−08	10.0	36.4	49				2	22	250	10.32	
10-4-C			142	719	3.0E−08	9.0	30.8	53				1	17	207	10.24	
10-5-B			143	174	1.1E−07	11.2	35.1	54					2	24	9.96	
9-2-A	FSW WM top	175	135	10 754	8.9E−09	10	52.9	80	10	80			70	953	10.77	46
9-3-B			140	2 311	2.1E−08	10.1	52.3	75					20	145	10.47	
9-4-C			148	90	5.3E−07	13.2	52.6	84					2	22	9.84	
11-1-D	PM	125	165	1 657	2.8E−09	7.5	36.6	90	10	80			1 459	1 596	9.24	
12-3-B	PM	175	135	14 681	1.3E−09	1.5	45.2	80	10	80	2	31	2 650	10 393	10.83	66
12-1-D			140	1 622	1.6E−08	2.7	42	83					13	120	10.40	
12-4-C			145	162	1.5E−07	5.1	38.9	86					4	31	9.95	

Table A4-7. Creep test results from the 2007 creep test study on friction stir welds, Andersson et al. (2007).

Test ID	Copper batch	Struct.	Temp. (ºC)	Stress (MPa)	Rupt. time (h)	Min creep rate (s^{-1})	Plastic strain on loading (%)	Elong. (%)	Red. in area (%)	Dia. (mm)	Gauge length (mm)	$t_{2\%}$ (h)	$t_{5\%}$ (h)	$t_{10\%}$ (h)	PLM (10^3)	n $d\varepsilon/dt = B^*\sigma^n$
LID75_1	TX104	PM lid	75	175	1 162	1.5E−08	9.3	43.6	90.2	10	80		6	145	6.30	
LID75_2				170	13 925	1.4E−09	10.3	43.4	91.0				2	2 840	6.59	78
LID75_3				180	175	5.3E−08	11.2	45.6	92.2				3	56	6.07	
LID75_5				170	9 585	3.6E−10	8.3	51.1	90.9			1 500	1 850	3 980	8.35	
TUB75_2	T18	PM tube	75	170	7 877	4.4E−09	10.1	52.7	91.6	10	80		971	3 570	6.52	58
TUB75_1				175	6 974	6.9E−10	14.3	47.1	90.6				100	2 266	6.51	
TUB75_4				180	120	1.3E−07	14.4	48.1	92.1				9		7.68	
WINR75_1	L21	CW inner	75	175	32	1.7E−07	10.7	47.4	89.1	10	60		25		5.87	47
WINR75_2				170	398	3.1E−08	10.8	47.5	86.2				7	149	6.17	
WINR75_3				160	6 271	2.3E−09	9.9	46.2	84.7				10	858	8.28	
WMI75_1	L21	WM inner	75	175	1 868	2.8E−08	13.8	63.8	89.6	10	50		1 565	1605	6.35	32
WMI75_2				170	2 207	1.1E−08	10.7	64.9	87.4				73	117	8.12	
WMY75_2	L21	WM outer	75	170	4 378	5.0E−10	14.2	65.3	82.9	10	50		30	560	6.45	124
WMY75_3				180	28	6.1E−07	15.2	65.1	90.1					83	7.46	
WYTT75_1	L21	CW outer	75	175	62	5.3E−07	13.5	54.3	92.8	10	60			20	5.95	95
WYTT75_2				170	835	3.3E−08	15.7	53.7	88.0				8	159	7.98	
HAZ75_1	L21	HAZ weld	75	175	25	1.3E−06	10.7	67.2	91.1	10	50			3	5.84	114
HAZ75_2				170	360	4.7E−08	16.4	66.2	90.8			5	27	179	7.85	

Table A4-8. Creep test results from the 2009 creep test study on cold worked copper, Martinsson and Andersson-Östling (2009).

Specimen	Cold work (%)	Temp (°C)	Stress (MPa)	Rupture time (h)	Min creep rate (s^{-1})	Plastic strain on loading (%)	Elong. (%)	Red. in area (%)	Dia. (mm)	Gauge length (mm)	PLM (10^3)	n $d\varepsilon/dt = B*\sigma^n$	Notes
CuCW12_4	12	75	205	100	2.00E−07	1.2	29.5	88.0	10	75	7.66	77	
CuCW12_1	12	75	200	599	4.07E−08	0.5	34.0	90.9	10	75	7.93		
CuCW12_2	12	75	196	2074	1.14E−08	0.4	29.2	88.7	10	75	8.11		
CuCW12_3	12	75	192	25844	1.08E−09	0.3	38.5	89.8	10	75	8.50		
CuCW24_4	24	75	235	171	9.63E−09	0.2	14.2	89.2	10	75	7.74	57	
CuCW24_5	24	75	230	3218	6.11E−10	0.2	11.4	90.8	10	75	8.18		
CuCW24_3	24	75	230	2448	6.43E−11	0.2	0.2		10	75	8.14		Interrupted
CuCW24_2	24	75	225	2369	9.18E−10	0.2	25.8	88.9	10	75	8.13		
CuCW24_6	24	75	223	8230	2.58E−10	0.2	12.6	88.8	10	75	8.32		
CuCW24_1	24	75	210	4009	4.03E−11	0.2	0.2		10	75	8.21		Interrupted
CuCW12_b	−12	75	205	0		4.7	14.1	91.2	5	50	6.53	60	
CuCW12_a	−12	75	185	56	1.37E−07	0.7	12.5	88.6	5	50	7.57		
CuCW12_e	−12	75	182	454	3.56E−09	2.2	13.3	86.9	5	50	7.88		
CuCW12_d	−12	75	178	176	4.44E−08	0.8	13.5	88.5	5	50	7.74		
CuCW12_c	−12	75	175	5440	1.04E−09	0.5	12.2	86.1	5	50	8.26		
CuCW15-e	−15	75	270	1849	3.49E−10	0.3	12.1	87.8	5	50	8.10	6	
CuCW15-b	−15	75	250	3112	2.02E−09	0.2	10.6	84.6	5	50	8.18		
CuCW15-f	−15	75	230	2480	1.73E−09	0.2	10.5	86.6	5	50	8.14		
CuCW15-i	−15	75	218	16638	6.19E−11	0.3	12.6	94.7	5	50	8.43		
CuCW15-d	−15	75	210	3451		0.2	0.3		5	50	8.19		Interrupted
CuCW15-h	−15	75	210	698	2.61E−09	0.4	10.5	89.0	5	50	7.95		
CuCW15-a	−15	75	185	451		0.3	0.2		5	50	7.88		Interrupted
CuCW15-c	−15	75	178	452		0.2	0.2		5	50	7.88		Interrupted

Table A4-9. Creep test results from the 2011 creep test study on the effect of long creep loading times, Andersson-Östling and Sandström (2011).

Specimen	Structure	Temp (°C)	Stress (MPa)	Rupture time (h)	Min creep rate (s^{-1})	Loading time (h)	Plastic strain on loading (%)	Elong. (%)	Red. in area (%)	Dia. (mm)	Gauge length (mm)	PLM (10^3)	n $d\varepsilon/dt = B*\sigma^n$	Notes
Anneal-1	forged lid	75	180	3	1,81E−03	1	16.9	17.1	92.0	5	50	7.13	114	
Anneal-2	forged lid	75	175	19	1,24E−04	1	23.8	14.6	90.1	5	50	7.41		
Anneal-3	forged lid	75	170	228	9,31E−06	1	23.2	21.4	61.6*	5	50	7.78		
Anneal-4	forged lid	75	165	79	5,83E−06	1	16.1	10.1	68.6*	5	50	7.62		interrupted
Anneal-7	forged lid	75	165	3696	6,94E−08	1	19.5	21.2	66.3*	5	50	8.20		
Anneal-8	forged lid	75	165	814	1,36E−06	24	26.2	10.8	89.7	5	50	7.97		interrupted
Anneal-5a	forged lid	75	165	2350	1,28E−06	24	23.2	19.0	38.7*	5	50	8.13		interrupted
Anneal-11	forged lid	75	165	1633	3,33E−06	719	25.4	14.9	63.7*	5	50	8.08		
Anneal-9	forged lid	75	165	3480	4,42E−07	2160	30.0	16.1	66.4*	5	50	8.19		
Anneal-10	forged lid	75	165	5134	3,38E−06	4320	33.9	17.7	63.9*	5	50	8.25		
Unanneal-1	Unnaneal	75	170	3115	1,97E−07	1	8.8	18.9		5	50	8.18		interrupted
Unanneal-2	Unnaneal	75	165	2817	2,22E−07	1	5.7	20.2		5	50	8.16		
Unanneal-3	Unnaneal	75	165	6526	6,94E−08	168	10.6	17.1		5	50	8.29		interrupted

Table A4-10. Creep test results from the 2011 creep test study on the effect of the processing line inclusions, *Wu (2011a)*.

Specimen	Structure	Temp (°C)	Stress (MPa)	Rupture time (h)	Plastic strain on loading (%)	Elong (%)	Red. in area (%)	Dia. (mm)	Gauge length (mm)	PLM (10^3)	n $d\varepsilon/dt = B*\sigma^n$	Notes
43E(PLI)	cross-weld	75	175	402	13.9	33.4	55.6	8	40	7.87		
43F(PLI)	cross-weld	75	170	3736	12.4	8.6		8	40	8.20		interrupted
122C(DFR)	cross-weld	75	175	303	13.9	50.0	87.9	8	40	7.82		
122D(DFR)	cross-weld	75	170	3546	13.6	4.8		8	40	8.20		interrupted
338D(JLH)	cross-weld	175	174	0.1	9.9	22.3	32.6	8	40	8.51		
43G(PLI)	cross-weld	175	136	5	8.7	22.1	41.5	8	40	9.28		
43H(PLI)	cross-weld	175	126	70	5.7	18.9	43.2	8	40	9.79		
122E(DFR)	cross-weld	175	136	2441	8.0	40.0	43.8	8	40	10.48		
122F(DFR)	cross-weld	175	126	2678	7.1	10.9		8	40	10.50		interrupted
PLI125-1	cross-weld	125	155	37	13.6	32.5	49.5	8	40	8.59		
PLI125-2	cross-weld	125	150	40	13.4	21.7	47.2	8	40	8.60		
PLI125-3	cross-weld	125	140	65	10.7	20.6	47.1	8	40	8.68		
DFR125-1	cross-weld	125	155	2972	11.1	11.0		8	40	9.34		interrupted
DFR125-3	cross-weld	125	160	607	16.4	49.3	87.9	8	40	9.07		

Table A4-10bis. Creep test results from the 2013 creep test study on the effect of indentations into annealed Cu-OFP, Mannesson et al. (2013).

Specimen	Structure	Temp (°C)	Stress (MPa)	Rupture time (h)	Min creep rate (s^{-1})	Loading time (h)	Plastic strain on loading (%)	Elong. (%)	Red. in area (%)	Dia. (mm)	Gauge length (mm)	Indentation depth (mm)	PLM (10^3)	n $d\varepsilon/dt = B*\sigma^n$	Notes
SKB 0-2	extruded tube	75	160	797	4.97E−09	0.24	14.9	9.4	-	12.8 x 8.1	80	0	-	12	Interrupted
SKB 0-3	extruded tube	75	167.0	235	1.07E−07	0.36	17.9	25.0	87.3	12.1 x 8.1	80	0	7.79		
SKB 0-4	extruded tube	75	163.0	1823	6.94E−08	0.37	17.4	17.9	84.5	12.1 x 8.1	80	0	8.09		
SKB 0-5	extruded tube	75	162.0	3022	7.78E−08	0.29	17.2	30.4	70.8	12.1 x 8.1	80	0	8.17		
SKB 1-1	extruded tube	75	161.3	810	1.06E−08	0.34	26.8	17.1	-	12.1 x 8.1	80	0.90	-	39.00	Interrupted
SKB 1-2	extruded tube	75	168.9	111	2.20E−07	0.37	20.3	22.8	86.7	12.1 x 8.1	80	1.04	7.67		
SKB 1-3	extruded tube	75	164.7	167	2.02E−08	0.35	16.9	28.8	73.5	12.1 x 8.1	80	1.02	7.73		
SKB 1-4	extruded tube	75	161.8	96	3.06E−08	0.23	17.2	33.3	88.4	12.1 x 8.1	80	1.05	7.65		
SKB 1-5	extruded tube	75	161.7	1871	4.17E−08	0.23	8.8	38.5	83.2	12.1 x 8.1	80	1.02	8.10		
SKB 15-1	extruded tube	75	164.1	644	4.15E−09	0.24	15.7	10.9	21.2	12.1 x 8.1	80	1.57	-	53.00	Interrupted
SKB 15-2	extruded tube	75	171.0	389	5.78E−08	0.28	17.5	22.7	83.3	12.1 x 8.1	80	1.52	7.86		
SKB 15-3	extruded tube	75	166.9	782	2.56E−08	0.34	16.1	27.2	73.1	12.1 x 8.1	80	1.52	7.97		
SKB 15-4	extruded tube	75	164.6	1785	1.30E−8	1.28	19.4	46.0	82.4	12.1 x 8.1	80	1.47	8.09		
SKB 15-7	extruded tube	75	173.1	192	8.60E−08	0.35	24.2	39.7	83.9	12.1 x 8.1	80	1.52	7.78		
SKB 2-1	extruded tube	75	166.5	644	7.22E−9	0.24	15.7	19	23.9	12.1 x 8.1	80	1.96	-	75.00	Interrupted
SKB 2-2	extruded tube	75	174.2	297	8.33E−08	0.35	17.7	22.6	85.9	12.1 x 8.1	80	2.01	7.82		
SKB 2-3	extruded tube	75	170.4	1080	1.51E−08	0.37	15.0	22.2	76.5	12.1 x 8.1	80	2.06	8.02		
SKB 2-7	extruded tube	75	176.4	135	2.06E−07	0.24	21.7	22.6	44.3	12.1 x 8.1	80	2.03	7.70		
SKB 2a-1	extruded tube	75	166.8	1389	4.21E−09	0.25	15.9	16.0	87.1	12.1 x 8.1	80	2.00	8.05	94.00	
SKB 2a-3	extruded tube	75	170.5	299	3.42E−08	0.34	16.7	13.5	69.7	12.1 x 8.1	80	2.07	7.82		
SKB 2a-4	extruded tube	75	165.2	3526	1.67E−08	0.33	18.1	34.6	92.9	12.1 x 8.1	80	2.06	8.19		
SKB 2a-7	extruded tube	75	171.9	207	7.17E−08	0.35	20.3	16.6	75.3	12.1 x 8.1	80	1.99	7.77		

Table A4-11. Creep test results from the 2014 creep test study on the effect of stress application variations, Mannesson and Andersson-Östling (2016).

Specimen	Structure	Temp (°C)	Stress (MPa)	Rupture time (h)	Min creep rate (s^{-1})	Loading time (h)	Loading 1 (%)	Loading 2* (%)	Loading 3* (%)	Elong. (%)	Red. in area (%)	Dia. (mm)	Gauge length (mm)	PLM (10^3)	Notes
P1	extruded tube	75	168	190		0.32	20.0			8.7	23.0	10	75	7.75	
P3	extruded tube	75	165	11 520	1.94E−07	0.36	10.9			21.1		10	75	8.37	
P4	extruded tube	75	160	22 713	1.39E−07	0.41	10.7			19.0		10	75	8.48	Interrupted
P2	extruded tube	75	168	2 767	7.22E−07	2+168+168	10.9	0.58	4.86	33.6	68.0	10	75	8.16	
P6	extruded tube	75	165	4 299	5.00E−07	2+168+169	9.4	2.59	3.30	25.1		10	75	8.22	
P7	extruded tube	75	160	13 234	7.22E−07	2+168+170	8.4	2.20	6.80	32.4		10	75	8.39	
N1	extruded tube	75	168	2 043	8.89E−07	2+1 000+1 000	11.1	0.70	3.18	34.6	67.9	10	75	8.11	
N2	extruded tube	75	165	2 681	3.67E−05	2+1 000+1 000	10.6	1.00	3.40	38.4	66.7	10	75	8.15	
N3	extruded tube	75	160	2 821	1.03E−06	2+1 000+1 000	12.1	1.40	0.60	39.4	68.9	10	75	8.16	

* Loading strain 2 and 3 is included in the creep strain when the total strain is calculated.

Table A4-12. Creep test results from the 2014 creep test study on the effect of copper with different NDT sound attenuation, Mannesson and Andersson-Östling (2014a).

Specimen	Structure	Temp (°C)	Stress (MPa)	Rupture time (h)	Min creep rate (s^{-1})	Loading time (h)	Plastic strain on loading (%)	Elong. (%)	Red. in area (%)	Width (mm)	Thickness (mm)	Gauge length (mm)	PLM (10^3)	n $d\varepsilon/dt = B*\sigma^n$
T64 175	extruded tube	125	155	13	2.01E−04	0.375	21.5	21.2	48.6	9	9	80	8.41	61
T64 165	extruded tube	125	145	463	7.83E−06	0.33	24.0	27.7	58.0	9	9	80	9.02	
T64 155	extruded tube	125	150	112	3.38E−05	0.27	23.7	30.9	55.7	9	9	80	8.77	
T64 185	extruded tube	125	140	858	3.33E−07	0.33	23.8	30.5	59.4	9	9	80	9.13	
T58 240	extruded tube	125	160	69	3.82E−05	0.35	23.2	16.3	74.7	9	9	80	8.69	20
T58 230	extruded tube	125	155	267	8.75E−06	0.23	22.2	26.7	87.3	9	9	80	8.93	
T58 220	extruded tube	125	145	1 018	2.51E−06	0.33	16.7	28.6	59.8	9	9	80	9.16	
T58 210	extruded tube	125	150	288	1.95E−05	0.35	17.6	32.2	55.3	9	9	80	8.94	
T58 200	extruded tube	125	140	581	2.39E−06	0.35	17.1	34.7	65.0	9	9	80	9.06	
T53 190	extruded tube	125	160	15	1.64E−04	0.33	23.8	16.4	80.8	9	9	80	8.43	30
T53 180	extruded tube	125	155	95	2.93E−05	0.28	22.8	22.3	52.0	9	9	80	8.75	
T53 170	extruded tube	125	145	448	1.44E−05	0.29	20.3	34.6	54.0	9	9	80	9.02	
T53 124	extruded tube	125	150	238	7.41E−06	0.39	18.0	28.3	56.2	9	9	80	8.91	
T53 114	extruded tube	125	140	1 445	1.50E−06	0.24	14.9	31.8	59.5	9	9	80	9.22	

Table A4-13. Creep test results from the 2014 creep test study on the effect of external indentations, Mannesson and Andersson-Östling (2014b).

Specimen	Indentation type	Temp (°C)	Stress (MPa)	Rupture time (h)	Loading time (h)	Plastic strain on loading (%)	Elong. (%)	Red. in area* (%)	Indentation depth (mm)	PLM (10^3)	Notes
NED 2	Cylinder	75	167	5870			39	84	0.50	8.27	Datafile corrupt, only basic data
NED 3	Cylinder	75	171	948	0.23	17.4	39	48	0.44	8.00	
NED 4	Cylinder	75	170	2923	0.36	18.1	34	50	0.50	8.17	
NED 1	Cylinder	125	161	315	0.35	19.4	40	48	0.40	8.95	
NED 5	Sphere	75	171	1935	0.28	17.8	45	47	0.51	8.10	
NED 6	Sphere	75	169	1773	0.37	18	59	50	0.50	8.09	
NED 7	Sphere	125	161	100	0.41	19.2	36	49	0.52	8.76	
NED 9	Cone	75	171	2469	0.33	19.3	46	44	0.63	8.14	
NED 10	Cone	75	169	1606	0.36	21.3	52	49	0.66	8.08	
NED 11	Cone	125	161	332	0.39	19	41	51	0.62	8.96	
NED 13	No indentation	75	165	4507	0.28	9.82	41	49	0.00	8.23	
NED 14	No indentation	75	163	8711	0.26	16.7	31	26	0.00	8.33	
NED 15	No indentation	75	170	996	0.37	15.6	44	48	0.00	8.00	

* All specimens with the exception of NED2 was stopped before final fracture, thus the reduction of area is shown as smaller than it would have been if the specimen had ruptured.

Table A4-14. Creep test results from the 2015 creep test study on the copper with different phosphorus contents, Wu and Sandström (2015).

Specimen	Temp (°C)	Stress (MPa)	Rupture time (h)	Min creep rate (s^{-1})	Loading time (h)	Plastic strain on loading (%)	Elong. (%)	Red. in area (%)	Dia. (mm)	Gauge length (mm)	PLM (10^3)	n $d\varepsilon/dt = B*\sigma^n$	Notes
REF50-8	125	155	4682	1.40E−10		18.3			10	50	9.42	28	Lab. move interrupt
REF50-9	125	160	4943	3.71E−10		18.6			10	50	9.43		Lab. move interrupt
REF50-10	125	155	5395	5.23E−10	4	19.3			10	50	9.45		Lab. move interrupt
REF50-11	125	160	12188	1.09E−09	3	18.7			10	50	9.59		Interrupted
REF50-12	125	173	4866	4.67E−09	10	21.1	62.4	80.6	10	50	9.43		
REF50-13	125	170	5182	5.53E−09	9	20.7	67.9	86.5	10	50	9.44		
MILP-8	125	155	6116	3.41E−10		21.5	50.3	81.1	10	50	9.47	46	Lab. move interrupt
MILP-9	125	155	5539	3.58E−10	12	20.1			10	50	9.45		Lab. move interrupt
MILP-10	125	160	8228	1.94E−09	10	19.6	38.3	49.5	10	50	9.52		
MILP-11	125	166	6379	2.56E−09	4	19.6			10	50	9.47		
MILP-12	125	170	100	5.03E−08	8	21.0	48.4	76.5	10	50	8.76		

Table A4-14. Continued.

Specimen	Temp (°C)	Stress (MPa)	Rupture time (h)	Min creep rate (s^{-1})	Loading time (h)	Plastic strain on loading (%)	Elong. (%)	Red. in area (%)	Dia. (mm)	Gauge length (mm)	PLM (10^3)	n $d\varepsilon/dt = B*\sigma^n$	Notes
M2HP-8	125	155	674	3.39E−09		29.3	48.0	86.6	10	50	9.09	19	
M2HP-9	125	160	0.02			19.2	45.6	87.5	10	50	7.28		
M2HP-10	125	165	535	3.14E−09		24.2	45.1	85.9	10	50	9.05		
M2HP-11	125	150	11890	3.44E−10	4	13.2			10	50	9.58		Interrupted
M2HP-12	125	160	0.23		6	19.1	45.9	68.9	10	50	7.71		
REF-1	75	180	3285	3.59E−10		22.2	53.8	90.1	10	50	8.18	59	Lab. move interrupt
REF-2	75	175	13221	3.18E−10		21.1			10	50	8.39		Lab. move interrupt
REF-3	75	190	35	3.04E−08		39.1	49.4		10	50	7.50		
M1LP-1	75	180	0.20			27.0	57.6	82.8	10	50	6.72		
M1lLP-2	75	175	5090	3.13E−10		27.2			10	50	8.25		Lab. move interrupt
M2HP-1	75	178	0.10			30.6	52.4	81.9	10	50	6.61		
M2HP-2	75	175	252	2.16E−08		30.3	46.0	78.9	10	50	7.80		

Table A4-15. Creep test results from the 2016 creep test study on phosphorus in copper (Andersson-Östling et al. 2018) and the 2017 follow-up creep study on Cu-OF and Cu-OFP at 175 and 215 °C (Danielsson and Andersson-Östling 2018).

Specimen	Temp (°C)	Stress (MPa)	Rupture time (h)	Min creep rate (s^{-1})	Plastic strain on loading (%)	Elong (%)	Red. in area (%)	Dia. (mm)	Width (mm)	Thickness (mm)	Gauge length (mm)	Indentation depth (mm)	PLM (10^3)	Notes
T-58-7	75	170	184	6.58E−06	12.3	22.3			12	8	80		7.75	
T58-8	75	170	38		18.7	22.7			12	8	80		7.51	
T58-9	75	170	148	1.50E−05	18.3	35.4			12	8	80		7.72	
T58-10	75	170	188	1.53E−05	19.2	36.0			12	8	80		7.75	
T58-11	75	170	24		24.0	28.3			12	8	80		7.44	
Cu-OF01	215	85	175	3.89E−07	0.3	0.8	0.4	10			75		10.85	
Cu-OFP02	215	85	13317	4.15E−08	8.6			10			75		11.77	Ongoing
Cu-OF03	175	85	1495	6.01E−08	0.1	1.3		10			75		10.38	

Table A4-16. Creep test results from the 2017 creep test study with continuous hydrogen charging, Leijon et al. (2018).

Specimen	Test type	Charge time (hours)	Temp (°C)	Stress (MPa)	Rupture time (h)	Dia. (mm)	Gauge length (mm)	Notes
H-creep_01	In situ hydrogen charging creep	96	22	140	93	5	50	Discontinued
H-creep_02	In situ hydrogen charging creep	95	22	140	92	5	50	Discontinued
H-creep_03	In situ hydrogen charging creep	103	22	140	100	5	50	Discontinued
H-creep_04	In situ hydrogen charging creep	17	50	185	3	5	50	Discontinued/large necking
H-creep_05	In situ hydrogen charging creep	1 009	22	170	1 006	5	50	Discontinued
H-creep_06	In situ hydrogen charging creep	116	50	172	113	5	50	Discontinued/charge unstable
H-creep_07	In situ hydrogen charging creep	98	22	175	95	5	50	Discontinued
H-creep_08	In situ hydrogen charging creep	118	50	172	115	5	50	Discontinued/charge unstable
H-creep_09	In situ hydrogen charging creep	172	50	172	169	5	50	Discontinued
H-creep_10	In situ hydrogen charging creep	172	75	172	169	5	50	Discontinued
H-creep_11	In situ hydrogen charging creep	101	75	176	98	5	50	Discontinued
H-creep_12	In situ hydrogen charging creep	260	22	176	257	5	50	Discontinued
H-creep_13	In situ hydrogen charging creep	16	75	176	13	5	50	Fractured
H-creep_14	In situ hydrogen charging creep	No charging	50	172	120	5	50	Discontinued
H-creep_15	In situ hydrogen charging creep	No charging	50	172	167	5	50	Discontinued
H-creep_16	In situ hydrogen charging creep	No charging	75	172	20	5	50	Discontinued

Table A4-17. Creep test results from the 2018 creep test study on copper welds with oxide particles, Björck et al. (2019).

Specimen	Structure	Material	Temp (°C)	Stress (MPa)	Rupture time (h)	Red. in area (%)	Dia. (mm)	Width (mm)	Thickness (mm)	Gauge length (mm)	PLM (10^3)	Notes
FS475175	FSW113 41/4	ref.mat.	75	175	545	88		8	8	4	7.91	
FS475135	FSW113_4	ref.mat.	75	135	13 507			8	8	4	8.40	Ongoing
FS475155	FSW113_4	ref.mat.	75	155	13 507			8	8	4	8.40	Ongoing
FS175155	FSW113 221/1	1 µm oxide	75	155	169	47		8	8	4	7.74	
FS175140	FSW113 199,5/1	1 µm oxide	75	135	181	50		8	8	4	7.75	
FS275175	FSW113 139/2	6–10 µm oxide	75	175	100	43		8	8	4	7.66	
FS275155	FSW113 154/2	6–10 µm oxide	75	155	425	42		8	8	4	7.87	
FS375175	FSW113 77/3	0 µm oxide	75	175	1 949	58		8	8	4	8.10	
FS375170	FSW113 76/3	0 µm oxide	75	170	534	90		8	8	4	7.91	
FS375135	FSW113 85/3	0 µm oxide	75	135	817	16		8	8	4	7.97	
FS375155	FSW113 79.5/3	0 µm oxide	75	155	2 106	32		8	8	4	8.12	
FT375155	FSW113 65/3	0 µm oxide	75	155	11 638			8	8	4	8.37	Ongoing
FS375115	FSW113 62/3	0 µm oxide	75	115	1 077	80		8	8	4	8.02	
FSW64175	FSW113 64/3	0 µm oxide	75	175	129	89	10			50	7.69	
FSW85155	FSW113 85/3	0 µm oxide	75	155	5 873		10			50	8.27	Ongoing
FSW88135	FSW113 88/3	0 µm oxide	75	135	3 162		10			50	8.18	Ongoing
FS675175	FSW113 242/6	0.1 µm oxide	75	175	288	91		8	8	4	7.82	
FS675155	FSW113 235/6	0.1 µm oxide	75	155	2 346	64		8	8	4	8.13	
FS675135	FSW113 270/6	0.1 µm oxide	75	135	4 098	88		8	8	4	8.22	Ongoing

Appendix 5

Tabulated data points for multiaxial, crack propagation and component tests in the reports in Appendix 1

Table A5-1. Creep test results from the 1988 creep test study on internally pressurised copper containers, Ivarsson and Österberg (1988).

Specimen	Outside diameter	Wall thickness	Internal pressure	Calculated hoop stress	Temp	Rupture time	Max diametral strain	Calculated plastic hoop strain on loading		
								PM	WM	Sim HAZ
	(mm)	(mm)	(MPa)	(MPa)	(°C)	(h)	(%)	(%)	(%)	(%)
1	19.8	2.83	39.2	117.5	110	35	7	1.43	0.68	0.18
2	19.9	0.91	10.3	107.5	110	285	6.9	0.93	0.33	0.13
3	19.9	2.85	29.4	88	110	697	4.6	0.35	0.07	0.06
4	19.95	0.95	7.85	78.5	110	-	-	0.2	0.03	0.04

Table A5-2. Creep test results from the 2009 creep test study on copper using notched multiaxial specimens, Wu et al. (2009).

Specimen	Test type	Copper batch	Structure	Temp (°C)	Stress (MPa)	Rupture time (h)	R (mm)	a/R*	Plastic strain on loading (%)	Notes
Cu-0.5-1	multiaxial creep	forged lid	PM	75	170	16782	5.64	0.5	0.29	Interrupted
Cu-0.5-2	multiaxial creep	forged lid	PM	75	180	12148	5.64	0.5	0.73	Interrupted
Cu-0.5-3	multiaxial creep	forged lid	PM	75	200	1133	5.64	0.5	1.38	
Cu-0.5-4	multiaxial creep	forged lid	PM	75	215	8	5.64	0.5	1.69	
Cu-0.5-5	multiaxial creep	forged lid	PM	75	195	2492	5.64	0.5	1.11	
Cu-2-1	multiaxial creep	forged lid	PM	75	170	16107	1.41	2	0.15	Interrupted
Cu-2-2	multiaxial creep	forged lid	PM	75	180	12145	1.41	2	0.31	Interrupted
Cu-2-3	multiaxial creep	forged lid	PM	75	200	13551	1.41	2	0.37	Interrupted
Cu-2-4	multiaxial creep	forged lid	PM	75	215	15417	1.41	2	0.78	
Cu-2-5	multiaxial creep	forged lid	PM	75	230	565	1.41	2	4.02	
Cu-2-6	multiaxial creep	forged lid	PM	75	225	685	1.41	2	3.29	
Cu-5-1	multiaxial creep	forged lid	PM	75	170	16107	0.56	5	0.13	Interrupted
Cu-5-2	multiaxial creep	forged lid	PM	75	180	11949	0.56	5	0.17	Interrupted
Cu-5-3	multiaxial creep	forged lid	PM	75	200	13550	0.56	5	-	Interrupted
Cu-5-4	multiaxial creep	forged lid	PM	75	215	9701	0.56	5	1.16	Interrupted
Cu-5-5	multiaxial creep	forged lid	PM	75	230	13727	0.56	5	2.75	Interrupted
Cu-5-6	multiaxial creep	forged lid	PM	75	245	20	0.56	5	4.03	
Cu-18-1	multiaxial creep	forged lid	PM	75	230	13725	0.15	18.8	2.23	Interrupted
Cu-18-2	multiaxial creep	forged lid	PM	75	240	13098	0.15	18.8	2.22	Interrupted
Cu-18-3	multiaxial creep	forged lid	PM	75	255	147.5	0.15	18.8	6.09	

* Notch acuity, a is half specimen diameter at base of notch, R is the notch root radius.

Table A5-3. Creep propagation test results from the 2011 study on Cu-OFP, Wu et al. (2011).

Specimen	Copper batch	Temperature (°C)	Reference stress (MPa)	Loading Load line Displacement (LLD) (mm)	CCG LLD (mm)	Minimum load line displacement rate (µm/h)	Time to rupture (h)	Ruptured/interrupted	Number of load increases
CCG215	T17	215	120	5.86	13.06	19.25	121		
CCG175	T17	175	122	6.06	22.38	2.25	812		
CCG75A	T17	75	165	10.43	2.57	0.0491	8 925	Interrupted	
CCG75R	T17	75	140–165	7.32	5.7	0.079 (at 150 MPa)	4 778	Interrupted	3
CCG22	T17	22	135–205	6.4	15.1	0.061 (at 143 MPa)	13 324	Interrupted	9

Appendix 6

Tabulated data points for hot tensile and creep tasting of nodular cast iron in the reports in Appendix 1

Table A6-1. Hot tensile testing of noudular cast iron, *Martinsson and Larsson (2009)*.

Specimen	E mod (GPa)	Rp0.2 (MPa)	Rm (MPa)	A_{50} (%)
A3	200	246	378	12.9
A4	159	244	381	12.5
R3	177	244	378	13.5
R4	151	247	379	13.0
T3A	203	242	378	14.9
T4A	215	242	359	9.1
Average	184	244	375	12.7

Table A6-2. Creep testing of nodular cast iron, Martinsson et al. (2010).

Specimen	Insert cast ID	Test type	Temperature (°C)	Stress (MPa)	Loading time (min)	Loading strain (%)	Testing time (h)	Notes
GAE1	I55	Creep and acoustic emission measurement	RT	280	10	0.54	2302	Interrupted
GAE2	I55		RT	260	10	0.27	2276	Interrupted
GAE3	I55		RT	240	10	0.18	2276	Interrupted
GAE4	I55		RT	220	10	0.15	2275	Interrupted
GAE5	I55		RT	200	10	0.11	2275	Interrupted
GAE6	I55		100	200	10	-	0	Loading test
G1	I30	Creep	100	350	10	-	0.1	Broken
G2	I30		100	150	10	0.12	35214	Interrupted
G3	I30		100	180	10	0.17	12628	Interrupted
G4	I30		100	210	10	0.34	75	Interrupted
G5	I30		100	240	10	1.07	75	Interrupted
G6	I30		100	210	600	0.31	11907	Interrupted
G7	I30		100	240	600	0.65	11787	Interrupted
T3B	I55	Creep	125	240	3	0.37	7245	Interrupted
T4B	I55		125	260	3	0.76	7210	Interrupted

Arkitektkopia AB, Bromma, 2020

SKB is responsible for managing spent nuclear fuel and radioactive waste produced by the Swedish nuclear power plants such that man and the environment are protected in the near and distant future.

skb.se